NUREG/CR-5876
PNL-8023

Full-Length Fuel Rod Behavior Under Severe Accident Conditions

Prepared by
N. J. Lombardo, D. D. Lanning, F. E. Panisko

Pacific Northwest Laboratory
Operated by
Battelle Memorial Institute

Prepared for
U.S. Nuclear Regulatory Commission

NUREG/CR--5876

TI93 005718

Full-Length Fuel Rod Behavior Under Severe Accident Conditions

Manuscript Completed: August 1992
Date Published: December 1992

Prepared by
N. J. Lombardo, D. D. Lanning, F. E. Panisko

Pacific Northwest Laboratory
Richland, WA 99352

Prepared for
Division of Systems Research
Office of Nuclear Regulatory Research
U.S. Nuclear Regulatory Commission
Washington, DC 20555
NRC FIN B2277

Abstract

This document presents an assessment of the severe accident phenomena observed from four Full-Length High-Temperature (FLHT) tests that were performed by the Pacific Northwest Laboratory (PNL) in the National Research Universal (NRU) reactor at Chalk River, Ontario, Canada. These tests were conducted for the U.S. Nuclear Regulatory Commission (NRC) as part of the Severe Accident Research Program. The objectives were to simulate conditions and provide information on the behavior of full-length fuel rods during hypothetical, small-break, loss-of-coolant severe accidents resulting in core degradation, in commercial light water reactors.

The FLHT test hardware and test operations are described. The thermal, hydraulic and mechanical response of the fuel rod bundle and insulating shroud are then described and analyzed. These results are then used to describe the full-length fuel damage behavior under coolant boilaway conditions. The influence of the coolant level on the onset and progression of fuel rod damage is first assessed through a correlation of the coolant level with the oxidation and melt fronts. Differences in damage progression behavior between rapidly and gradually decreasing coolant levels are assessed.

The oxidation behavior for variations in length of uncovered fuel bundles is examined and the effect of test duration on the oxidation-induced damage assessed. Next, an analysis is made of the hydrogen generated, including the fraction of steam converted to hydrogen, the timing of release, and the effect of Zircaloy melting on the generation rate. The material relocation behavior of these full-length tests is then evaluated and integrated with the results of similar short-length, in-pile severe fuel damage tests. Differences in test design and operations are assessed relative to differences observed between the short- and full-length test end-state picture. Finally, an assessment of models incorporated into the Severe Core Damage Analysis Program (SCDAP) is made from a comparison of the code predictions and the test data from three of the FLHT tests.

Contents

Abstract iii

Executive Summary ix

Acknowledgments xiii

Acronyms xv

Definitions xvii

1 Introduction 1

1.1 Objectives of the CBDP Program and the FLHT Tests 1
1.2 Test Operations 3
1.3 Test Results 3
1.4 Report Overview 3

2 FLHT Hardware Design and Test Operations 5

2.1 Hardware Design 5

2.1.1 Test Train Assembly 5
2.1.2 Steam Closure Cave and Effluent Control Module 8
2.1.3 Data Acquisition and Control System 10

2.2 Test Operations 10

2.2.1 Pretest Installations and Checkout 11
2.2.2 Commissioning and Calibration 11
2.2.3 Preconditioning Operation 11
2.2.4 Coolant Boilaway/Severe Damage Transient 12
2.2.5 Post-Test Examinations 12

3 Thermal, Hydraulic, and Mechanical Behavior of the FLHT Tests 15

3.1 Overview of Thermal Response and Damage Progression 15
3.2 Thermal Response 16

3.2.1 Component Heatup 16
3.2.2 Temperature Gradients 18

3.3 Hydraulic Response 21

3.3.1 Coolant Level Behavior 21
3.3.2 Bundle Flow Resistance During Damage Progression 22

Contents

3.4 Mechanical Behavior 23

3.4.1 Fuel Rod Failure 23
3.4.2 Cavity Failures 24

4 Evaluation of FLHT Severe Accident Phenomena 27

4.1 Correlation of Coolant Level with Cladding Temperatures 27

4.1.1 Coolant Level at the Onset of Damage Conditions 27
4.1.2 Fuel Uncovered for Autocatalytic Oxidation and Melting 29

4.2 Oxidation Behavior 31

4.2.1 Temperature Escalation and Burn Front Progression 31
4.2.2 Oxidation in the Steam-Cooled Region 33
4.2.3 Influence of Test Time and Boiloff Type on Oxidation 34

4.3 Hydrogen Generation 35

4.3.1 Hydrogen Generation Rate and Integral Hydrogen Released 35
4.3.2 Effect of Zircaloy Melting on the Release of Hydrogen 37

4.4 Material Relocation Behavior 38

4.4.1 Observed Relocation Behavior 39
4.4.2 Assessment of SFD Test Relocation Behavior 41

5 SCDAP Code Analyses of FLHT Tests 47

5.1 Description of SCDAP 47
5.2 Overview of SCDAP Predictions with Major FLHT-Test Parameters 47
5.3 SCDAP Assessment of the FLHT-5 Test Data 48

5.3.1 SCDAP FLHT-5 Model 48
5.3.2 Comparison of Bundle and Shroud Temperatures 49
5.3.3 Comparison of Bundle Oxidation and Hydrogen Generation 51
5.3.4 Comparison of Fission Gas Release 52

6 Conclusions 55

7 References 57

Figures

2.1 FLHT test general hardware arrangement 5
2.2 FLHT test train axial schematic 7
2.3 Detailed FLHT test train axial schematic 7
2.4 FLHT general reactor core cross section 7
2.5 Detail of the shroud 7
2.6 Flow paths in the steam closure cave and effluent control module 9
3.1 FLHT-5 cladding, liner, and saddle temperature histories--Level 88 16
3.2 Cladding heatup rates after dryout for FLHT-4 and -5 Level 96 17
3.3 Comparison of FLHT-2 steam and cladding temperatures 17
3.4 Cladding and liner heatup rate for FLHT-5 Level 96 17
3.5 Liner and saddle heatup rate for FLHT-5 Level 96 18
3.6 FLHT-5 cladding axial temperature profiles prior to the initial oxidation excursion 18
3.7 FLHT-2 cladding temperature deviation from average--Level 100 locations 19
3.8 FLHT-2 cladding temperature deviation from average of the three rods--Level 92 19
3.9 FLHT-2 cladding temperature deviation from average--Level 72 20
3.10 FLHT-2 cladding temperature deviation from average--Level 60 20
3.11 FLHT-5 average cladding to average liner temperatures and temperature difference--Level 96 20
3.12 Coolant level decrease for the FLHT-2, -4, and -5 tests 21
3.13 Comparison of cladding dryout and TDR coolant level data for the FLHT-5 test 22
3.14 Comparison of TDR liquid level response 23
3.15 Comparison of fuel rod failure temperatures 24
4.1 Effect of decreasing liquid level on peak cladding temperature for the step-change flow reduction transients 28
4.2 Effect of decreasing liquid level on peak cladding temperature for the FLHT-1 variable flow reduction transient boilaway 28
4.3 Correlation of liquid level with the oxidation burn front for FLHT-2 29
4.4 Comparison of initial and final oxidation excursion locations with liquid level for FLHT-5 30
4.5 FLHT-5 cladding temperature response illustrating the downward oxidation progression 31
4.6 FLHT-5 cladding temperature response illustrating the termination of the downward burn 32
4.7 FLHT-5 saddle temperature response illustrating the upward burn 32
4.8 FLHT-5 saddle temperature as a function of time and elevation 33
4.9 Comparison of calculated oxidation and nuclear LHGR during FLHT-5 heatup 33
4.10 Overview of the FLHT oxidation progression 34
4.11 FLHT-2 hydrogen generation rate calculated from NTF and for fully converted inlet flow 36
4.12 FLHT-4 hydrogen generation rate calculated from NTF and for fully converted inlet flow 36
4.13 FLHT-5 hydrogen generation rate calculated from NTF and for fully converted inlet flow 37
4.14 Partitioning of hydrogen production for the FLHT-5 test 37
4.15 Thermocouple responses identifying FLHT-2 material relocation events A-E 39
4.16 Axial schematic of FLHT-2 material relocation events 41
4.17 Predicted impact of shroud radial heat losses on cladding axial temperature gradients 43
4.18 Illustration of the influence of fission-to-chemical power ratio on local temperatures 44
4.19 Changing nature of FLHT axial temperature gradients 45

4.20 Characterization of boiloff-type axial temperature gradients 45
5.1 SCDAP nodalization of the FLHT-5 test 48
5.2 Measured and predicted cladding and liner temperatures at Level 80 for FLHT-5 49
5.3 Measured and predicted cladding temperatures for FLHT-5 versus elevation, at 100 s intervals 50
5.4 Measured and predicted saddle temperatures at Level 64 for FLHT-5 50
5.5 Measured and predicted saddle temperatures at Level 136 for FLHT-5 50
5.6 Measured and predicted hydrogen generation rates 51
5.7 Predicted and measured xenon fractional release rates for FLHT-5 52

Tables

1.1 Summary of major parameters for full-length high-temperature severe fuel damage tests in the NRU reactor 2
2.1 FLHT test train features 6
2.2 FLHT test parameters 11
3.1 Comparison of coolant level behavior for FLHT tests 21
4.1 Hydrogen generation and oxidation summary 36
4.2 Summary of steam consumption for in-pile SFD tests 38
4.3 Overview of FLHT-2 recorded material relocation events 40
4.4 Evaluation of material relocation behavior in both short- and full-length SFD tests 42
4.5 Comparison of fission and chemical powers 44
5.1 Post-test SCDAP predictions for FLHT tests compared with measured data 48
5.2 Measured and SCDAP predicted hydrogen generation and zircaloy oxidation for FLHT-5 51
5.3 SCDAP predicted FLHT-5 zircaloy oxidation 52
5.4 FLHT-5 fission gas release measurements and predictions 52

Executive Summary

Four full-length high-temperature (FLHT) tests of the Coolant Boilaway and Damage Progression (CBDP) Program were conducted to provide data for assessing computer models that predict coolant boilaway, fuel heatup, melting, and hydrogen release that occur during the early phase of severe reactor accidents. The FLHT tests were also conducted to investigate full-length fuel damage progression and phenomena in order to confirm the behavior of short-length severe fuel damage tests.

The four FLHT tests contribute data and insights unique to severe fuel damage (SFD) behavior because of the dynamically-changing coolant level with full-length fuel and a constant fission power level that simulated decay heat levels--parameters that lead to prototypic axial temperature profiles under coolant boilaway conditions and oxidation-induced damage progression. Additionally, two of the FLHT tests in the series were conducted for extended times (up to 1 hr) under severe damage conditions, lengths of time that exceed other SFD tests. Together, these aspects of the FLHT tests permitted a unique assessment of a variety of SFD phenomena. A summary of the significant damage progression phenomena associated with these tests and their impact on key issues are presented below.

Effect of Coolant Boilaway

Two types of coolant boilaways were evaluated by the FLHT tests: 1) a rapid boilaway where the coolant level decrease to the steady state elevation occurred within 10 min as a result of a large step-change decrease in the coolant flow rate and 2) boilaway where the coolant level decrease was gradual due to the slow reduction in the coolant flow rate. The primary differences in the damage progression behavior for the different types of coolant boilaways are 1) the coolant level at which rapid oxidation (oxidation excursion) takes place and 2) the mechanism responsible for the downward progression of the oxidation burn front. The coolant level is considerably lower for the rapid boilaway tests when the initial oxidation excursion occurs. For these tests in which the coolant level deceased rapidly, the downward progression of the oxidation burn front is driven by the steepening axial temperature gradients. In the extended boilaway test, the downward progression of the oxidation burn front is controlled by the coolant level decrease.

Oxidation-Induced Damage Progression

The axial extent of the oxidation-induced damage was dependent on the rapid boilaway test on the test time at high temperature. In the longer duration FLHT tests, an upward progression of the oxidation burn front was noted following the downward burn. Whereas the downward burn was controlled by the rapidly changing axial temperature profiles, the upward burn was controlled by the nearly complete oxidation of Zircaloy at lower elevations. As a result, the upward burn progressed at a slower rate but occurred over a longer length of fuel. The bulk of the time at high-temperature for the tests of longer duration, therefore, took place with an upward burn based on sequential thermocouple measurements. Because of the disrupted geometry and oxidation that took place during the downward burn, the oxidation accompanying the upward burn in this previously oxidized region was less intense. However, in the initially steam-starved upper elevations above the initial oxidation excursion, the subsequent oxidation within the burn front appeared as vigorous as the downward burn. Although there existed a steam-cooled region just above the dryout front where temperatures remained below the oxidation excursion temperature and rapid oxidation did not take place, significant oxidation of the cladding took place, resulting in highly embrittled cladding. Thus, essentially all of the exposed fuel rod cladding can be oxidized and damaged in a protracted coolant boilaway accident.

Hydrogen Generation

The results from the FLHT tests support the conclusion that no physical phenomena exist that would terminate the hydrogen generation during severe accidents aside from complete consumption of the available Zircaloy, as demonstrated in the FLHT-5 test. The phenomenon of

material relocation, although it did not terminate hydrogen production, was consistently found to cause a temporary reduction in the production rate; however, this temporary reduction has little influence on limiting the total hydrogen released. The mechanism for reducing hydrogen generation is the removal of hot materials from the high-temperature oxidation zone into a cooler zone. As the lower, and cooler, regions became heated as the oxidation excursion zone progresses downward, the hydrogen generation was found to return to fully-consumed conditions. During the tests, because little material relocated from the high-temperature region to the steam-cooled region above the coolant, hydrogen generation continued until either termination of the test or, as in the case of FLHT-5, complete consumption of the available zircaloy. Thus, for severe accidents where steam production continues, only the Zircaloy below the coolant/steam interface would not be expected to participate in the production of hydrogen.

Material Relocation

The relocation of molten materials was tied to the passage of the oxidation burn front. The material relocation behavior can be described as heterogeneous, with UZrO melting, relocating, and reheating as the oxidation burn front moved downward. The loss of bundle region thermocouples precluded the collection of data on the material relocation during the upward burn. The axial extent of the material relocation was generally within the spacing of the grid spacers, e.g., <0.5 m. This relocation distance was not great enough to remove significant quantities of material from the high-temperature oxidation region to the steam-cooled region or the coolant pool; thus, oxidation and the accompanying hydrogen generation continued.

Cohesive blockages did not form at the bottom of the fuel bundle as were typically found in the short-length Power Burst Facility (PBF) SFD tests. The difference in the end-state blockage formation was attributed to differences in test design and operation. The short-length tests have intrinsic design and operational features that promote the formation of large cohesive blockages, particularly at the lower elevations. These features include steep axial temperature gradients resulting from the short-length high fission power levels and the proximity of inlet region structures to the damage region.

Conversely, the design and operational features of the full-length tests make the formation of large cohesive melts less likely because of smaller fission power levels, relatively larger radial heat losses, and larger distances between the melt zone and inlet fixtures.

While the effects of fission power level, radial heat losses, axial temperature profiles, and end-effects all are inextricably tied to the material relocation phenomena observed in these SFD tests, quantification of each of these effects, particularly the difference in radial heat losses and fission- to-chemical power ratio, was not attempted. It was concluded, however, that the difference in observed blockage in the lower elevation is due primarily to non-prototypic axial temperature profiles in the short-length tests and the proximity of inlet fixtures. Other aspects of material relocation behavior, such as the correlation of the oxidation burn front to the melt zone and the axial distance of the material relocation, were consistent between the full-length FLHT tests and the short-length tests.

Assessment of Severe Accident Behavior Code Models

An assessment of models incorporated into the Severe Core Damage Analysis Program (SCDAP_ severe accident computer code was made between the code predictions and test data for three of the FLHT tests. The heatup portions of the transient were relatively well predicted; however, significant differences between predicted and measured results were noted in the coolant level decrease and in the total hydrogen generated and fission products released. The predicted hydrogen and fission product release amounted to 50% of the measured data. These differences were attributed to deficiencies in the material relocation model. The underpredicted integral hydrogen and fission product release noted in this assessment could lead to underpredicted source terms for the late-phase severe accident behavior, and perhaps, underpredicted risk.

Conclusions

The results from the FLHL tests provide well-characterized data for evaluating the effects of coolant boilaway and core damage progression in an LWR. The tests provided the opportunity to investigate integral

severe accident phenomena in full length LWR-type fuel bundles under boilaway conditions. The test data and analysis supported the regulatory issue of hydrogen generation in boiling-water BWRs during a severe accident. The tests were used to confirm the validity of most of the results obtained from separate effects and short-length integral tests. Not confirmed were coherent blockage and lack of gross fuel swelling. The tests were used to help validate SCDAP for the early stage of a severe accident. We believe because of an inadequate fuel rod relocation model that the oxidation and hydrogen generation were incorrectly predicted by the code as the test data made evident. Fission product releases were also inadequately predicted but we believe that improvements in the fuel rod relocation model would also improve the fission product release predictions.

Acknowledgments

The work on the FLHT-1, -2, -4, and -5 tests spanned the years 1984 to 1987, excluding post-irradiation examinations. During this period, many individuals at the Pacific Northwest Laboratory (PNL), EG&G Idaho, two consultants, Chalk River Nuclear Laboratories (CRNL), and the U.S. Nuclear Regulatory Commission (NRC) made significant contributions to these successful tests. Listed below are the key contributors to this program. However, as is always the case with a large-scale irradiation test program, there are more contributors than can be named. Those whose names have not been included know that their contributions have been invaluable to the success of the program.

PNL

Gordon Anderson designed and built the special electronic systems for the liquid level time domain reflectometer sensors that continuously measured the liquid level within the fuel bundle region, the shroud molten metal penetration detectors that help protect the reactor during the tests, and the electrical heaters in the upper plenum of the test train. He also helped with pretest instrument checks. He was assisted by Gene Wallace, Bev Taylor, and Tom Conroy.

Dale Fitzsimmons was the test director for the last two tests and significantly upgraded the experiment operations plan for those tests.

Max Freshley provided management oversight and was a key interface among PNL, CRNL, and the NRC.

Bob Goodman was responsible for test train instrumentation. He was supported by Bill Norton and Tom Fish.

Galen Hesson performed thermal hydraulic analyses and was the test director for the first two tests.

Walt Hensley was responsible for fission product measurements and analysis for the later tests.

Dave Hurley designed, fabricated, assembled, checked out, operated and modified the effluent control module. He was assisted by Duane Hobbs and Steve Burnum.

Urban Jenquin was responsible for test nuclear analyses including fission product production, radiation levels, and shielding analyses.

Loyd King was responsible for the test train design and post-test examinations; he also helped with test operations. He was assisted by designers Dave Hagerty, Ken Keene, Craig Sumner, and Andy Anthony. Also assisting were Bob Hagen, Don Smith, and Chuck Bigelow during post-test examinations.

John Nageley provided editorial guidance and improved the clarity of many parts of the test report. Others who worked on earlier drafts of the report include Dave Hilliard, Nancy Waugh, S. Kesterson, R. Moreno, and J. Moore.

LeeRoy Parchen was in charge of QA and the fabrication of the later test trains.

Chuck Bigelow assembled the test trains and helped put them into the reactor.

Ron Page was responsible for making flexible electrical connections for the test train instruments. He was assisted by Steve Faber, Tom Fish and Billy Norton.

Jim Pilger was responsible for the earlier test train fabrication development, actual fabrication and assembly. He was assisted by Stu Allison, Chuck Bigelow, Jim Vining, Ron Page, Billy Norton, Steve Faber, John Lester, and Norm Davis.

Bill Rausch did the development of the necessary software for the test data acquisition and control; he also operated the computer during the tests.

Glenn Russcher was responsible for the safety analyses of the earlier tests.

Nancy Wildung processed the millions of data points and converted them into visual representations. She was helped by Tracy Klem, Brian Reed, and Gary Springer.

Consultants

August Cronenberg performed key safety analyses for off-normal energetic events as well as for fission product transport and deposition.

Mark Wismer made major contributions to every aspect of the tests, design, assembly, setup and checkout, especially in trouble-shooting instrument problems; he was the interface between the test director and the computer control systems during the tests and helped perform post-test fuel bundle and shroud examinations.

EG&G

Jack Hartwell performed fission product release measurements and analysis.

CRNL

Just as there are more PNL staff who contributed to the success of these tests than can be named here so also are there more CRNL staff than can be named here. However, the following CRNL staff provided major contributions to the success of most if not all the FLHT tests: Mike Atfield, Don Burton, Terry Chapman, Paul Fehrenbach, Nancy Howden, Neil Keller, Pat Kelly, Bob Lovoie, Ivan Martin, Bernie McCambridge, Bill McCrea, Danny Nishimura, Bill Shorter, Dave Thompson, and Dave Wilder.

NRC

This program was initially under the management of Bob van Houten and, after his retirement, temporarily under Bob Wright then under Tom J. Walker. This program was part of the U.S. NRC Severe Accident Research Program that was initially headed by Mel Silberberg and later by Farouk Eltawila. Ralph Meyer made timely, valuable contributions.

Acronyms

ADD	antideposition device
ALPM	actual liters per minute
BWR	boiling-water reactor
CBDP	Coolant Boilaway and Damage Progression (Program)
CRNL	Chalk River Nuclear Laboratories
DACS	data acquisition and control system
DOE	U.S. Department of Energy
ECM	effluent control module
EFPH	effective full-power hour
EPRI	Electric Power Research Institute
EOP	Experiment Operations Plan
FLHT	full-length high-temperature (tests)
HBR	H. B. Robinson (Reactor)
HEPA	high-efficiency particulate air (filter)
ID	inside diameter
INEL	Idaho National Engineering Laboratory
LCS	loop control system
LHGR	linear heat generation rate
LOCA	Loss-of-coolant accident
LWR	light water reactor
MFM	mass flowmeter
MMPD	molten material penetration detector
MS	mass spectrometer

NTF	noncondensable turbine flowmeter
NRC	U.S. Nuclear Regulatory Commission
NRU	National Research Universal (reactor)
OD	outside diameter
PBF	Power Burst Facility (reactor)
PHM	palladium hydrogen meter
PNL	Pacific Northwest Laboratory
PTE	post-test examination
PT	pressure transducer
PWR	pressurized-water reactor
RCS	reactor control system (in other literature RCS often means reactor coolant system)
RT	room temperature
SARP	Severe Accident Research Program
SCC	steam closure cave
SCDAP	Severe Core Damage Analysis Program
SFS	Severe Fuel Damage
SFD/ST	Severe Fuel Damage/Source Term (Program)
slpm	standard liter per minute
SNL	Sandia National Laboratory
SPND	self-powered neutron detector
TC	thermocouple
TCM	thermal conductivity meter
TD	theoretical density
TDR	time-domain reflectometer (liquid level detector)

Definitions

Significant words and phrases used in this report are defined below:

Assembly	(Also referred to as fuel rod assembly or fuel assembly)- The 11 or 12 full-length fuel rods held in a square lattice array by grid spacers.
Bundle	(Also referred to as fuel rod bundle or fuel bundle)- A term commonly used to designate the fuel rod assembly and its characteristics (e.g., bundle coolant flow and bundle oxidation power).
Boilaway Transient	The extended operation at 23- or 30-kW bundle nuclear power and low makeup flow (~1.26 g/s) when the coolant boiled away and the rods heated up, experienced cladding temperature escalation, melting, and accelerated oxidation resulting in severe bundle damage.
Carriers	Pieces of Zircaloy occupying the corners of the assembly that shield the thermocouple (TC) leads and route them, i.e., "carry" them to exit points from the assembly extremities.
Caves	Lead-lined boxes containing and shielding various components within the steam closure cave/effluent control module (SCC/ECM).
Cavity	The spaces in the shroud or plenum area that were pressurized with inert gas and monitored for pressure during the test; e.g., the shroud insulation cavity, the plenum insulation cavities, and the shroud molten material penetration detector (MMPD) cavity.
Closure	(Also referred to as closure plug)- The specially designed fixture at the top of the test train that provides a pressure seal for the reactor pressure tube and permits penetration of makeup flow lines, time-domain reflectometer (TDR) lines, plenum drain line, bundle effluent line, and test train instrument leads.
Gamma Thermometer	A device for measuring liquid level and axial power distribution that can be thought of as a solid stainless steel rod with internal thermocouples along its length, residing in a Zircaloy guide tube in one of the cells of the square lattice of the fuel assembly. (In FLHT-5, a steel rod in a Zircaloy sleeve was used to simulate the gamma thermometer used in FLHT-4 to keep the two tests similar with respect to power distribution and material contents.) Neither FLHT-1 nor FLHT-2 tests contained a gamma thermometer.
Makeup Flow	(Also referred to as makeup)- The inlet water flow to the bundle, especially after the boilaway has begun. This small flow "makes up" for some of the water coolant loss due to steaming.
Level	The elevation in inches above the bottom of the FLHT fuel column.
Plenum	The 4-m-long Zircaloy tube (effluent line) leading from the top of the fuel bundle to the closure, including insulated heaters. The upper plenum is the approximately 3-m-long heated section beginning 1-m above the top of the bundle; the lower plenum is the unheated approximately 1-m section below the heated section. The two plena are separated by a metal diaphragm. Above the upper plenum is an evacuated double-walled plenum section leading through the closure.

SCC/ECM	A combined acronym denoting the steam closure cave (SCC) and the effluent control module (ECM).
Shroud	The insulated multicomponent structure surrounding the fuel bundle. The components (listed in order from inside to outside) include the liner, zirconia insulation tiles, Zircaloy saddles, inner round, MMPD cavity with wire wrap, and the outer Zircaloy round. The oxidation of the liner (and the carriers) is included with that of the bundle in the measurement of bundle oxidation power and hydrogen generation because it is impossible to distinguish the separate contributions of these components during accelerated bundle oxidation.
Liner	The Zircaloy lining around the fuel bundle shroud, which separates the bundle from the zirconia insulation in the shroud.
Test Train	The combined FLHT test apparatus inserted in the National Research Universal (NRU) Reactor pressure tube, including fuel bundle, shroud, plenum, and closure fixture (approximately 9 m long).
Time-Domain Reflectometer (TDR)	A device for sensing liquid level in the test train. It consists of a tube running the full length along the outside of the test train in the bypass annulus and is held at constant pressure by means of a vent line. By electronic means, the water level is measured based on the time delay of reflected electronic signals. The tube interconnects the bottom of the fuel bundle and the top of the plenum and acts like a manometer with the fuel bundle as one leg; therefore, the tube acts like a stand pipe, indicating the collapsed liquid level in the fuel bundle.

1 Introduction

Through the Severe Accident Research Program (SARP),[1] the U.S. Nuclear Regulatory Commission (NRC) is conducting or participating in numerous experiments to study the behavior of reactor core materials during severe accident conditions. As part of the SARP, the NRC sponsors the Coolant Boilaway and Damage Progression (CBDP) Program at Pacific Northwest Laboratory (PNL).[2] In the CBDP Program, instrumented, insulated assemblies of full-length (3.7-m) light-water reactor (LWR) fuel rods are subjected to coolant flow reductions while operating at low fission heat ratings which simulate decay heat. This procedure simulates possible loss-of-coolant (LOCA) accident conditions in LWR cores. The consequent coolant boilaway, heatup of the exposed rods, and exothermic oxidation reaction of the hot Zircaloy cladding with steam result in cladding melting, fuel liquefaction, material relocation, hydrogen generation evolution, and fission product release.

A series of four CBDP tests was conducted by PNL in the National Research Universal (NRU) reactor at Chalk River Nuclear Laboratories (CRNL), Ontario, Canada, beginning in 1985. These tests, designated full-length high-temperature (FLHT) experiments, featured a gradual increase in the severity of peak cladding temperatures, hydrogen generation rate, and length of time at maximum conditions, as noted in Table 1.1

This report presents analyses of the data from the FLHT-1, -2, -4, and-5 tests.[3] Although some analysis of the FLHT-1 test data is presented, the majority of the analysis and conclusions of severe fuel damage progression and behavior focused on the FLHT-2, -4 and -5 tests because of their longer time at high temperature.

[1]Partners in this program with NUC include nuclear organizations from the following countries: Belgium, Canada, England, Finland, Federal Republic of Germany, Italy, Japan, the Netherlands, Republic of China (Taiwan), Republic of Korea, Spain, Sweden, Switzerland, France, Russian, and Mexico.

[2]Operated for the U.S. Department of Energy by Battelle Memorial Institute under Contract DE-AC06-76RLO 1830.

[3]FLHT-3 was conceptualized but not conducted.

1.1 Objectives of the CBDP Program and the FLHT Tests

The objectives of the CBDP Program were to 1) obtain well-characterized data for evaluating the effects of coolant boilaway and core damage progression in a LWR and 2) investigate integral severe accident phenomena in the full-length fuel bundle and under prototypic conditions to address important regulatory issues. The data are used to confirm the validity of results obtained from separate-effects tests sponsored by the NRC at PNL and other laboratories and to validate computer models that describe reactor behavior during severe accidents. Only by having validated models can a thorough assessment of risk be obtained and strategies developed for preventing or mitigating accidents resulting from the loss of reactor coolant.

Instrumentation of the FLHT test trains provided date on temperature, pressure and flow rate. These data were obtained to assess the following severe accident phenomena:

- coolant boilaway behavior for full-length fuel bundles at decay heat levels
- axial temperature distributions of full-length fuel bundles as a function of coolant level
- the timing and rate of hydrogen generation and the effect of cladding melting on the hydrogen generation
- the oxidation behavior of full-length fuel rods under protypic axial temperature profiles and constant steam supply
- the effect of time-at-high-temperature on the damage progression and the amount and types of damage
- full-length material relocation phenomena under prototypic axial temperature distributions

Table 1.1 Summary of major parameters for full-length high-temperature severe fuel damage tests in the NRU Reactor[1]

Test Designation	Test Date	Number of Preirradiated Rods[3]	Approximate Pre-Test Fuel Preconditioning (Time at 670 kW) Assembly Nuclear Power), h	Nominal[2] Assembly Nuclear Power, kW	Peak Cladding[4] Temperature Achieved, K	Peak Hydrogen Production Rate, mg/s[5]	Time at Peak Temperature,[6] min	Final Liquid Level, m	Average Heatup Rate K/s[7]
FLHT-1	3/85	0	0.0	23	2300	140	<1	1.5	NM
FLHT-2	12/85	0	0.0	23	2500	210	4.5	0.9	3.1
FLHT-3[7]									
FLHT-4	8/86	1	1.0	23	2600	174	30	0.86	2.6
FLHT-5	5/87	1	5.0	>30	2600	182	60	0.76	3.5

[1]All tests to date have been conducted with a nominal bundle inlet flow of 1.3 g/s during the boilaway transient.
[2]The fission power was confirmed by calorimetry of the water-filled bundles. The voided region of the bundle is estimated to have lower power increases of 15% based on neutronics. calculations.
[3]Total rods per assembly are 12 (FLHT-1, -2) and 11 (FLHT-4 -5). The preirradiated rods have a nominal burnup of 28 MWd/kgU and wre discharged in May of 1975.
[4]Best estimate values based on interpretation of thermocouple data.
[5]Peak assembly heat generation rate due to oxidation (in kW) equals 0.15 times the peak hydrogen production rate in mg/s.
[6]Time after onset of cladding melt temperatures (2100 K).
[7]Heatup rate at bundle midplace from saturation (467 K) to 1700 K. Not applicable for FLHT-1.
[8]Conceptualized but not performed.

- cladding/grid spacer interactions
- flow channel blockage behavior
- fission product release and transport.

1.2 Test Operations

In each FLHT test, a 12-rod assembly of full-length pressurized-water reactor (PWR) rods was subjected to low coolant flow of ~0.1 g/s/rod while operating at either 23 or 30 kW, i.e., at ~2% to 3% of normal commercial LWR rod fission power to simulate decay heat. The fuel rod assembly was contained in an insulating shroud and operated in a pressure tube within the NRU reactor. The pressure tube was connected to a recirculating pressurized water loop, which provided exterior cooling for the shroud. The operating time following the onset of cladding melt temperatures (~2100 K) was increased from test to test, starting with less than 1 min for FLHT-1 and reaching 60 min for FLHT-5.

Other test variations included 1) the use of an irradiated PWR rod (FLHT-4 and -5); 2) the time period of pretest full-power bundle operation to "precondition" the fuel pellets;[1] and 3) the addition of an actual or simulated gamma thermometer in place of one of the fuel rods in the 12-rod assembly. During the tests, cladding temperatures were monitored along the length of the fuel rod bundle using high-temperature thermocouples[2] (TCs); bundle inlet water and exit steam flow were measured with turbine flowmeters; the evolution of hydrogen was measured by several methods; and the release and transport of fission products were monitored by several gamma spectrometers. A shielded effluent control module (ECM) on top of the reactor conducted the hot, pressurized, radioactive effluent past the hydrogen meters and gamma spectrometers. As the ECM condenses steam, it maintains system pressure with a pressure control valve and pressurized nitrogen injection.

[1]Preconditioning was performed to provide fuel pellet cracking and to increase the fission product inventories, especially iodine.
[2]W-5Re/W-26Re, BeO insulated, Zr/Ta sheath.

1.3 Test Results

All the FLHT tests conducted to date produced extensive and severe fuel rod damage, with the severity and extent of the damage increasing with each subsequent test. Following the flow reduction that initiated the transient, the coolant boiled away and the rods dried out and heated until an autocatalytic oxidation reaction began between the steam and the Zircaloy cladding. This oxidation reaction concentrated in a "burn front" of limited axial extent (<0.2 m) that initially moved rapidly downward in the bundle, then traveled slowly upward. The high-temperature portion of the FLHT-5 boilaway transient was deliberately extended to 60 min which permitted the burn front to reach the top of the rods. Within the burn front, peak temperatures exceeded the Zircaloy melt temperature by as much as 500 K and significant fractions of gaseous and volatile fission products were released. The damage region was as much as 3-m long.

1.4 Report Overview

The hardware designs and test operations for the four tests are reviewed in Section 2. An overview of the fuel bundle thermal, hydraulic and mechanical response is then presented in Section 3. With this understanding, an evaluation of the key severe accident phenomena investigated by the FLHT test program is presented in Section 4. Covered in this section are detailed discussions on the effect of coolant level on cladding temperatures, oxidation burn front and melt progression; an evaluation of the oxidation progression behavior within and outside the burn front region; the timing and amount of hydrogen released, including the effect of cladding melting; and finally, an assessment of full-length material relocation behavior. Similarities and differences in severe accident behavior between the full-length FLHT tests and short-length in-pile tests are presented in Section 4 to identify length-effects. Finally, a comparison of Severe Core Damage Analysis Program (SCDAP) predicted test behavior with the actual FLHT test behavior is presented in Section 5, and areas for model improvement are identified.

2 FLHT Hardware Design and Test Operations

The FLHT tests all used similar hardware and followed similar test operations. In this section, a description is given of the hardware, test operations and the test-to-test variations.

2.1 Hardware Design

Overall the test train and associated hardware for the FLHT tests is designed to accomplish the following: 1) provide for a controlled coolant boilaway; 2) accommodate temperatures at least as high as 2500 K within the fuel bundle; 3) measure and record key temperatures, flow rates, and pressures; 4) maintain control of pressures and flows; 5) sample the effluent; and 6) provide for operating safety and public safety throughout the course of tests.

The FLHT test hardware consists of the following four components plus the NRU reactor: test train assembly, steam closure cave, SCC, effluent control module, ECM, and a data acquisition and control system, DACS.

The general arrangement of these components during a test in the NRU reactor is shown in the Figure 2.1. During a boilaway transient two coolant systems are used. The test train external coolant system continuously circulates sub-cooled, pressurized water around a closed loop piping system. The water cools the external surfaces of the test train assembly. The second system is a once-through circuit that supplies sub-cooled, pressurized water from a storage tank to the fuel bundle inlet region. This water then flows up among the fuel rods, the upper plenum, through the closure, SCC, ECM and finally into a storage tank. These coolant systems are also shown in Figure 2.1.

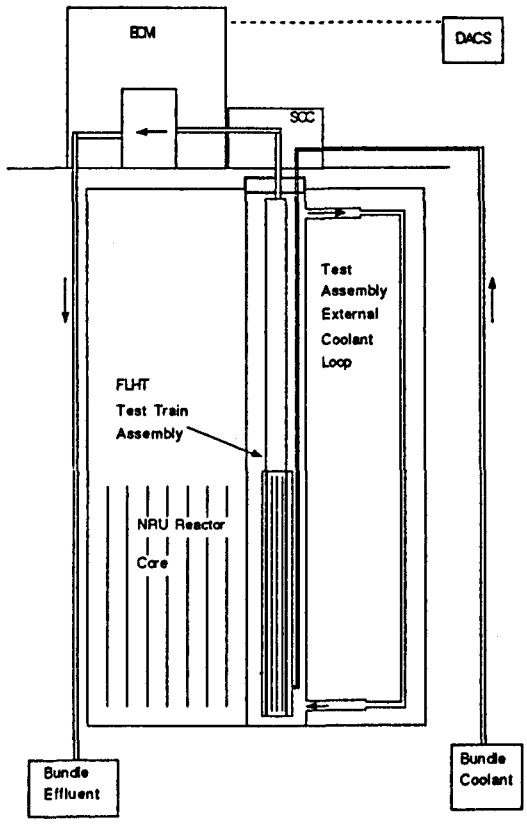

Figure 2.1 FLHT test general hardware arrangement

2.1.1 Test Train Assembly

The test train assembly is about 9 m long and hangs inside a pressure tube in the NRU reactor. The assembly consists of almost equal lengths of upper plenum and reactor core sections plus short sections at each end, a closure section at the top end and an inlet section at the bottom end. The closure section seals the assembly to the reactor pressure tube and is the pressure boundary for all instrument lines and flow tubes that exit the test train assembly. The upper plenum section connects the closure to the core sections of the assembly. In addition to providing this mechanical function it provides a thermally insulated and in the FLHT-4 and -5 tests electrically heated flow path for the fuel bundle effluent. The reactor core section of the test train assembly consists of a highly instrumented fuel bundle and thermally insulated shroud. The inlet region mechanically supports the fuel bundle, provides an entrance for bundle coolant and is a pressure boundary for all bundle instrument lines. Most of the test instruments are located within the reactor core section and several are located within the upper plenum section. Figure 2.2 is a schematic of an axial view of the test train assembly.

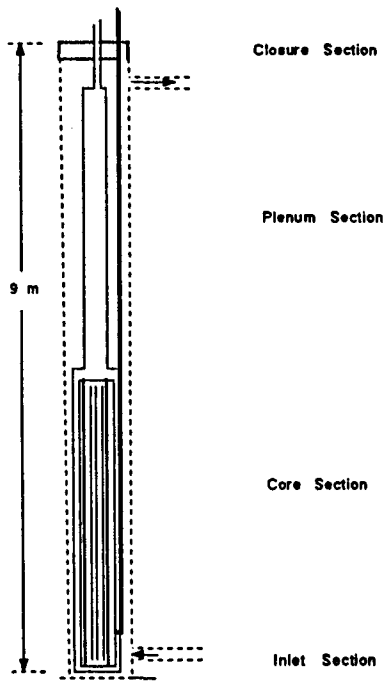

Figure 2.2 FLHT test train axial schematic

Generally, the test trains used in the FLHT tests comprise the following: 1) either an 11- or 12-rod assembly of 3.7-m-long fuel rods, 2) an insulating shroud surrounding the fuel rod bundle, and 3) a 2.5-cm-ID 4-m-long effluent line, or "plenum," leading from the top of the bundle to a closure plug at the top of the reactor pressure tube. Primarily, differences among the FLHT test trains are in the number of unirradiated and irradiated rods included and in the method for heating the plenum walls; a summary of the test trains features is presented in Table 2.1. A detailed axial layout of the test train components is shown in Figure 2.3. The fuel bundle contains positions for 12, 3.7 m long LWR type fuel rods in a square array with a 1.3 cm pitch. Eight either Inconel or Zircaloy grids maintain the rods in position. Each rod contains enriched UO_2 pellets that are slotted as required to make room for thermocouple leads. Thermocouples are spot welded to the inside of the fuel rod cladding at various elevations and azimuthal positions. The leads for the fuel rod thermocouples and other thermocouples that measure bundle coolant temperatures exit from the bottom of the test assembly and are routed up along side the assembly exterior. The thermally insulated shroud surrounds the fuel bundle and isolates it thermally and hydraulically from the

Table 2.1 FLHT test train features

Item	FLHT-1	FLHT-2	FLHT-4	FLHT-5
Total number of fuel rods	12	12	11	11
Number of irradiated rods	0	0	1	1
Gamma thermometer[1] (occupying an interior rod position)	No	No	Yes	No[(a)]
Spacer grid material	8 Inconel	8 Inconel	8 Inconel	4 Inconel 4 Zircaloy
Insulator material	Zirconia	Zirconia	Zirconia+Thoria[2]	Zirconia
Rod fill gas pressure, MPa	1.4	1.62	0.5	0.5
Method of plenum heating	None	Superheated Steam	Electrical Heaters	Electrical Heaters

[1]The gamma thermometer for FLHT-5 was replaced by a "dummy" stainless steel rod.
[2]A 10.2-cm-long length of thoria was located at the top of the insulated shroud.

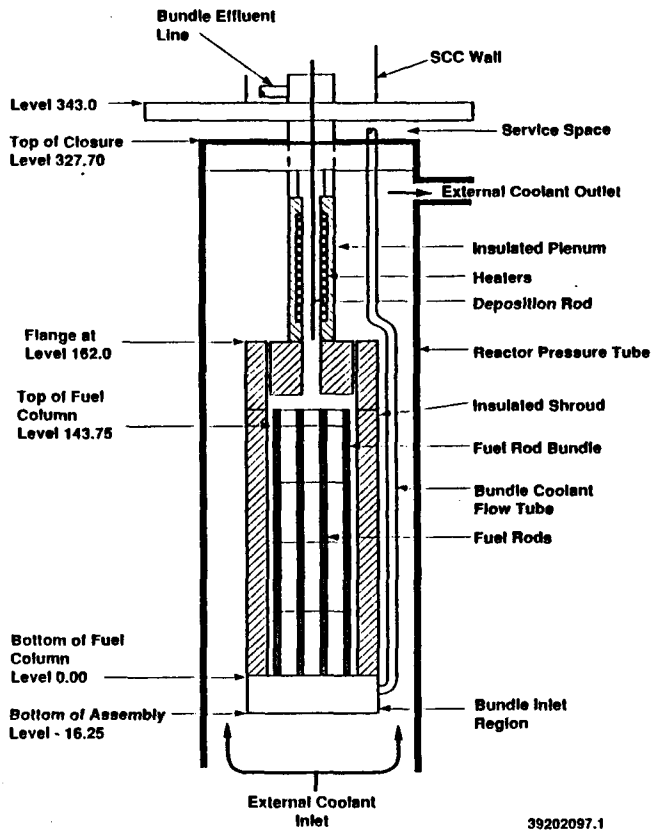

Figure 2.3 Detailed FLHT test train axial schematic. Levels are elevations in inches from the bottom of the fuel column.

reactor. Some radial heat losses occur and the effect of these losses will be discussed later in this report.

2.1.1.1 Fuel Rod Bundle

A cross section of the fuel bundle and shroud is shown in Figure 2.4 and a detailed shroud configuration is shown in Figure 2.5. The fuel bundle consists of a 4 x 4 square array designed as a subsection of a 17 x 17 PWR assembly. The four corner positions of the 4 x 4 array holds angled Zircaloy pieces in place of fuel rods. These angled Zircaloy pieces called "carriers" are used to route thermocouple wires down the fuel assembly to where they exit the bottom of the test train. In FLHT-1 and -2, the remaining 12 positions were occupied by 12 unirradiated fuel rods containing UO_2 pellets with 2.0% ^{235}U enrichment.

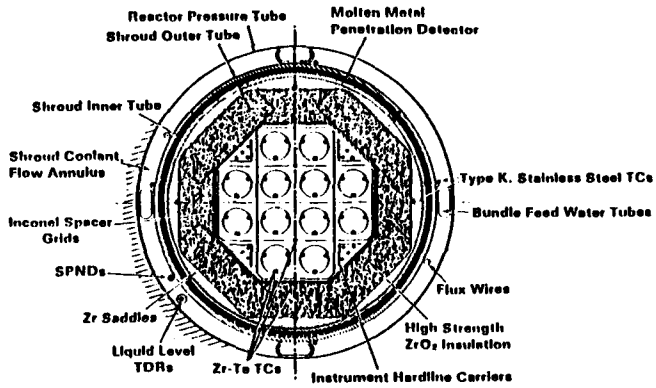

Figure 2.4 FLHT general reactor core cross section. Top to bottom rows are labeled A, B, C and D. Left to right columns are labeled 1, 2, 3, and 4.

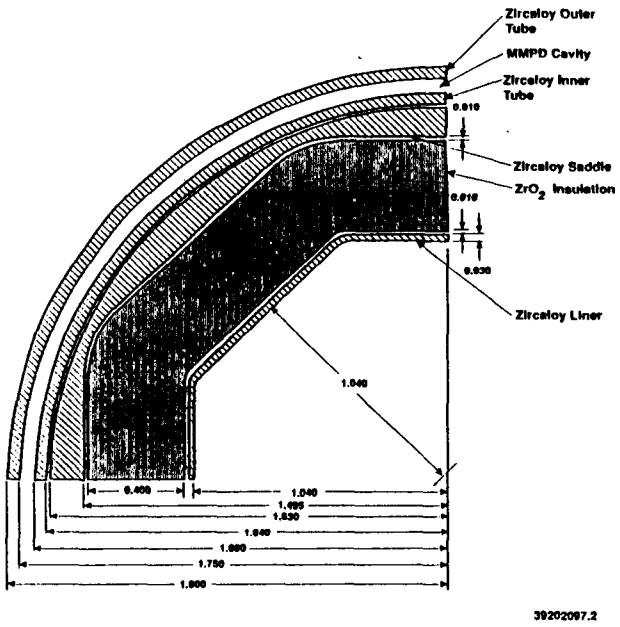

Figure 2.5 Detail of the shroud (dimensions in inches)

In FLHT-4 and -5, ten unirradiated rods (containing 1.76% enriched UO_2 pellets) and one irradiated rod of equivalent effective enrichment comprised the array, together with one gamma thermometer (a stainless steel

tube containing differential thermocouples) or an equivalent "dummy" rod.

2.1.1.2 Insulated Shroud

An insulated shroud composed of 6 layers of materials surrounds the fuel rod assembly. The innermost layer next to the fuel rods is a Zircaloy liner, 0.5 mm thick. The liner surface facing the fuel rods takes an active part during the boilaway transient by reacting with steam similarly to the nearby fuel rod cladding. On the exterior of the shroud liner, 1-cm-thick interlocking insulation tiles of low-density zirconium dioxide forms an octagonal cross section. On the exterior of these insulating tiles, Zircaloy "saddle" pieces provide the transition from the octagonal inner shape to the circular outer cross section of the shroud. On the exterior of the saddles, two concentric full-length Zircaloy tubes provide an instrumented, pressurized annulus to detect the possible melt-through of molten materials, molten metal penetration detector (MMPD) from the fuel rod assembly. The reactor pressure tube surrounds the outer round, and the external coolant flow annulus separates the two.

2.1.1.3 Test Train Instrumentation

The fuel bundle and shroud instrumentation for the tests includes the following:

- thermocouples to monitor cladding heatup and liquid level position attached 1) to the inner surface of the fuel rod cladding, 2) near grid spacers, 3) in the hardline carriers, and 4) inside the shroud liner (10- to 20-cm spans between thermocouples groups)

- thermocouple pairs located on the exterior of the saddles at 20-cm axial intervals, from 1.4 m to 3.4 m above the bottom of the fuel stack. These thermocouples monitored the radial heat flow and provided shutdown control.pressure transducers (PTs) connected via capillary tubing to the unirradiated fuel rods, the melt-detection, and insulation cavities (plenum and shroud regions)

- liquid level detectors [time-domain reflectometers (TDRs)] located on the test assembly external surfaces that measured the assembly collapsed liquid level via connections through the top and the bottom of the test train.

In FLHT-1 and -2, plenum instrumentation included thermocouples on the plenum inner wall (liner) and outer wall (outer round). In FLHT-4 and -5, additional instrumentation in the plenum region included 1) the control thermocouples for the electrical heaters, 2) thermocouples spaced along a 5-m-long 1-cm-dia stainless steel rod suspended in the plenum, and 3) thermocouples on the plenum exterior at 45-cm intervals. The stainless steel rod was called the "deposition rod" because its purpose was to collect deposits of fission products released from the fuel bundle.

2.1.2 Steam Closure Cave and Effluent Control Module

The steam closure cave (SCC) is a lead structure that provides radiation shielding for the bundle effluent line between the locations where it penetrates the test train assembly closure to where it enters the effluent control module. This part of the effluent line is about 2 m long and is otherwise in an accessible area above the reactor.

The effluent control module (ECM) is a lead structure like the SCC and contains the valves, instruments and electronic logic to control the bundle effluent pressure and therefore the pressure within the bundle coolant region. It also samples the effluent, condenses all effluent steam, measures hydrogen, and gamma spectra of released fission products.

The SCC and ECM used in the FLHT tests are designed to provide shielding and secondary confinement for the part of the effluent line that is exterior to the reactor. These two major components are interconnected as shown in Figure 2.6. As shown in the figure, the effluent line exits through the closure section then enters first the SCC and then the ECM compartments before terminating at a bundle effluent storage tank. The ECM contains a condenser and separator for separating noncondensable gas from the effluent stream. Also included in the ECM is a multistage filter that traps fission product iodine that bypasses the condenser.

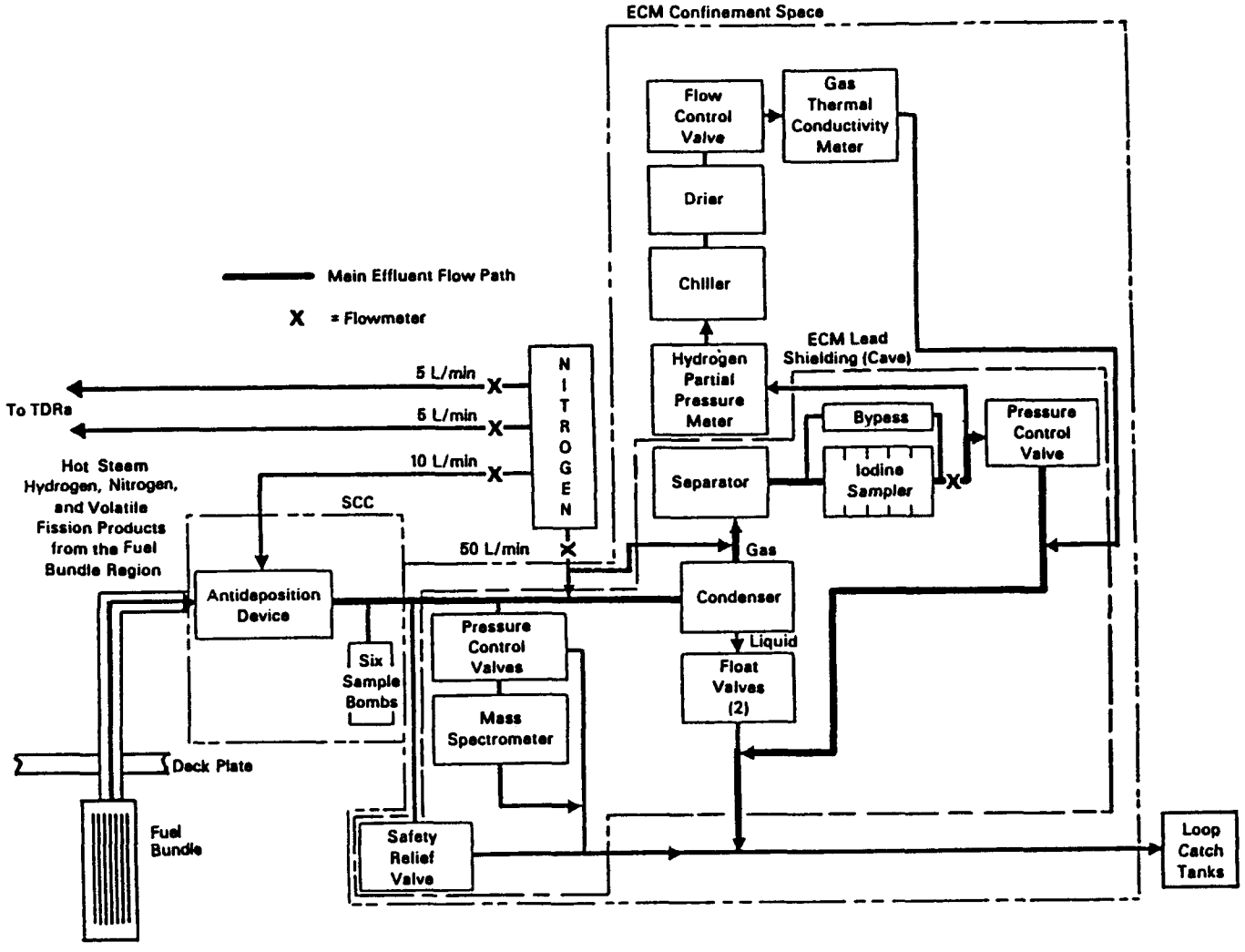

Figure 2.6 Flow paths in the steam closure cave and effluent control module (specific to FLHT-5 but representative of all FLHT tests)

Two sample lines branch from the main effluent line inside the ECM confinement. During the tests, the one upstream from the condenser conducts a sample through a mass spectrometer (MS) to measure hydrogen/steam ratios and fission gas fractions.[1] The line downstream from the condenser conducts a gaseous stream sample through a heater to a palladium hydrogen-partial-pressure meter (PHM),[2] then through a chiller to a gas thermal conductivity meter (TCM).[3]

Both instruments measure the hydrogen fraction in the sample mixture. The most accurate hydrogen measurement is obtained by the ECM noncondensable line turbine flowmeter, as described below.

Also during the tests, pressurized nitrogen is injected upstream from the condenser in the ECM through an electrically operated throttle valve. The system pressure of the ECM and inside the test train is controlled at 1.38 MPa (185 psig) by a pressure control valve downstream from the condenser. A nitrogen flow of 45-60 slpm (RT)[1] sweeps the effluent through the

[1]Not employed in FLHT-1.
[2]FLHT-4 and -5 only.
[3]Used in all FLHT tests.

condenser and the sample line to the waste line. A much larger flow of nitrogen [4100 slpm (RT)] is injected into the <0.1 MPa waste line to keep the hydrogen fraction safely below the 4 vol% flammability limit. Nitrogen is also injected into the two TDR liquid level sensor lines and into an antideposition device (ADD) in the effluent line at the SCC [total of 20 slpm (RT)]. This known and constant nitrogen flow also permits the deduction of the hydrogen evolution from the noncondensable gas turbine flowmeter (NTF) in the gaseous effluent line downstream from the condenser. By subtracting the total nitrogen injection from the total measured noncondensable flow, the most accurate hydrogen release rate is obtained.

The ECM provides the required penetrations and controls for "services," i.e., chiller water, condenser water, heater tape/control thermocouples for the main effluent line and sample lines, and electrical connections for the pumps and valves as well as beam ports (shielding penetrations) for gamma spectrometers to measure fission product transport and deposition at the following locations:[2]

- effluent inlet to the ECM
- gas and liquid lines waste exiting the ECM
- three stages of the multi-stage iodine filter
- condenser region.

2.1.3 Data Acquisition and Control System

The overall system of computer, peripherals and software is designated the data acquisition and control system (DACS). It is located in a room about 30 m from the reactor top face, along with a similar CRNL system called the loop control system (LCS). The DACS provides remote adjustment of the ECM nitrogen injection flow throttle valve. In addition, the DACS supplies a remote setpoint control function to the ECM pressure controller that controls a valve in response to the pressure transducer readout, to maintain test-train/ECM system pressure. The DACS also provides set points to the CRNL flow controller on bundle inlet flow during the boilaway transient. During the transient, the DACS automatically opens and closes the valves to six effluent sample bombs in the SCC according to a preset program.

The output from the 250 test-train and ECM instruments is scanned and recorded up to five times per second during the transient phase of the experiment. This data are fed through an analog/digital converter to a super minicomputer. The computer is programmed and configured by PNL to 1) convert the raw signals to calibrated values in engineering units, 2) display the real-time data and ongoing history, and 3) store the data on disks and rapidly transfer the data to magnetic tapes. Later the data tapes are further reduced to once-per-second files at PNL for plotting and analysis.

The DACS also has automated shutdown control ("trip control") on the reactor via comparator functions against various "trip points." The trip points include high saddle temperature, high effluent temperature, and low system pressure.

2.2 Test Operations

The FLHT test operations include up to five phases:

1. pretest installations and checkout - reactor at zero power
2. commissioning and calibration - reactor at zero power
3. preconditioning operation (FLHT-4 and -5 only) - reactor at full power
4. coolant boilaway/severe damage transient - reactor at 5% of full power
5. post-test examinations.

[1]Standard liter per minute, room temperatures. Volume occupied by a given mass of gas at a specified temperature and pressure, referred to as standard conditions (STP). Although standard pressure is always defined as 760 Torr or mm of Hg (14.7 psia), several temperatures have been defined as standard. Here standard temperature is defined as 21°C (70°F), i.e., room temperature.

[2]An additional measure of fission product release was provided by CRNL: the Ci-MeV product of the noble fission gases (Xe + Kr) exhausting through the NRU reactor stack was measured with an existing calibrated Geiger counter system.

These five phases are described briefly below. The test-to-test operations differ primarily in the length of preconditioning, in the assembly nuclear power, and in the hold period at high temperature.[1] These differences are summarized in Table 2.2.

2.2.1 Pretest Installations and Checkout

The test trains are designed and built at PNL and then shipped to CRNL where an irradiated rod (if used) is installed in an open position of the fuel bundle. The assembly of the test train is completed by bolting the plenum to the shroud sections. The assembled test train is pressurized to insure no leaks are present. The instruments are then given a final check and then heavily shielded assembly is loaded into the reactor and closure seal is made, leak tested and pressure checked. Following the installation of the test train into the reactor the SCC/ECM modules are installed and all piping connections are made, leak checked and pressure checked.

2.2.2 Commissioning and Calibration

The commissioning phase of the tests is conducted with the reactor shutdown. The purpose of this phase is to test and verify key components, measurements, controls, and procedures. At the DACS, the various timers and trip functions are verified using simulated test data. At the top of the reactor, final pressure leak tests are performed on the test train and ECM piping and components.

Superheated steam is then injected from an external source into the test train plenum region to verify the ability of the plenum and ECM electrical heaters to keep the plenum above saturation temperature (excluding FLHT-1) and to maintain a desired temperature profile along the plenum length. Other important commissioning activities include the following:

- operation of the ECM condenser and pressurizer systems with steam flow
- operation of the hydrogen monitors (i.e., the MS, PHM, and TCM) at expected steam/nitrogen flows and temperatures
- operation of the liquid level sensors and the gamma thermometer during controlled draining of the plenum and the fuel bundle.

Unique to FLHT-5 was an in situ test of the hydrogen monitors whereby known hydrogen/nitrogen mixtures were injected at the entrance to the ECM. This calibration test provided data on instrument response times and on transit times to the various instruments.

2.2.3 Preconditioning Operation

In the preconditioning phase of each test, about a day before the beginning of the boilaway transient, the reactor is operated at full power for a predetermined period for two purposes: The first is to "precondition" the fuel pellets, i.e., to subject them to prototypic

[1]Defined as the time following onset of Zircaloy melt temperature (assumed 2100 K).

Table 2.2 FLHT test parameters

Test parameters	FLHT-1	FLHT-2	FLHT-4	FLHT-5
Preconditioning period, h	0.0	0.0	1.0	5.0
Bundle nuclear power from calorimetry, kW	23	23	23	30
Makeup flow rate during boilaway and heatup, g/s	Variable	1.4	1.26	1.21
Duration of operation following onset of Zircaloy melt temperature, min	< 1	4.5	30	60

thermally-induced cracking. The cracking promotes typical fuel-cladding gap closure and opens pathways for fission product release and enhances the prototypicality of the pellet mechanical behavior during the severe damage portion of the experiment. The second purpose is to build an inventory of medium-lived radioactive isotopes that could be used in post-test gamma-scanning to assess the extent of the volatile fission product release and deposition.

The preconditioning assembly power actually achieved at full reactor power ranged from 670 kW for FLHT-4 to 700 kW for FLHT-5, corresponding to a rod axial peak linear heat generation rate (LHGR) of 26 to 27 kW/m; these levels were considered sufficient based on tests with LWR-type fuel rods that determined a cracking threshold for a single through-diameter crack at < 20 kW/m and for the typical 4-8 crack pattern at 20 to 25 kW/m (Lanning 1982).

2.2.4 Coolant Boilaway/Severe Damage Transient

The planned operation of the boilaway includes bringing the reactor to low power (~5% of full power) with 1-kg/s bypass flow and 0.13-kg/s bundle coolant flow. After calorimetry and stabilization at 23-kW or 30-kW bundle nuclear power, the plenum section is drained and heated,[1] and the assembly inlet flow is reduced to 9.4 g/s (75 lb/h) to arrive at a steady-state dryout front position ~0.7 m below the top of the fuel column. The bundle calorimetry and plenum drain/heatup operations are pretransient operations that are conducted before the boilaway transient.

The coolant boilaway is started by making a rapid reduction in the bundle inlet flow to ~1.3 g/s (10 lb/h).[2] Less than 10 min after flow reduction, temperatures in the bundle increase rapidly as the exothermic oxidation reaction accelerates. The hold time from the first attainment of cladding melt temperatures (2100 K) to the termination of the experiment varies from test to test, as presented previously in Table 2.2.

2.2.5 Post-Test Examinations

Post-test examinations include 1) axial gamma-scans of the deposition rods, copper flux wires, and test train assembly; 2) a visual examination that includes removal of a portion of the shroud to create a "window" to reveal the fuel bundle region, and 3) detailed metallography and gamma tomography of various cross-section and axial segments of the fuel bundle.

In FLHT-4 and -5, the first major planned post-test activity was to remove and scan the 4-m-long deposition rod that was suspended in the plenum above the fuel bundle region. After scanning the deposition rod, the piping and electrical connections between the SCC, ECM, DACS, and the test train were disconnected or severed. Then the SCC and ECM were removed from the top of the reactor and the test train was removed from the reactor. For all tests, the test train is gamma-scanned after it is removed from the reactor and before it is stored in a spent fuel storage pool several months awaiting a post test visual examination.

[1]The plenum region was heated by superheated steam injected into the plenum region in FLHT-2; electrical heaters were used in FLHT-4 and -5. The plenum region was not heated in FLHT-1.

[2]The FLHT-1 experiment operation differed from the sequence described above. The test plan called for a 16-step reduction in bundle inlet flow until a peak cladding temperature of 2150 K was attained; this was to be followed by test termination. However, no means existed for heating the components above the bundle region (i.e., plenum, closure, and vertical outlet piping) and the limited superheat of the steam generated in the bundle region was insufficient to keep those surfaces above the saturation temperature. Consequently, condensate formed and fell back into the bundle region, making the bundle liquid level difficult to control. Operator adjustments to obtain higher steam superheat to heat the plenum caused the liquid level to fall below the Level-80 (2.0-m) elevation for a sustained period. Autocatalytic oxidation of the cladding eventually occurred resulting in temperatures reaching 2300 K. The test was terminated coincident with the oxidation excursion.

The visual examination of the fuel rods includes cutting a 90° window, ~3 m long along one side of the shroud to expose in sequence the outer round, inner round, saddles, insulation, liner, and an outer pair of fuel rods. Each window generally includes the severe damage and steam-cooled regions. An extensive photographic record is made of the fuel bundle and shroud as viewed through the window. This record aids the post-test interpretation of the on-line instrumentation record.

On concluding this examination, the exposed area is sealed in epoxy resin and sectioned for later hot cell examination. On-going activities include metallography and gamma tomography of fuel bundle and shroud transverse cross sections and gamma tomography of test train segments cut from the fuel bundle region. The objective of these activities is 1) to determine the degree of oxidation and fuel dissolution that occurred, 2) to determine the extent of change in the bundle region flow area and 3) to estimate the peak temperatures achieved after the thermocouples have failed.

3 Thermal, Hydraulic. and Mechanical Behavior of the FLHT Tests

In this section, the key thermal, hydraulic, and mechanical results of the FLHT tests are presented. The results that are presented here are intended to provide a comprehensive picture of the thermal, hydraulic, and mechanical behavior of the FLHT tests that will be used in Section 4.0 to analyze and assess severe damage phenomena associated with the FLHT tests.

First in this section, an overview of the FLHT test thermal response and damage progression is provided. This overview is followed by an analysis of the heatup rates and axial and radial temperature gradients recorded during the heatup of the bundle and the shroud. Next, results of the hydraulic response of the fuel bundle region to the changing coolant makeup rate are summarized and analyzed; included is a discussion of the changing bundle flow resistance with time. Finally, results on the mechanical response of the bundle and shroud are summarized and analyzed; included are the data on fuel rod cladding failure at different internal pressures.

3.1 Overview of Thermal Response and Damage Progression

The initiating event for the FLHT-2, -4 and -5 tests was a step change in the bundle coolant flow rate while at constant power. Immediately following the flow reduction to 1.3 g/s, the coolant began to boil away as a result of the power/cooling mismatch. As the coolant level dropped and the cladding surfaces dried out, the cladding immediately began to heat up: at first almost adiabatically; then at a decreasing rate due to increased heat transfer; and, finally, at an increasing rate as oxidation heat generation began to increase. The heatup phase of the tests culminated at 1600 to 1700 K in a rapid temperature escalation, >10 K/s, signaling the onset of an autocatalytic oxidation reaction. The peak cladding temperatures attained during the escalation were not accurately determined because the cladding thermocouples failed at ~2400 K. The peak cladding temperatures were, however, estimated to have been in the 2500 K range for FLHT-2 and ≥2600 K for FLHT-4 and -5, based on behavior of the thermocouples on the liner and preliminary data from visual and metallurgical examinations.

A localized, rapidly downward-moving oxidation "burn front" developed at a non-dimensional elevation of approximately 0.7 (Level 100) as a result of the initial oxidation excursion; it progressed down past the midplane of the fuel assembly toward the steam-cooled region just above the coolant pool. Within the downward moving burnfront, cladding temperatures exceeded the oxygen-saturated Zircaloy [Zr(O)] melt temperature, resulting in local cladding material relocation and fuel dissolution. The axial extent of the burn front was relatively confined, generally within the 0.2 m distance between cladding thermocouples. The downward progression of the burn front occurred as a result of the developing axial temperature profiles and the decreasing coolant level, both of which together allowed progressively lower axial levels to reach oxidation excursion temperatures to consume the steam thereby denying Zircaloy at higher elevations from reacting.

During the tests, as the burn front reached the steam-cooled region above the coolant pool (e.g., Level 30 to Level 52 in FLHT-5),[1] temperatures were too low (below ~1700 K) to initiate autocatalytic oxidation. Without the rapid oxidation that accompanies autocatalytic oxidation, steam was available for consumption in the upper elevations; this steam then fueled an upward-moving burn front. This front slowly moved up through the damaged bundle midsection and then along the relatively unoxidized upper section (above Level 100) toward the top of the bundle. The upward progression continued until the test was terminated. Thus both a downward and upward progression of the oxidation excursion zone was noted in full-length tests FLHT-4 and -5. Note that the FLHT-1 and -2 tests were terminated before the start of the upward burn.

The upward burn front progressed to the top of the fuel rods in FLHT-5, resulting in essentially complete

[1]Level is defined as the elevation, in inches, above or below the bottom of the fuel stack.

consumption of the exposed Zircaloy and then a significant reduction in the rate of hydrogen generation. The FLHT-5 test then continued operation for ~1000 s past the major reduction in bundle oxidation during which damage continued, primarily from the nuclear heating component. Thus, the FLHT-5 test represented two distinct accident regimes--one in which chemical power was the major contributor to damage progression and a second less vigorous regime in which damage was induced by a nuclear-dominated heating component.

3.2 Thermal Response

An understanding of the thermal response of the bundle and shroud used in these tests is important in developing conclusions regarding, for example, oxidation and melt relocation behavior and the effect of radial heat losses. To develop this understanding, the following is an analysis of the results obtained during the heatup of fuel rod bundle (cladding) and shroud (liner and saddle). Analyzed are the radial and axial temperature gradients in the fuel bundle region--from cladding dryout to the onset of the autocatalytic oxidation.

3.2.1 Component Heatup

Discussed below is the co-planar heatup of the cladding, liner and saddles, followed by a discussion of the relative heatup rates.

3.2.1.1 Cladding, Liner and Saddle Thermal Response

The temperature history of the cladding, liner, and saddle at Level 88 is shown in Figure 3.1. The heatup of the various components at this elevation typifies that of the FLHT tests. Some variation to this typical response occurs with local failure of the fuel rod and shroud cavities, molten material relocation, and eutectic reactions. During the tests, the cladding heated up rapidly at the onset of dryout; then less rapidly as radiation heat transfer to the liner, carriers, and other fuel rods increased; then more rapidly again as the autocatalytic oxidation reaction started. The liner underwent a similar temperature history but, because it was indirectly heated, dryout occurred later and the heatup was less rapid. When rapid oxidation of the fuel rod cladding occurred, however, the added heat from the oxidation reaction

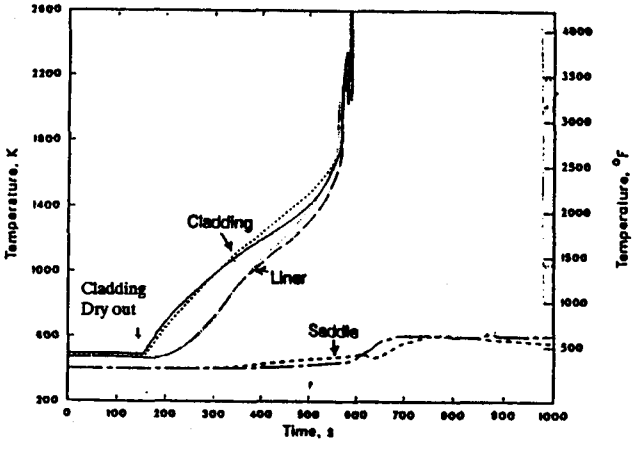

Figure 3.1 FLHT-5 cladding, liner, and saddle temperature histories-level 88

caused the liner temperature to escalate. The additional heat generated by the liner was effective in reducing the radial heat losses from the rods during the period of liner oxidation (see Section 3.2.2).

The saddle thermocouples located on the outside of the zirconium dioxide insulation responded slower than the cladding temperature by 150 to 200 s and attained much lower peak temperatures because of the low thermal conductivity insulation that separated the saddles from the high-temperature bundle region (see Figure 3.1). The saddle thermocouples survived the test and therefore provided data on both the downward passage of the burn front at ~1050 s and the upward passage at ~2500 s. The ability of these thermocouples to survive and therefore record the upward burn front progression after the failure of the thermocouples on the cladding and on the liner is crucial to determining the full scope of damage progression in the FLHT tests.

3.2.1.2 Heatup Rate

A typical post-dryout cladding heatup rate (dT/dt averaged over 10-s intervals) is plotted for FLHT-4 and -5 at Level 96 in Figure 3.2. As designed, the heatup rate was slightly higher for the FLHT-5 test (~0.5 K/s) due to the higher fission heat rate. Initially, on dryout, a step change increase in the cladding heatup rate occurred, reaching 5 K/s (i.e., adiabatic). The heatup rate then steadily decreased as a result of increasing

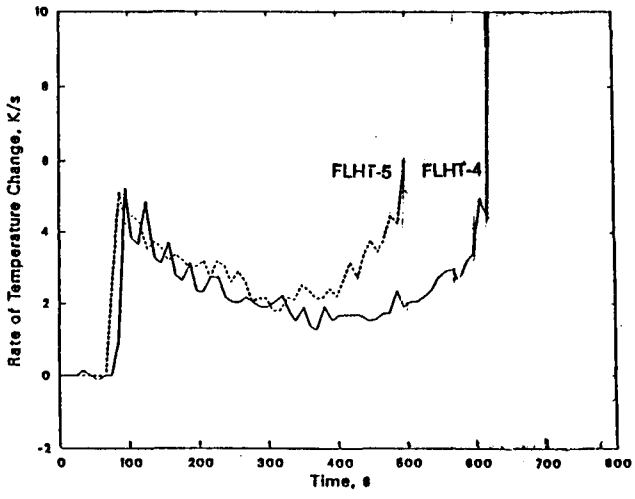

Figure 3.2 Cladding heatup rates after dryout for FLHT-4 and -5 Level 96

convective and radiation heat transfer before beginning a steady increase from the metal-water reaction energy release.

The decrease in the heatup rate immediately following dryout of the cladding was caused by the developing convective heat transfer component. The temperature difference between components was small, and absolute temperatures were low enough that radiation heat transfer was relatively small; yet the temperature difference between the cladding and steam was quite large. This phenomena is best illustrated in a plot of the FLHT-2 cladding and steam temperatures at Level 84 and Level 84.5, respectively,[1] shown in Figure 3.3. As shown, heatup of the steam above the saturation temperature took an additional 45 s after dryout, during which time the cladding-to-steam temperature difference increased to as much as 200 K; in contrast, the temperature differences among fuel rods was on the order of 10 K.

Approximately 200 s after dryout, the cladding-to-steam temperature difference stabilized as did the convective heat transfer component. During this time, fuel rod temperatures reached high enough levels where radiation heat transfer became significant. This conclusion is

[1]The thermocouples that measure the steam temperature are positioned in the flow stream, just below (< 4 cm) the grid spacer.

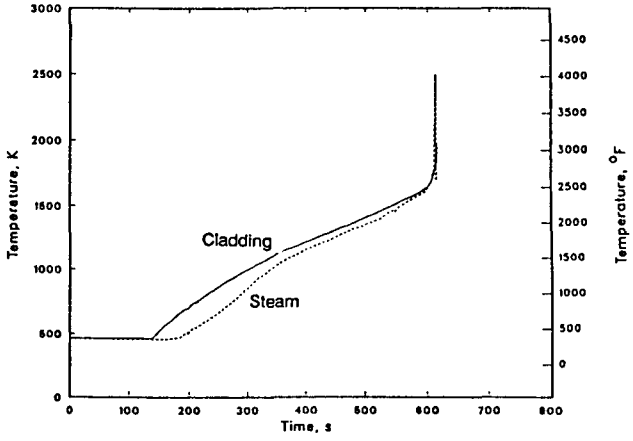

Figure 3.3 Comparison of FLHT-2 steam and cladding temperatures

supported by the liner heatup rate (dT/dt) exceeding that of the cladding as shown in Figure 3.4.

During the FLHT-5 boilaway transient, shortly after the increase in radiation heat transfer to the liner (and elevated liner temperature), radial heat transfer to the external coolant began to increase
This is evident from the sharp increase in the saddle temperatures at Level 96 (Figure 3.5) at 800 s. It is important to note that during the initial 400 s when the bundle region and liner were at high temperatures the

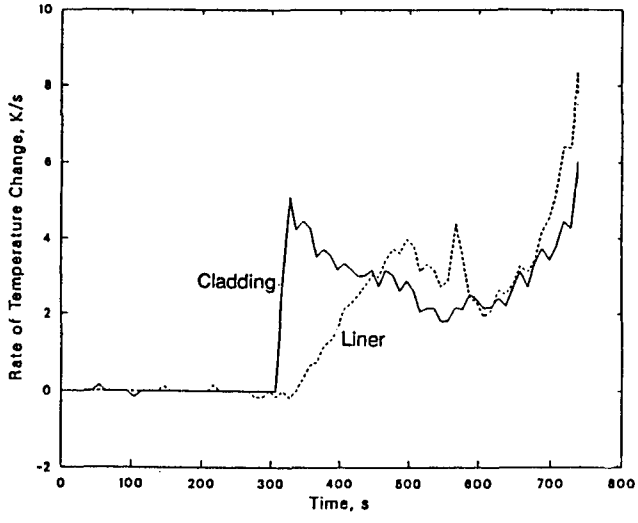

Figure 3.4 Cladding and liner heatup rate for FLHT-5 Level 96

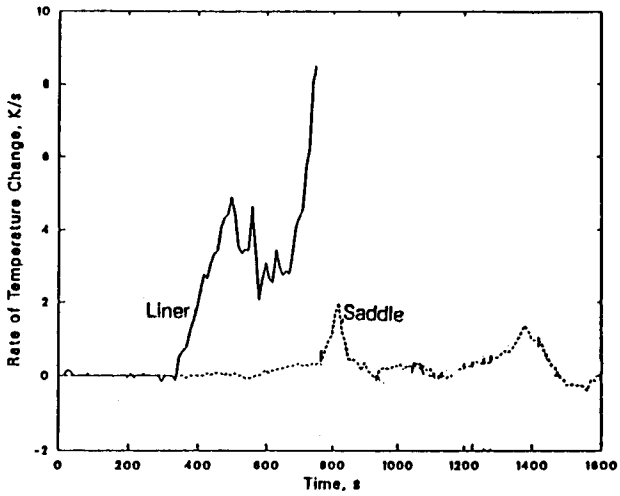

Figure 3.5 Liner and saddle heatup rate for FLHT-5 Level 96

local heat losses were negligible and the bundle and liner heatup were essentially adiabatic. This adiabatic behavior of the bundle and liner at this time in the transient is confirmed in the discussion of bundle heat losses in Section 4.4.

As observed from the cladding axial temperature profiles (Section 3.2.2.1), the oxidation power begins to affect the temperature rise rate when cladding temperatures exceed 1400 K, about 150 s before autocatalytic conditions are achieved. The initial impact of the oxidation power was to offset the decrease in the cladding heatup rate. As the chemical power contribution increased further, however, the heatup rate was essentially doubled to 5 K/s. Shortly after this time, at temperatures near 1700 K autocatalytic oxidation behavior was recorded, with cladding thermocouple rise rates greater than 10 K/s. Thermocouples began to fail near 2400 K.

3.2.2 Temperature Gradients

Presented in the next two sections are illustrations of the axial and radial temperature gradients recorded following dryout of the fuel rods. First, cladding axial temperature gradients that developed following the decrease in coolant level are presented to illustrate the transition between the nuclear and oxidation-driven temperature increase. Next, the radial temperature gradients between fuel rods, the fuel rods and liner, and between the liner and saddle are presented to give insights into the transient nature of the radial heat losses.

3.2.2.1 Axial Temperature Gradients

The FLHT tests have provided the only experimental data on full-length cladding axial temperature gradients under coolant boilaway conditions. Cladding axial temperature gradients recorded during the FLHT-5 test from the initiating flow reduction to escalation are shown in Figure 3.6. In this figure, the cladding temperatures are plotted versus axial position at 50-s intervals, beginning with flow reduction (0 s) and ending with the initial autocatalytic reaction (500 s).

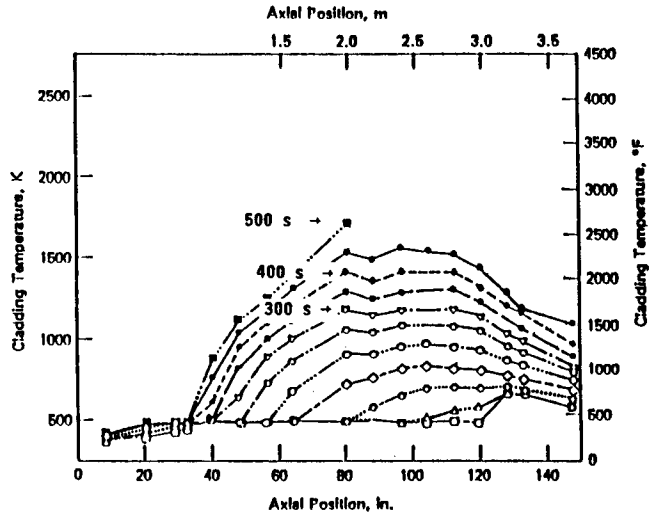

Figure 3.6 FLHT-5 cladding axial temperature profiles prior to the initial oxidation excursion (at 50 s intervals beginning with the flow reduction)

A general steepening of the axial temperature gradient above the coolant pool occurs as the level of coolant decreases and approaches its steady-state position. The larger gradient is a result of the decreasing steam flow and the increasing length of the fuel rods uncovered. During the time interval from 450 and 500 s, the axial gradient between Level 60 and Level 80 increased

directly as a result of the oxidation energy release; this occurred between 1400 to 1500 K, and is consistent among all the FLHT tests.

The dynamically changing axial temperature gradients illustrated in Figure 3.6 are important in interpreting the observed material relocation behavior and in the length of fuel uncovered that can lead to the onset of rapid oxidation. A more detailed discussion of the impact of full-length temperature gradients on severe fuel damage progression is presented in Section 4.

3.2.2.2 Radial Temperature Gradients

The rod-to-rod and rod-to-liner temperature gradients are evaluated from the FLHT-2 test data because of the number of thermocouples per plane (3 versus 2 in FLHT-4 and -5). Deviations in the temperatures of the fuel rods (from the average reading of 2 or 3 rods on a plane) are presented for Level 100, 92, 72, and 60 in Figures 3.7 through 3.10, respectively. In these figures, the temperature deviation of two of the exterior "guard" rods and one of the inner four "test" rods are displayed. The trends indicated in these figures show only a slight temperature difference (~10 K) following the uncovery of the fuel rods, with the deviations increasing with time and the onset of the oxidation excursion. Generally, the temperatures of interior test rods exceed the temperatures of the guard rods. An exception is at Level 60, see Figure 3.10, where the thermocouple in the exterior Rod 1B is located on the bundle interior side of the rod and shows temperatures similar to the interior Rod 2C.

Of the four axial levels displayed, the initial peak temperature location (Level 100) shows the largest deviation over the course of the transient. This larger deviation is a result of significantly higher temperatures recorded by the inner test thermocouples on Rod 2B. At the other elevations (e.g., Levels 92, 72, and 60), the temperature deviations are much less, generally within ±25 K, up until rapid oxidation takes place, where upon the deviation increases due to the positive feedback effect of the metal-water reaction. Before this time the temperature gradient across the fuel rod bundle is relatively small and, as discussed below, the major heat loss from the fuel rods is radiation heat transfer to the liner. Thus, it is not until the onset of rapid oxidation that the fuel bundle begins to show local effects or the characteristics of a more heterogeneous heatup. The increasing

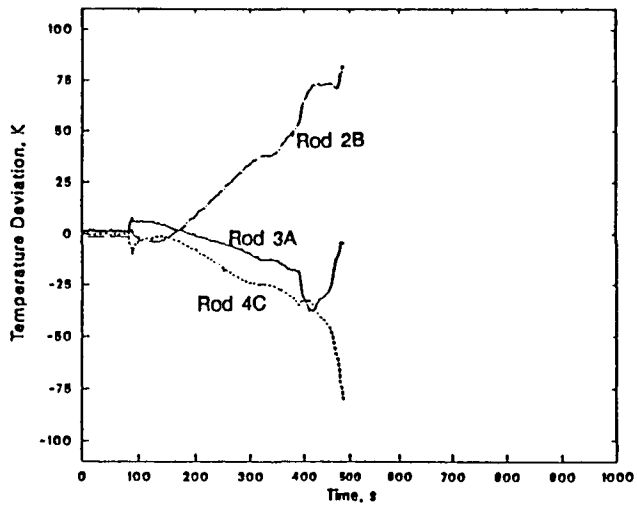

Figure 3.7 FLHT-2 cladding temperature deviation from average--Level 100 locations. (Refer to Figure 2.4)

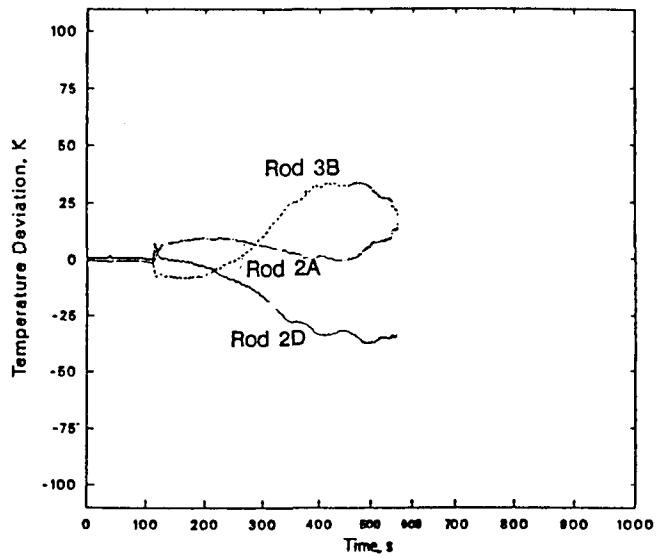

Figure 3.8 FLHT-2 cladding temperature deviation from average of the three rods-- Level 92. (Refer to Figure 2.4.)

heterogeneity of the heatup that accompanies the onset of rapid oxidation is one factor that influences the subsequent material relocation behavior (Section 4.4).

An examination of the rod-to-liner (average rod to average liner) temperature gradient at Level 96 is

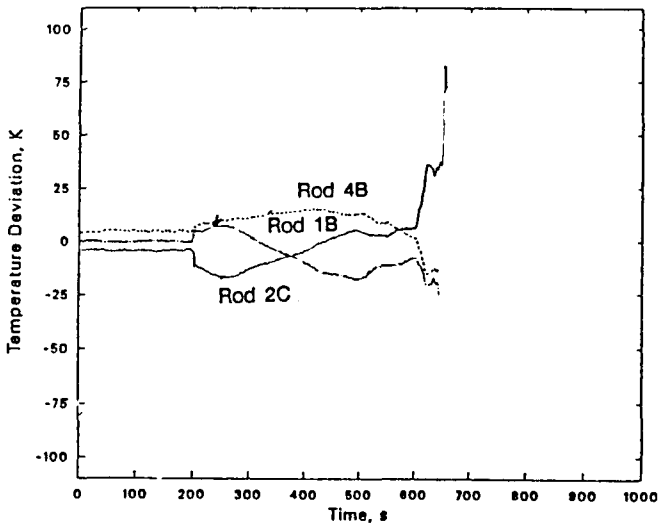

Figure 3.9 FLHT-2 cladding temperature deviation from average--Level 72. (Refer to Figure 2.4.)

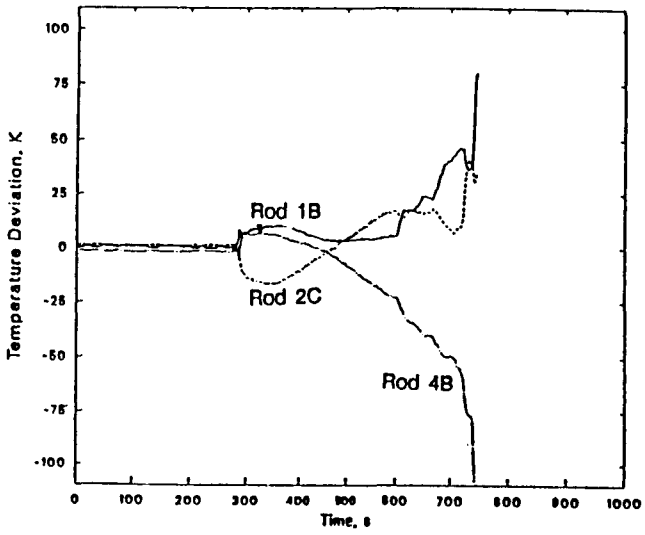

Figure 3.10 FLHT-2 cladding temperature deviation from average--Level 60. (Refer to Figure 2.4.)

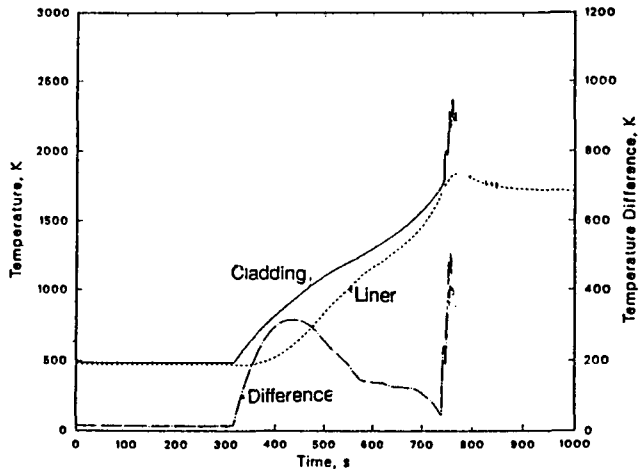

Figure 3.11 FLHT-5 average cladding to average liner temperatures and temperature difference--Level 96

presented for the FLHT-5 test in Figure 3.11.[1] Shown in this figure is the rod-to-liner temperature difference as well as the rod and liner average temperatures. Because the liner was heated indirectly, liner heatup was delayed by as much as 50 s, resulting in a large radial temperature gradient that developed immediately following uncovery of the rods (similar to the cladding-steam gradient). This radial gradient increased steadily following cladding dryout, exceeding 300 K before decreasing, as a result of increasing radiation heat transfer. Radiation heat transfer from the rods continued to reduce the rod-to-liner temperature gradient until oxidation of cladding and liner begins. Because rapid oxidation of the liner generally occurred at lower temperatures and slightly earlier than the oxidation of the cladding (Figures 3.1 and 3.4), the gradient at the time of cladding oxidation excursion was greatly reduced. In this particular example, the peak rod-to-liner gradient was reduced from 300 K to less than 50 K as a result of liner oxidation.

The effect of the liner oxidation reducing the rod-to-liner temperature gradient was noted in all FLHT tests.

[1]Component average temperatures are the arithmetic mean of two or more thermocouples on a plane. For example, thermocouples from Rods 2A and 3D make up the cladding-average value and liner thermocouples from the 90 and 270 degree orientation make up the average liner value at Level 96.

The reduction of the radial temperature gradient that occurs with autocatalytic liner oxidation is, therefore, important in promoting and maintaining material relocation conditions during the period of liner oxidation, particularly in the FLHT tests where the fission power component is not increased to overcome radial heat losses.

3.3 Hydraulic Response

The decrease in the coolant level caused by the reduction in coolant flow rate is the principal hydraulic response of the FLHT tests. A secondary effect of the coolant level decrease is the change in flow resistance that occurs as a result of melt relocation and Zircaloy oxidation. In this section, the coolant level and bundle flow resistance responses are presented and discussed. Insights into the effect of different bundle power levels and different coolant flow histories on the coolant level history are included in the discussion of coolant level behavior. Correlation of the coolant level with the onset and progression of damage is presented in Section 4.1.

3.3.1 Coolant Level Behavior

The initiating event for the FLHT-2, -4 and -5 tests was a step-change reduction in the bundle inlet flow rate while constant nuclear power was maintained. The reduced inlet flow rate was typically about 10 percent of the pretransient flow rate. The coolant level decrease that followed was characterized by an exponential decay as illustrated in Figure 3.12. A summary of the coolant level behavior is presented in Table 3.1.

The differences in the boildown behavior among the three experiments relate directly to the differences in the average coolant flow rate of the coolant and differences in fission power levels.[1] As indicated previously in Table 2.2, the average makeup flow rate was approximately 10% greater for FLHT-2 than for FLHT-4 and -5; however, as shown in Figure 3.12, this small difference had little effect on the boildown histories for the

[1]Other parameters that affect the liquid level include inlet coolant temperatures, system pressure, and axial power profile. An inlet coolant temperature of 360 K and system pressure of 1.38 MPa were employed for the 3 tests; a chopped cosine-shaped axial power profile was assumed to be identical.

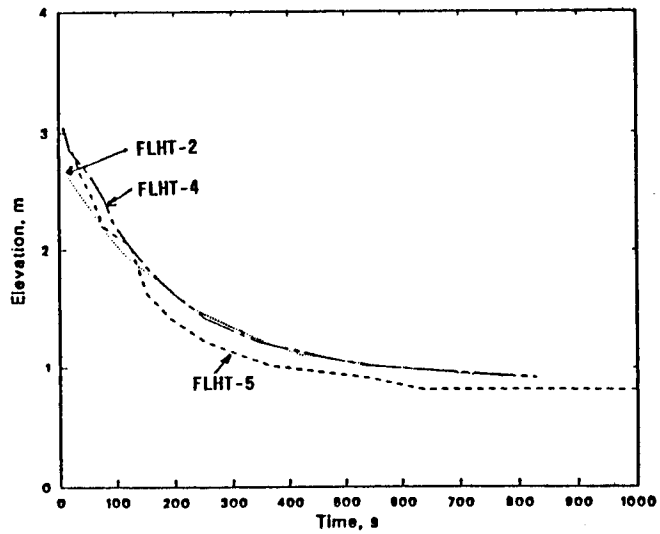

Figure 3.12 Coolant level decrease for the FLHT-2, -4, and -5 tests

Table 3.1 Comparison of coolant level behavior for FLHT tests

Parameter	FLHT-2	FLHT-4	FLHT-5
Time to reach steady-state level, s	780[1]	850	630
Final coolant level, m	0.9	0.86	0.76
Percent of fuel length uncovered, %	75	77	79
Average coolant level velocity, cm/s[2]	0.25	0.25	0.34

[1]FLHT-2 was terminated just before attaining steady state.
[2]Velocity from pretransient to final coolant level.

23 kw FLHT-2 and -4 tests. In addition, in each of the FLHT tests, the inlet flow rate fluctuated ±20% in response to fluctuations in the pressure control system.

In spite of the fluctuations that occurred, however, the coolant level decrease was generally smooth and continuous.

The higher bundle nuclear power for FLHT-5 versus FLHT-4 (30 versus 23 kW) resulted in a faster boildown rate and lower asymptotic coolant level, as shown in Table 3.1 and in Figure 3.12. The more rapid boildown, coupled with a faster heatup rate after dryout, brought the peak temperature of the FLHT-5 cladding to the oxidation excursion temperature (~1500 to 1700 K) earlier than in the lower power FLHT-2 and -4 tests. The slightly different initial "pretransient" coolant levels for each of the FLHT tests did not significantly alter the subsequent course of the transient.

An assessment of how the changing coolant level influences the damage progression sequence is presented in Section 4.

3.3.2 Bundle Flow Resistance During Damage Progression

An increase in the resistance to the flow of coolant in the bundle has been observed to occur during the longer duration FLHT tests as a result of the following phenomena: 1) fuel rod ballooning (FLHT-2) and bowing, 2) melt relocation, and 3) the volume increase from the oxidation of the Zircaloy cladding and liner following the beginning of rapid oxidation. The effects of these phenomena are evaluated in the following.

The coolant levels versus time plotted in Figure 3.12 are derived from data on the dryout of the thermocouples on the cladding. Another measurement of the coolant level was made by the two TDR tubes located in the bypass flow annulus between the FLHT shroud and the NRU reactor pressure tube. These tubes functioned like a manometer because they were connected to the bundle region above and below the top of the fuel columns. The level measured by the TDRs is that of the subcooled liquid in the measurement tube; this is essentially the bundle region collapsed coolant level.[1] A comparison of the coolant level as indicated by the TDRs and cladding thermocouples is presented in Figure 3.13. Although a sizeable difference in the indicated coolant level is noted, correcting for the density difference in the TDR measurement tube reconciled the two measurements early into the transient (<1000 s).

[1]Coolant level without the presence of steam bubbles.

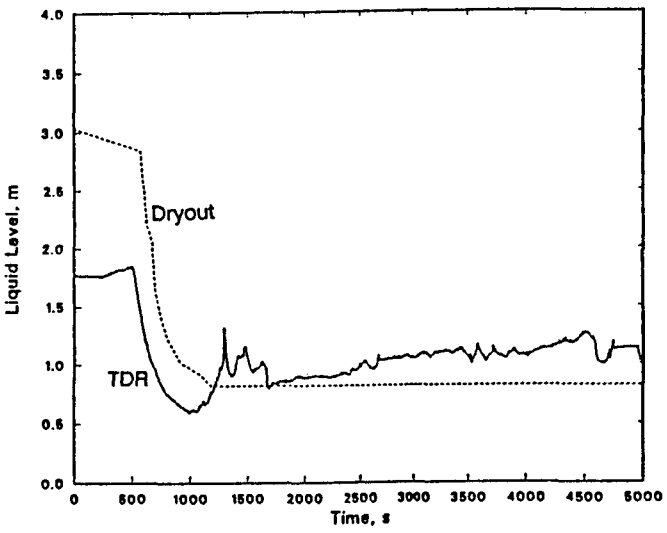

Figure 3.13 Comparison of cladding dryout and TDR coolant level data for the FLHT-5 Test

As the coolant level approached its steady state position, however, the TDR began to indicate a collapsed level above that indicated by the dryout data. This behavior can be explained by an increasing flow resistance in the bundle region--an effect that tends to force coolant from the bundle region into the TDR, thereby increasing the indicated collapsed coolant level.

The increase in the TDR response at 1000 s is consistent with the conclusion that resistance in the bundle flow increases during damage progression resulting from the three phenomena noted above. An increase in the bundle flow resistance/blockage as inferred from the TDR readings was consistently observed following the initial oxidation excursion in each of the FLHT boilaway tests; the longer the time at high-temperature, the larger the indicated flow blockage. It was calculated that a blockage of the bundle flow equal to 99% of the initial bundle flow area[2] would be required to increase the TDR level 0.2 m above the coolant level indicated by the thermocouples as in FLHT-5. The slight decrease in the TDR-indicated level following reactor shutdown at 4500 s was due to the collapse of voids in the bundle region. The subsequent increase at 4700 s was due to the initiation

[2]Calculated from the isentropic compressible flow equations assuming a driving force equal to the TDR-indicated height increase above the collapsed level, 0.2 m.

of the nitrogen bundle purge flow, used to sweep the remaining stagnant hydrogen and fission products out of the test train, for measurement and disposal.

The TDR recorded a continually increasing collapsed bundle coolant level from 1600 s to the test termination, reflecting a continually increasing degree of flow blockage. Some fluctuation is noted from 3500 to 3900 s, the approximate time when hydrogen generation (bundle oxidation) begins to significantly decrease. Interestingly, during the time of minimal hydrogen generation (4000 to 4500 s), the TDR indicates increasing flow blockage, suggesting bundle geometry changes were occurring with nuclear heating only. This is of interest because damage appears to continue without a contribution from oxidation.

The effect of different fuel rod failure mechanisms on the bundle flow resistance can be assessed in a comparison of the TDR response between FLHT-2 and FLHT-5. The rod pressure in the FLHT-2 test exceeded that of the system pressure; therefore, ballooning of the fuel rods was the failure mechanism and contributed to an early increase in the bundle flow resistance. In FLHT-5, on the other hand, the failure mechanism was the collapse of the fuel rods; with no increase in fuel rod area, the increase in bundle flow resistance was delayed until the onset of melt relocation. The delay in the bundle flow resistance increase is illustrated in the comparison of the TDR responses for FLHT-2 and -5 shown in Figure 3.14. The change in slope of the TDR level was coincident with the onset of fuel rod failure in FLHT-2 as opposed to occurring coincident with the onset of the oxidation excursion in FLHT-5. The earlier 180 s increased resistance in the bundle flow measured by the TDR in FLHT-2 is attributed to the change in geometry from the ballooning of fuel rods.

3.4 Mechanical Behavior

The mechanical response of the fuel rod cladding during the heatup to melt conditions is an important aspect of severe damage fuel behavior. The cladding failure temperature, as well as the time from dryout to failure, are important information obtained from the FLHT tests. This information is presented below, along with an assessment of the impact of shroud cavity failures.

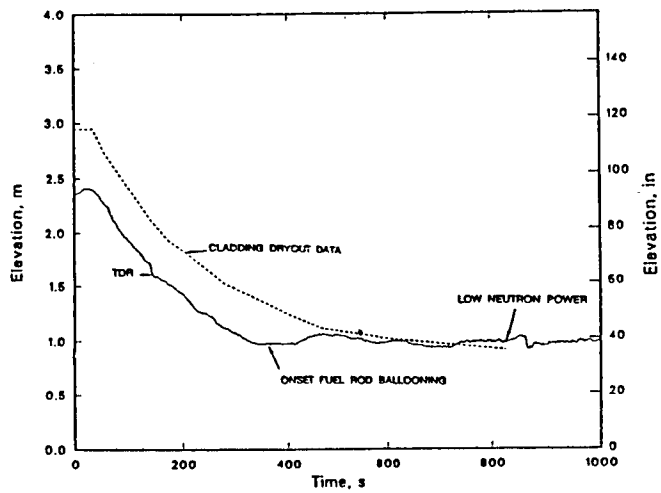

a) Fuel Rod Ballooning (FLHT-2)

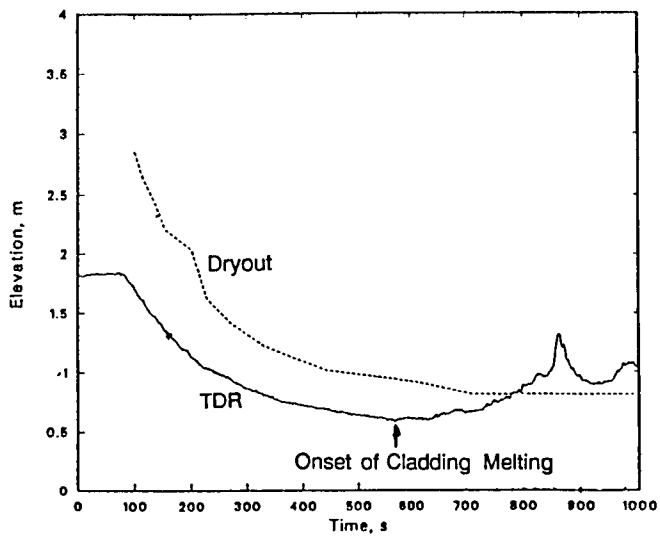

b) Fuel Rod Collapse (FLHT-5)

Figure 3.14 Comparison of TDR liquid level response

3.4.1 Fuel Rod Failure

The FLHT-2 test fuel rod internal pressure (1.62 MPa) was set to higher than the system pressure (1.38 MPa) to replicate PWR-type conditions and failure mechanisms (ballooning), whereas the internal pressure was set to lower levels (~0.4 MPa) in FLHT-4 and -5 to replicate

boiling-water reactor (BWR)-type conditions and failure mechanisms (collapse). As expected, the higher internal pressure of the fuel rods in FLHT-2 resulted in fuel rod failure at lower temperatures. This effect is shown in Figure 3.15, which plots the fuel rod pressure with peak cladding temperature for FLHT-2 and FLHT-5. Fuel rod failure occurred at a peak cladding temperature of 1250 K for the high-internal pressure rods of FLHT-2 compared with 2300 K for the low-internal pressure rods of FLHT-5. Failure of all the instrumented fuel rods occurred essentially simultaneously where ballooning was the failure mechanism; a slightly greater variation in time was noted where fuel rod melting was the failure mechanism, as in FLHT-4 and -5.

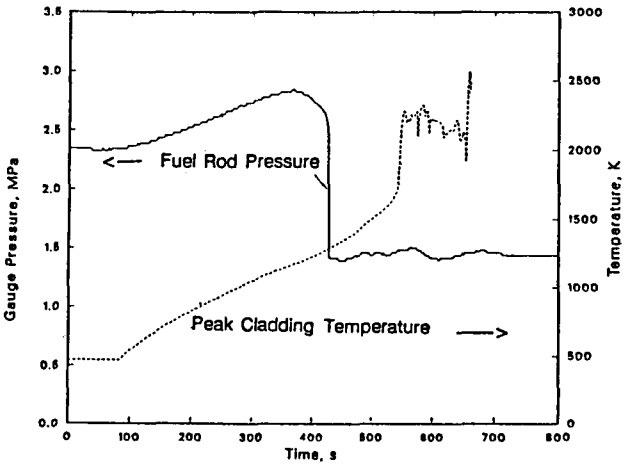

a) Fuel Rod Ballooning (FLHT-2)

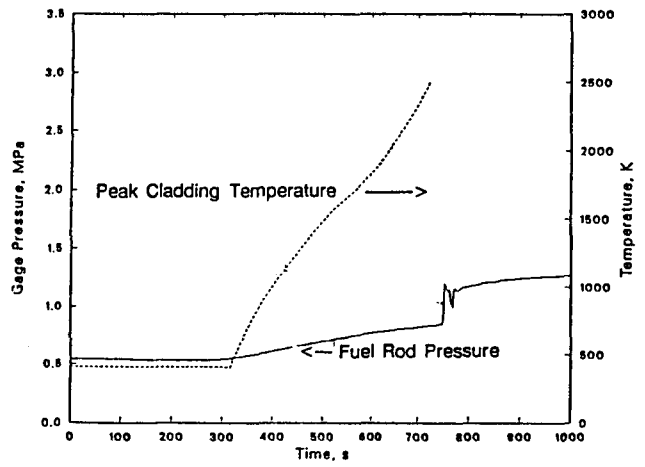

b) Fuel Rod Collapse (FLHT-5)

Figure 3.15 Comparison of fuel rod failure temperatures

With the fuel rod pressure below the system pressure fuel rod failure resulted in brief local temperature changes (no local effects were observed with fuel rod pressures higher than the system pressure). The magnitude of the temperature change and the direction (increase or decrease) was dependent on the thermocouple position relative to the breach location. Local temperature changes were generally less than 250 K and quickly decayed to pre-breach values.

3.4.2 Cavity Failures

There were a number of sealed cavities in the FLHT test train that were subjected to high temperatures and were therefore susceptible to failure: the fuel rods, the shroud insulation cavity, and two cavities in the plenum region. Cavity failure was a function of the cavity backfill pressure, the location of the cavity relative to the high temperature region, and the time at temperature.

Failure of the cavity that contained the porous shroud insulation occurred in each of the FLHT tests. The failure of this cavity by liner oxidation was expected and therefore the initial pressure of this cavity was set to minimize the pressure differential between the bundle region and insulation cavity at the time of failure. By minimizing the pressure differential, injection of hot gasses from the bundle region into the shroud was limited, as was the impact on the shroud thermal conductance. Generally, the shroud insulation cavity failed just before the initial oxidation excursion, and the pressurization of the insulation cavity to reduce the effluent ingress was successful.

Failure of the plenum cavities occurred only in the longer duration tests, i.e., FLHT-4 and FLHT-5. Failure of these cavities occurred subsequent to the initial oxidation excursion. Because these cavities were at a pressure considerably below the system pressure, diversion of some of the bundle effluent into the plenum cavity occurred over a brief period of time. This diversion of the bundle effluent resulted in a brief reduction

of the system pressure and a temporary reduction in the bundle hydrogen generation as measured by the ECM. The total volume of gas that entered the plenum cavity was limited because of the limited void volume of the zirconium dioxide insulation within the cavity. Again, local perturbations were noted in the deposition rod temperatures adjacent to the breach location; these temperature fluctuations (increase or decrease) were dependent on the location of the thermocouples relative to the breach location.

In conclusion, although cavity pressure changes occurred at discrete times during the FLHT tests, the impact of these pressure changes on the damage progression phenomena and the interpretation of test results was minimal.

4 Evaluation of FLHT Severe Accident Phenomena

Analysis of the data obtained from the FLHT tests were used to enhance the understanding of severe accident behavior and damage progression as presented in this section. First, the effect of coolant boilaway on damage progression is assessed. This is data that is unique to the FLHT tests. An assessment is made of the length of bundle uncovered, the time required for the onset of damage and the effect of coolant level decrease on the damage progression. Next, an assessment of the oxidation behavior of the tests is made from the burn front behavior, the effect of test time and boiloff type, and an evaluation of oxidation in the steam-cooled region above the coolant region. An assessment of the hydrogen generation is made by evaluating the rate and timing of the hydrogen generation, and includes an assessment of the effect of Zircaloy melting on the hydrogen generation. Finally, the material relocation behavior of the tests is evaluated and then assessed by comparing the FLHT test data with data from in-pile short-length severe fuel damage (SFD) tests.

Data from each of the tests was selectively highlighted to illustrate key severe accident phenomena. The FLHT-1 test was used to evaluate the effect of a simulated extended boilaway accident and demonstrate that damage conditions can be achieved with a relatively small fraction of the fuel bundle uncovered. The material relocation events that occurred early in the FLHT-2 test were used to illustrate how material relocation can temporarily decrease hydrogen generation but also how it can continue in the absence of a complete flow blockage. The FLHT-4 test results were used to illustrate the additional damage that can result from longer times at high temperature. Finally, the FLHT-5 test results were used to demonstrate the progression from the onset of rapid oxidation to complete consumption of the available Zircaloy.

4.1 Correlation of Coolant Level with Cladding Temperatures

When evaluating the severe accident phenomena that occur during the FLHT boilaway tests, correlating the coolant level with cladding temperatures provides valuable insights into the following phenomena: 1) the coolant level at the onset of damage, 2) the time from dryout and length of exposed fuel rod required to reach autocatalytic oxidation (damage) conditions, and 3) the effect of a decreasing coolant level on the progression of the oxidation front. Each of these phenomenon is presented and discussed below.

4.1.1 Coolant Level at the Onset of Damage Conditions

The FLHT boilaway tests are representative of a low power,[1] low-pressure (1.4 MPa) small-break LOCA with either 1) a step-change constant makeup rate, as in FLHT-2, -4, and -5, or 2) a variable makeup rate, as in FLHT-1. The step-change constant makeup tests are considered rapid boilaways because the reduction in makeup rate is large, resulting in a rapid coolant level decrease. The variable makeup FLHT-1 test is considered an "extended" boilaway, because the reduction in makeup rate is small and the coolant level decrease slow or "extended" in time.

Extended boilaway transients can result in 1) a higher coolant level at the onset of rapid oxidation and, therefore, a larger steaming rate and a potentially larger chemical power contribution leading to potentially higher temperatures, 2) a thicker oxide buildup on the surface of the fuel rod before the excursion, and 3) a slower moving burn front. The two most significant effects--the higher chemical power contribution and a slower moving burn front--were not assessed in the FLHT-1 test because of the early test termination. The difference in the coolant levels at the onset of rapid oxidation was assessed for the different boilaway types, however, and the results are presented below.

The effect of decreasing coolant levels on peak cladding temperatures is presented in Figure 4.1 for the FLHT-2, -4 and -5 tests and in Figure 4.2 for the FLHT-1 test. The coolant level at excursion is consistent among the

[1]The FLHT-2 rod average power of 0.52 kW/m-rod is equivalent to a decay heat of 2.5% of full power for a 2440 MW PWR 630 s after shutdown.

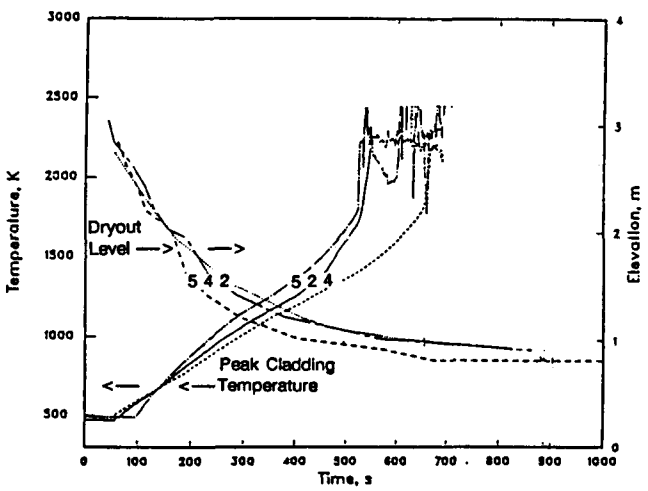

Figure 4.1 Effect of decreasing liquid level on peak cladding temperature for the step-change flow reduction transients (FLHT-2, -4, and -5)

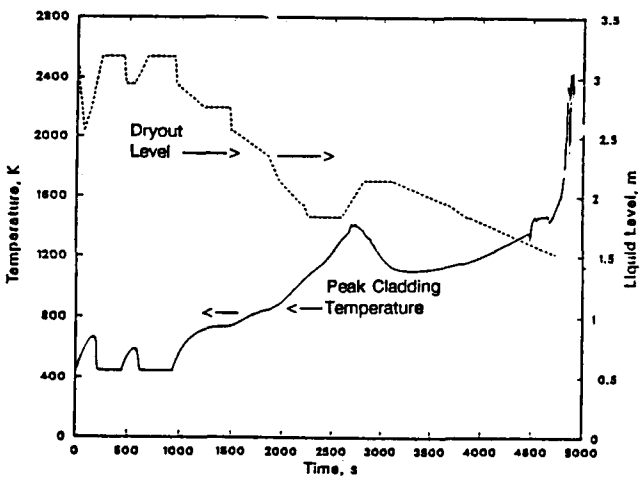

Figure 4.2 Effect of decreasing liquid level on peak cladding temperature for the FLHT-1 variable flow reduction transient boilaway

three rapid boilaway tests, generally at the 1-m elevation or with approximately 70% of the fuel rod uncovered. (The FLHT-5 excursion initiated at a slightly lower coolant level due to the more rapid coolant level decrease.) In the FLHT-1 test, the bundle makeup rate and coolant level varied considerably over an extended period of time, resulting in an oxidation excursion when the coolant level was at the 1.5-m elevation or when only 60% of the length of the fuel rods was uncovered.

The difference between the excursion coolant level for the extended FLHT-1 boilaway and the more rapid FLHT-2, -4 and -5 boilaways can be viewed as the difference between a "quasi-steady-state" and a transient approach to damage conditions. For example, in FLHT-1 the level decreased from 2.9 to 2.1-m in 1300 s; quasi-steady-state axial temperature distributions were, therefore, expected because of the gradual level decrease. In FLHT-2, though, the same decrease in coolant level took only 115 s, a rate of decrease that prohibited fully developed axial profiles, and hence peak temperatures from being established. For this reason, a lower coolant level and therefore a greater length of fuel was exposed at the time oxidation excursion conditions were achieved in FLHT-2.

4.1.1.1 Recovery from the Onset of Damage Conditions

The length of fuel rod that can be uncovered without resulting in an oxidation transient is a complex function of the following: decay heat level and axial power profile, coolant makeup rate and temperature, system pressure, oxide buildup, and radial heat losses. Associated with the length of the uncovered fuel bundle is the consideration at what point recovery can be achieved before the onset of damage. For example, can an oxidation excursion and the subsequent fuel damage be avoided by accident recovery strategies such as reflood and pressure relief? Although discussions of accident management and recovery strategies are outside the scope of this report, the FLHT-1 test does provide some valuable insights into the effectiveness of coolant reflood in an attempt to reduce cladding temperatures before the onset of rapid oxidation.

A brief discussion of the accident recovery experience of the FLHT-1 test is, therefore, presented below.

The portion of the FLHT-1 transient shown in Figure 4.2 can be partitioned into three distinct phases: 1) an initial boilaway from 1000 s to 2700 s in which the coolant level dropped from 3.2 m to 1.8 m, 2) a reflood phase from 2700 s to 3200 s during which a temporary

increase in makeup rate increased the coolant level to 2.1 m, and 3) the final phase of the boilaway in which the coolant level decreased to 1.5 m, leading to an oxidation excursion in the upper elevations of the fuel bundle.

During the initial boilaway phase, the peak cladding temperature (Level 120; 2650 s) began exhibiting a temperature rise rate characteristic of the rapid oxidation that occurs above temperatures of 1400 K (see Figures 3.1 and 3.6). Given the behavior of FLHT-2, -4, and -5, autocatalytic oxidation was only a little over a minute away. It is noteworthy from an accident mitigation viewpoint that the autocatalytic oxidation was averted in FLHT-1 by a rapid increase in inlet makeup flow, i.e., reflood. In fact, a relatively minor increase in the coolant level, approximately 0.3 m, was extremely effective in cooling the bundle; it not only terminated the heatup but also reduced the peak cladding temperature by over 300 K.

As the reflood rate was subsequently intentionally decreased, however, the coolant level once again began to steadily decrease, resulting once again in increasing cladding temperatures. As the coolant level gradually dropped below the 1.5-m elevation (Level 60), autocatalytic oxidation occurred and the test was then terminated.

The coolant level at the time of the excursion initiation was consistent with the coolant level when an apparent excursion was avoided, indicating that the additional oxide buildup on the Zircaloy cladding that occurred after reflood had little impact on the onset of the rapid reaction.

4.1.2 Fuel Uncovered for Autocatalytic Oxidation and Melting

The coolant level and location of the oxidation excursion zone during FLHT-2 are correlated in Figure 4.3. From this figure, it is possible to assess the following: 1) the time from cladding dryout to initiation of the oxidation excursion (line "A" in Figure 4.3); 2) the length of fuel rod uncovered for oxidation excursion conditions (line "B" in Figure 4.3); and 3) the influence of the coolant level decrease on the progression of the oxidation burn front. Also indicated in this figure is the time the Zircaloy melt temperature is exceeded, a relationship

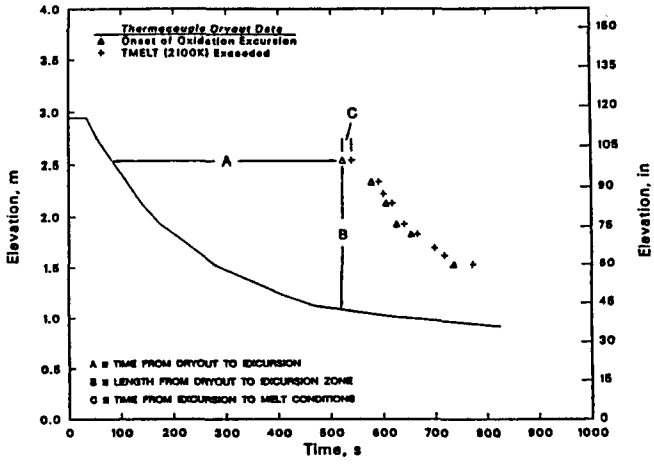

Figure 4.3 Correlation of liquid level with the oxidation burn front for FLHT-2

that will be used later to provide insights into the material relocation behavior. Each of these unique aspects of full-length severe fuel damage behavior is discussed below.

4.1.2.1 Time From Dryout to Oxidation Excursion

A consistent time interval from cladding dryout to the initiation of oxidation excursion (line "A") was observed for the levels that experienced autocatalytic oxidation behavior (Levels 60 through 100), indicating that the cladding heatup rate (energy generation minus heat removal) over this axial region was fairly uniform. Moreover, the uniform time to excursion translates into uniform oxide thickness buildup before the onset of melt relocation conditions.

The time from dryout to excursion can also be viewed as the time during which actions can be taken to recover from the conditions that could eventually lead to fuel damage. Again, for the FLHT-2, -4, and -5 tests, this time was fairly short (~450 s). The recovery from situations that could potentially lead to fuel damage such as coolant boilaways will depend strongly on the timing and effectiveness of the actions taken, e.g., coolant injections and pressure relief. As reported earlier, the FLHT-1 test did demonstrate that fuel damage can be avoided at temperatures just below the autocatalytic by increasing the coolant level for the bundle.

4.1.2.2 Length of Fuel Rod Uncovered for Oxidation Excursion

The axial distance from the dryout front to the burn front (Figure 4.3, line "B") was found to decrease with decreasing elevation. This phenomena is attributed to the transient nature of a rapid boilaway--as Level 100 underwent an oxidation excursion, axial temperature profiles were still developing, requiring as much as 1.5 m of heated length to attain conditions necessary for the start of an oxidation excursion. By the time Level 60 underwent rapid oxidation approximately 200 s later, however, coolant level and steaming rate changes were minimal and steady-state axial temperature profiles were being approached. Under these conditions, the distance from the dryout location to the excursion zone decreased to as little as 0.6 m.

Based on the length of fuel rod between the dryout level and the excursion zone shown in Figure 4.3 and an oxidation excursion temperature of 1700 K, the axial temperature gradients from the dryout front to the excursion region in the rapid boilaway tests increased from 8 K/cm to 20 K/cm in just over 2 min. The effects of these changing axial gradients and the distance from the dryout front to the excursion zone on material relocation behavior are discussed in Section 4.

For the extended boilaway FLHT-1 test where quasi-steady state conditions existed, the length from the dryout front to the excursion zone was as great as 1.5 m (Figure 4.2). Because the rate of coolant level decrease was much less in the FLHT-1 test than in the other FLHT rapid boilaway tests, the change in the distance from the dryout level to the excursion zone and the axial temperature gradients would have been much less if the test had been allowed to proceed.

4.1.2.3 Influence of Coolant Level on Oxidation Front Progression

The combination of the rate of coolant level decrease and the rate at which the axial temperature profiles develop determines the velocity of the oxidation burn front. In the rapid boilaway FLHT-2, -4, and -5 tests, the progression-to-damage was not so much driven by the decrease in coolant level as it was by the increase in the axial temperature gradient. For these tests, the large reduction in the coolant makeup rate (80 to 90%) that initiated the excursions is essentially equivalent to a termination of the coolant flow. This led to the rapid decrease in the coolant level shown in Figure 4.1 where the coolant level approached its steady-state position while the axial temperature profiles were still developing. The result of this is that the coolant level changed very little while an extensive length of fuel underwent autocatalytic oxidation. A demonstration of the relative change in the liquid level position and the position of the oxidation burn front is provided in Figure 4.4; the temperatures of the initial oxidation excursion level (Level 96) and the lowermost oxidation excursion levels (Level 56), along with the coolant level history for FLHT-5 are plotted. As shown, in less than 3 min, the damage progressed over 1.2 m of the 3.7-m-long fuel rod bundle while the coolant level decreased only 10 cm, from 1.3 to 1.2 m. Thus, for the rapid boiloff tests, the progression of the oxidation burn front is primarily determined from the developing axial temperature profiles, and not from the rate of liquid level decrease.

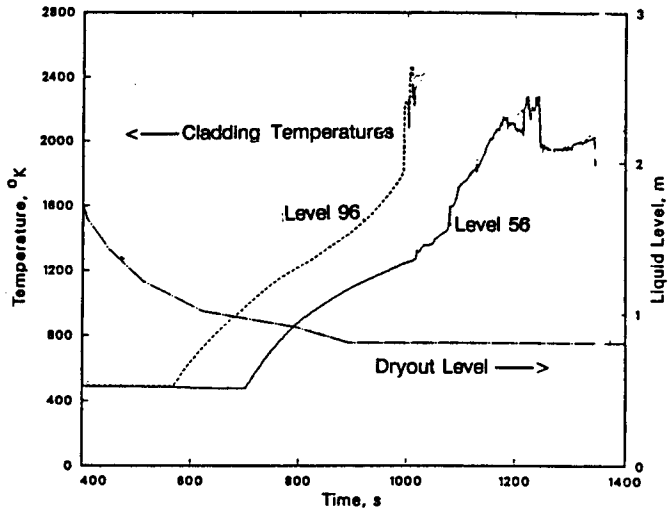

Figure 4.4 Comparison of initial and final oxidation excursion locations with liquid level for FLHT-5

For extended boilaway-type transients, however, e.g., FLHT-1, the progression of damage is more closely tied to the rate of the decrease of coolant level. Again, this difference can be viewed as the difference between a "steady-state" and transient approach to damage conditions. Further insights into the speed and axial extent of

the damage progression are provided in the discussion on oxidation behavior (Section 4.2).

4.1.2.4 Progression of the Melt Zone

In all tests, the Zircaloy melt temperature was exceeded shortly after the onset of the oxidation excursion, generally within 20 s as shown in Figure 4.3, line "C." The progression of the "melt temperature zone" shown in this figure is one of many important factors that control material relocation behavior and is closely tied to the progression of the oxidation burn front. In FLHT-2, the rapid downward progression of the melt temperature zone early in the transient resulted in an increased number of relocation events when compared to later in the transient when the high-temperature zone progressed more slowly (see Section 4.3). Again, during slow boil-away tests, the progression of the melt zone, like the oxidation front, is controlled by the rate of coolant level decrease and progresses by temperature profile development.

4.2 Oxidation Behavior

Presented below is an assessment of the oxidation behavior of the constant makeup FLHT tests. The establishment, progression, and termination of the oxidation burn front during the tests is detailed along with an evaluation of the steam consumption below the location of the burn front.

4.2.1 Temperature Escalation and Burn Front Progression

One aspect of full-length damage progression with continued steam production is the downward then upward progression of the oxidation burn front. Whereas only a downward progression was noted in FLHT-1 and -2 due to the relatively short test times both a downward and an upward progression occurred in the longer duration FLHT-4 and -5 tests. Because complete oxidation of the uncovered Zircaloy occurred in FLHT-5, the results of this test will used to illustrate the characteristics of the burn front progression.

Following the initial oxidation excursion, a localized zone (<0.2 m)[1] of oxidation reaction formed that then progressed downward from Level 96 toward Level 48 during the time from 1000 to ~1200 s. The downward progression of the burn front is illustrated in Figure 4.5, which plots the cladding temperature histories from Level 96 to Level 40. The downward progression occurred as a result of the developing axial temperature profiles (see Figure 3.6) in the lower axial levels reaching autocatalytic reaction temperatures of 1600 to 1700 K. After initiation of the autocatalytic reaction all remaining steam was consumed, effectively eliminating the potential for oxidation excursions in the upper elevations. This downward progression of the burn front continued until about 1200 s when the front arrived in the vicinity of Level 48, the upper level of the steam-cooled region above the dryout front.[2]

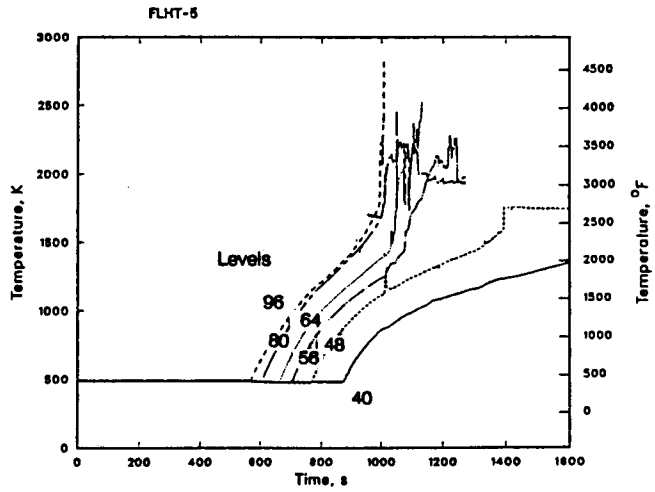

Figure 4.5 FLHT-5 cladding temperature response illustrating the downward oxidation progression

[1]The oxidation front was judged to be less than 0.2 m (8 in.) long due to the discrete thermocouple response observed between thermocouples spaced 0.2 m apart.

[2]Thermocouple data shows Level 56 underwent an oxidation excursion; the next lowest thermocouple measurement plane at Level 48 did not display autocatalytic behavior (although it was affected by material relocation). Thus the lowest level that experienced an oxidation excursion was estimated to be Level 52, midway between the two thermocouple measurement elevations.

The downward progression of the oxidation burn front was eventually terminated as quasi-steady-state conditions were reached; that is, when the coolant level and axial temperature profiles were no longer changing. This progression is illustrated in Figure 4.6, which shows stable cladding temperatures just above the coolant pool. The slight variation in temperature shown was a direct result of small variations in the coolant level position. The steam-cooled and the oxidation-induced damage regions are also delineated in this figure.

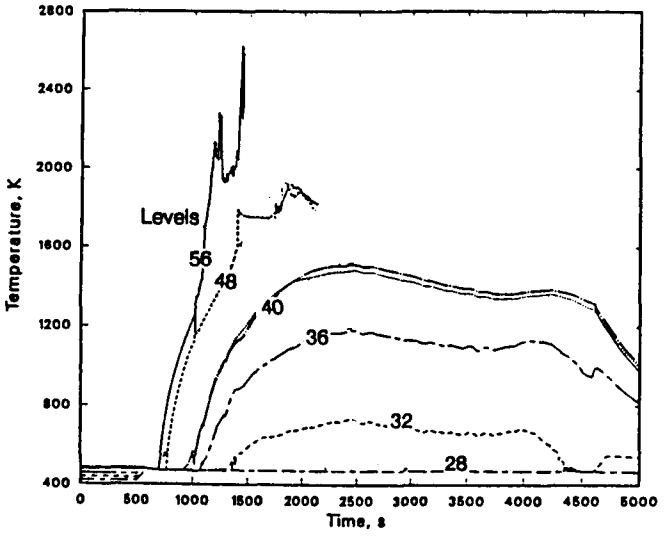

Figure 4.6 FLHT-5 cladding temperature response illustrating the termination of the downward burn

With constant conditions existing above the coolant pool and without fresh metal available for oxidation, an upward moving burn front was established. This upward moving front consumed all available steam, preventing the steam from fueling rapid oxidation in the higher elevations. The upward burn continued from its origin to the top of the fuel rods; this effectively terminated the high hydrogen generation phase of the test (see Section 4.3).

Elevations that participated in the upward burn included the portion of the bundle that participated in the downward burn, e.g., Levels 48 through 96, and regions that had been steam-starved during the downward burn, e.g., Levels 100 through 144. Unlike the downward progression, the progression of the upward burn was not driven by the transient decrease in coolant level and developing temperature profiles but, rather, by full consumption of the available Zircaloy in an axial region. As a result, the velocity of the upward burn was considerably slower than the downward burn and less definable, because the bulk of the bundle region instrumentation was damaged in the downward progression. Given the discrete response of the protected saddle thermocouples, however, the region of intense oxidation in the upward burn was again less than 0.2-m long.

The progress of the upward burn front is shown by the successive peaks in the saddle thermocouples (Figure 4.7). Note that the relatively unoxidized surfaces at Level 112 and above reacted as vigorously during the upward burn as did the levels that underwent the downward burn (e.g., Level 80).

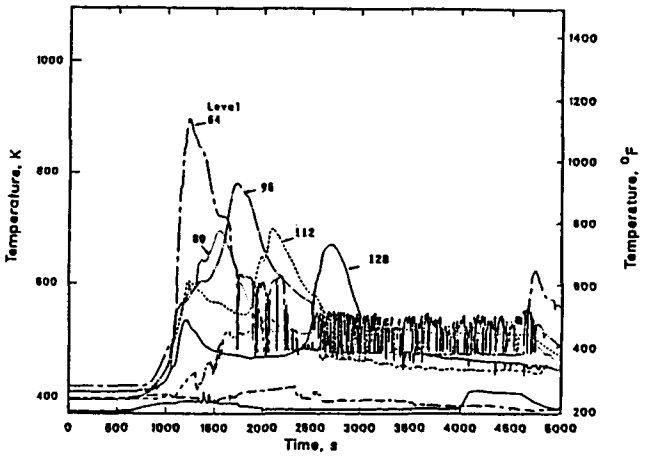

Figure 4.7 FLHT-5 saddle temperature response illustrating the upward burn

A somewhat different perspective of the progression of the oxidation burn front is presented in the 3-dimensional plot of saddle temperatures shown in Figure 4.8. Regions that underwent both downward and upward burn displayed a much less vigorous oxidation reaction on the upward burn due to the oxide layer buildup that occurred during the downward progression.

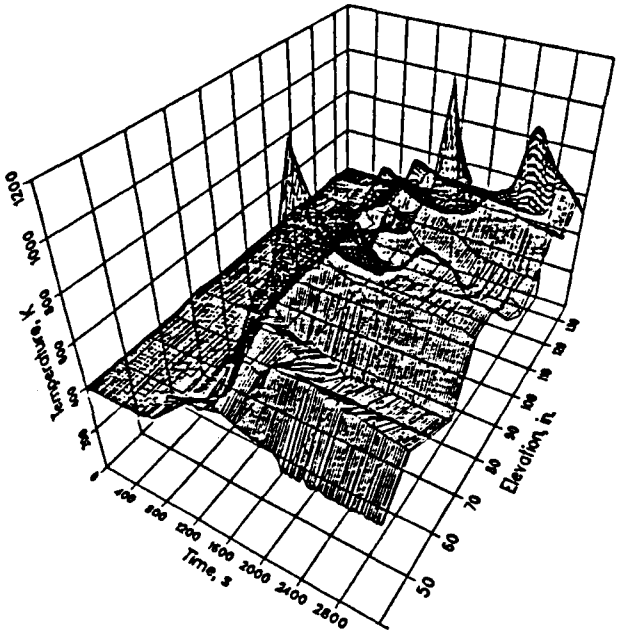

Figure 4.8 FLHT-5 saddle temperature as a function of time and elevation

Cladding regions steam-starved in the downward burn were unaffected by the hydrogen-rich environment and eventually reacted vigorously once steam became available. Based on the responses of the saddle thermocouples shown in Figures 4.7 and 4.8, the oxidation reactions accompanying the once steam-starved regions in the upward burn are shown as being as vigorous as the reactions associated with the initial downward burn.

Because of the existence of the upward burn, it is obvious that complete oxidation of the available Zircaloy did not take place within the initial downward burn front; this result may, however, differ for different boiloff scenarios with slower coolant level and burn front velocities, i.e., extended boiloffs.

4.2.2 Oxidation in the Steam-Cooled Region

Although considerable fuel rod damage occurred while the coolant level approached steady-state conditions, there existed a short length of exposed fuel just above the dryout front that, because of sufficient steam cooling, did not reach autocatalytic conditions. This lower boundary of the severe damage region region is physically defined by the coolant level and the (T >2100 K) and is easily determined from the responses of the thermocouples shown in Figure 4.6. The steam-cooled region was the largest in FLHT-1 due to the higher coolant level and hence steaming rate, and was the smallest in FLHT-5 due to the higher fission power level. The length of the steam-cooled region is was on the order of 40 cm. Within the bulk of the steam-cooled region, significant oxidation of the cladding took place; even in the relatively short time at high temperatures during FLHT-2, most of the cladding in this region was converted to white stoichiometric ZrO_2; the cladding in this region was extremely brittle and prone to fracturing. Thus, while autocatalytic oxidation was not manifest in the steam-cooled region, significant oxidation and embrittlement of the cladding occurred.

The oxidation LHGR during FLHT-5 was evaluated by using the measured cladding carrier, liner temperatures, the known surface areas of the components, and the oxidation kinetics of Cathcart-Pawel (1977). The results of these calculations are shown in Figure 4.9 where the computed oxidation LHGR in kW/m is plotted versus axial position at various times and compared with the nuclear (fission) LHGR. The calculated oxidation heat rates shown in this figure are provided for the heatup portion of the transient prior to the initial oxidation

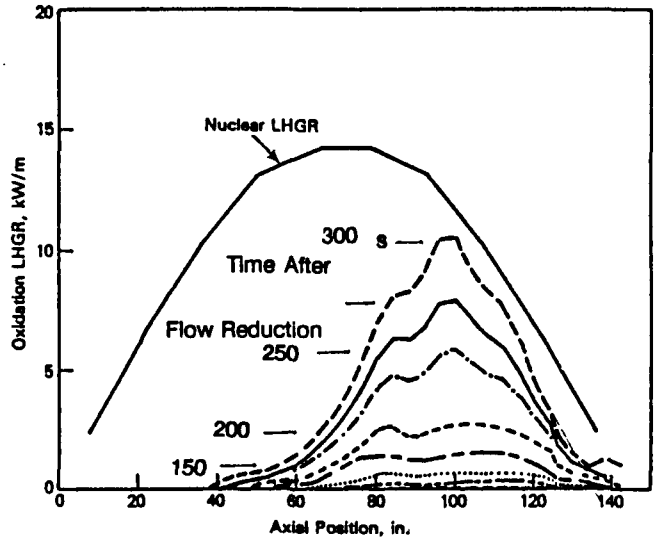

Figure 4.9 Comparison of calculated oxidation and nuclear LHGR during FLHT-5 heatup

excursion. As shown, oxidation is occurring over a significant portion of the heated length and consuming a fraction of the available steam. In fact, just before the initial excursion, approximately 35% of the available steam was consumed below the oxidation excursion location (based on a steady-state steaming rate of 1.26 g/s), with the peak linear heat generation rate from oxidation equalling the peak nuclear heat generation rate.

Assuming that the remaining steam is consumed by the local oxidation excursion and that the excursion zone is 0.2-m long, the peak oxidation power is calculated to exceed 68 kW/m which is roughly four times the nuclear LHGR.

Using this same method, the cumulative oxidation just before escalation can be calculated. The maximum amount of cladding oxidation was computed to be less than 8%, indicating that greater than 90% of the Zircaloy oxidation in the FLHT-5 test assembly occurred after the initial oxidation excursion.

4.2.3 Influence of Test Time and Boiloff Type on Oxidation

An overview of the oxidation and damage progression of the four FLHT tests is presented schematically in Figure 4.10. Illustrated in this figure is the relationship between the initial oxidation front location, the asymptotic or final coolant level, and the termination of the

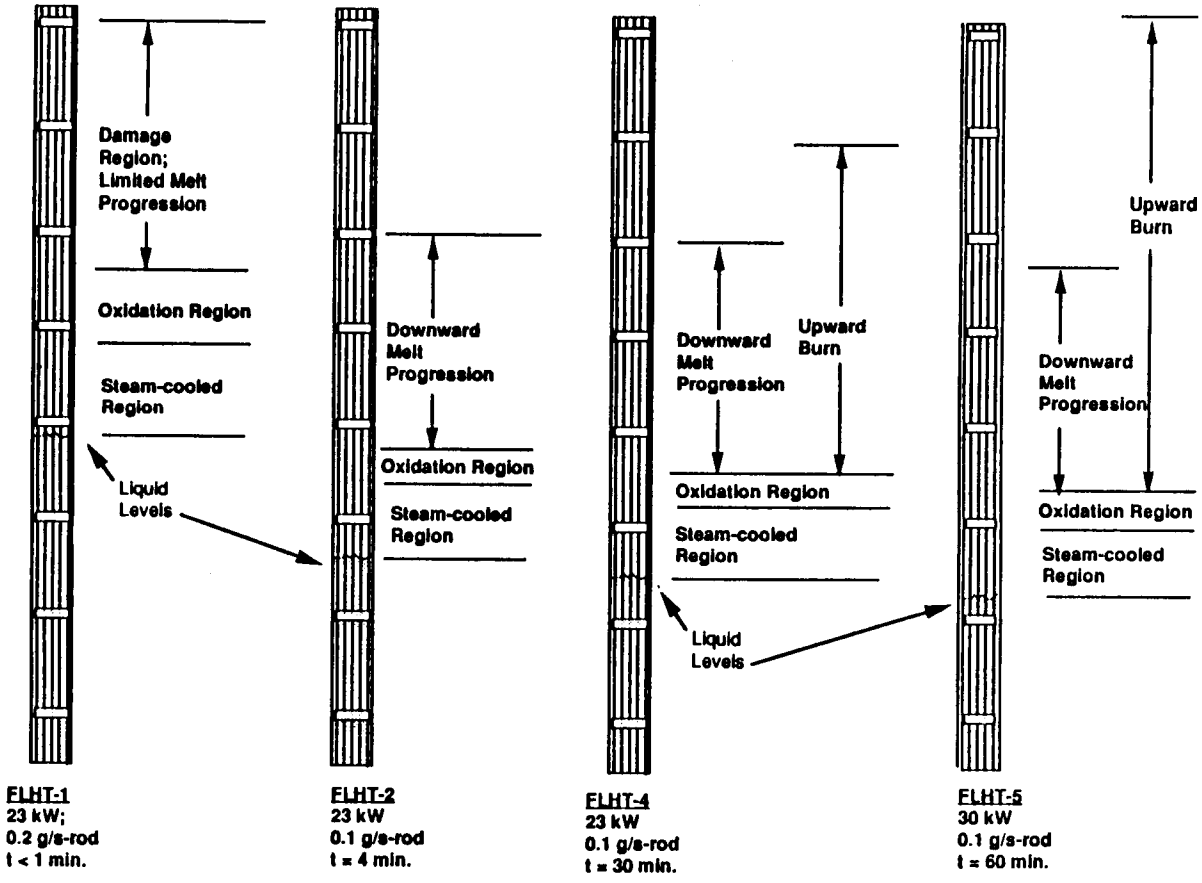

Figure 4.10 Overview of the FLHT oxidation progression

downward and upward burns. Also shown in this figure is the oxidation and steam-cooled regions; the damage in these regions is characterized, respectively, by white, highly-embrittled, oxidized cladding completely converted to ZrO_2, and undamaged cladding with a dark protective oxide layer.

As shown in the figure, only a small fraction of the uncovered fuel remains undamaged, with this fraction being affected by the test time and the boilaway type. The damage that occurred was entirely oxidation induced, i.e., the simulated decay fission power levels and radial heat losses were such that Zircaloy melt temperatures could not be achieved in these tests without the local chemical power from oxidation. For the FLHT-1 extended boilaway, the length of the undamaged steam-cooled region was expanded and was located higher in the bundle; coupled with the high coolant level and the short test time, the axial extent of the damage region is the smallest of the tests. Conversely, the oxidation-induced damage is greatest for the 1-hr-long FLHT-5 test.

4.3 Hydrogen Generation

Hydrogen generation during the FLHT boilaway transients was measured by a combination of up to four different instruments--a mass spectrometer (MS), thermal conductivity meter (TCM), palladium hydrogen meter (PHM), and a noncondensable turbine flowmeter (NTF). The MS, TCM, and PHM essentially measured the percentage of hydrogen[1] in the nitrogen carrier gas flow. The NTF provided a measurement of the hydrogen generation by measuring the combined nitrogen/hydrogen mixture flows through the NTF and subtracting the nitrogen sweep gas flow. The NTF responded almost instantly (~5 s) to changes in hydrogen generation because it was located closest to the hydrogen source (<10 m) and on the main noncondensable gas line in the ECM. The MS and TCM had considerably longer delay times (3 to 8 min) as these two instruments were located further downstream from the hydrogen source and were located on the sample line. The lower gas velocity in the sample line,[2] coupled with the increased distance from the hydrogen source, significantly increased the transit time to the mass spectrometer and TCM to 150 s and 420 s, respectively (longer transit times were noted for FLHT-4 and -5 than for FLHT-2 due to added components and 1 piping in the ECM). Because of the instantaneous response time, reliability and demonstrated accuracy of the NTF, the discussions of hydrogen generation rate, total release, and timing will focus solely on the NTF measurements.

In this section, the rate of hydrogen generation and integrated release are presented for each of the FLHT tests, along with assessments of the timing of the hydrogen release and the amount of hydrogen produced before and after the onset of Zircaloy melting, i.e., at 2100 K ±100 K. A summary of the hydrogen release data and inferred oxidation behavior is presented in Table 4.1.

4.3.1 Hydrogen Generation Rate and Integral Hydrogen Released

The real-time rates for hydrogen generation for the three step-change transient FLHT tests as measured by the NTF[3] are presented in Figures 4.11 through 4.13. Also plotted in these figures is the equivalent hydrogen generation represented by full conversion of the inlet ordinate axes of Figure 4.11 are the same, and it is seen that the measured hydrogen rates from about 700 to 850 seconds equals the theoretical amount of hydrogen that could be produced from the total quantity of the water fed into the bundle. The two scales on the ordinate axes of Figures 4.12 and 4.13 are different to show the close relationship of the measured values to the calculated values. If the ordinate scales had been equal, the curves would be one on top of the other. The characteristics of hydrogen generation for each of the tests are compared and discussed below, and conclusions are made regarding the extent of steam consumption, the effects of material relocation, and the potential for long-term hydrogen release in severe accidents.

[1]The MS measured the weight ratio of hydrogen, krypton, and helium to nitrogen in the gas stream, whereas the PHM measured the partial pressure of hydrogen in the gas stream. Output of the TCM was in percentage of hydrogen.

[2]The sample line flow rate was limited to 250 cc/min by throttling valves in the sample line. The flow rate in the main noncondensable line in the ECM was ranged from 90 L/min to 240 L/min. Thus the sample line flow rate was less than 1% of the main noncondensable effluent flow.

[3]Hydrogen release data was computed from the output of several pressure, temperature and flow sensors.

Table 4.1 Hydrogen generation and oxidation summary

Parameter	FLHT-1	FLHT-2	FLHT-4	FLHT-5
Peak generation rate, mg/s	140	210	174	182
Average generation rate, mg/s	N/A	140	140	90
Total release g	31	44	240	340
Percent of hydrogen released after 2100 K	0	90	95	95
Percent of bundle Zircaloy consumed	8	12	61	86
Peak oxidation power, kW	21	32	26	27

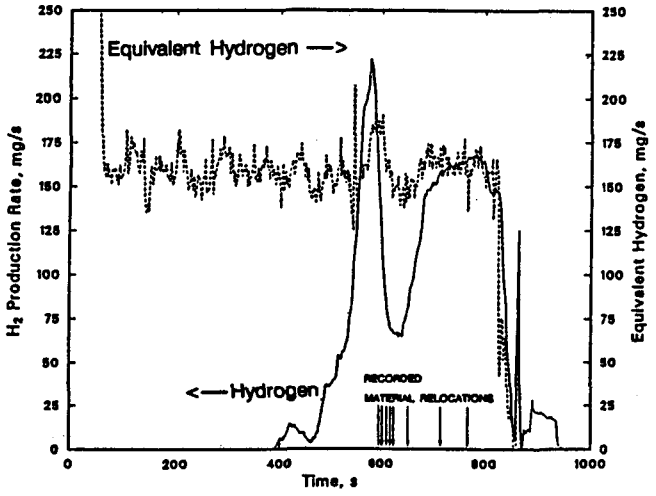

Figure 4.11 FLHT-2 hydrogen generation rate calculated from NTF and for fully converted inlet flow

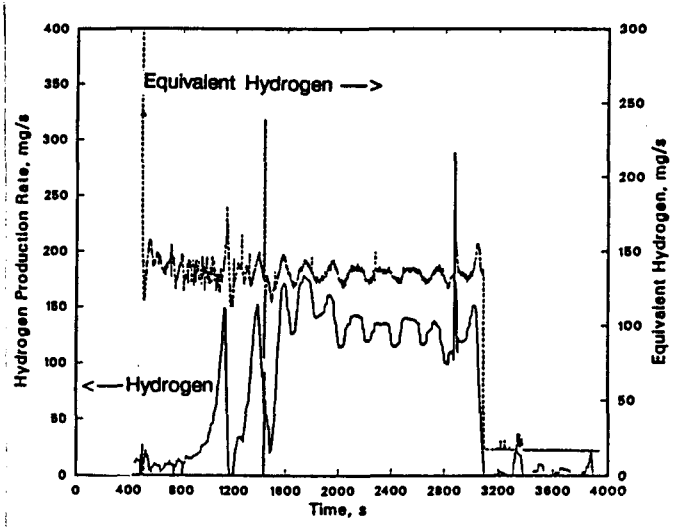

Figure 4.12 FLHT-4 hydrogen generation rate calculated from NTF and for fully converted inlet flow (Note different ordinate scales.)

Several consistent phenomena are observed with respect to the generation of hydrogen during the FLHT tests. First, each of the tests operated under steam-starved conditions during the majority of the high-temperature transients, a condition that is not surprising given the steaming rate (~0.1 g/s-rod) and high temperatures achieved. As a result, fluctuations in the coolant makeup rate were therefore directly translated into the fluctuation in the hydrogen generation rate. Second, the onset of measurable hydrogen generation is essentially coincident with the onset of autocatalytic oxidation. This conclusion is illustrated in Figure 4.14 of the FLHT-2 hydrogen generation versus the peak cladding temperature and is supported in an assessment of hydrogen generation behavior from in-pile test data by Cronenberg et. al (1990). Third, all but a few percent of the total hydrogen generated during the course of the transients occurred before the onset of cladding melting; but more importantly, no physical mechanisms were found to limit hydrogen generation once the oxidation excursion started.

Two other significant phenomena observed were the reduction in hydrogen generation that occurred as a result of molten material relocation during the FLHT-2 test and the termination of significant oxidation in

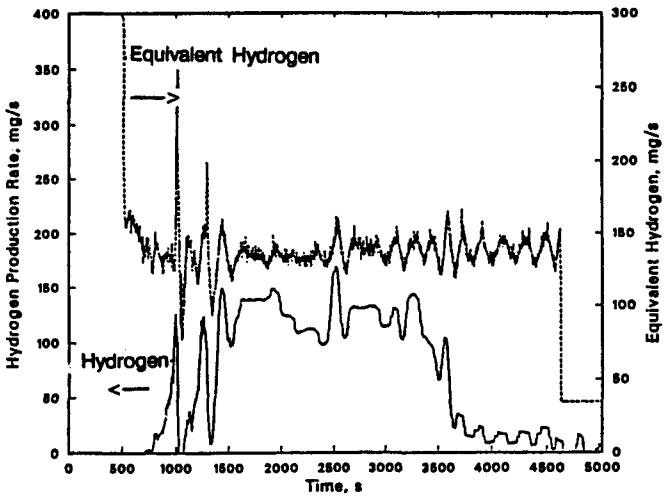

Figure 4.13 FLHT-5 hydrogen generation rate calculated from NTF and for fully converted inlet flow

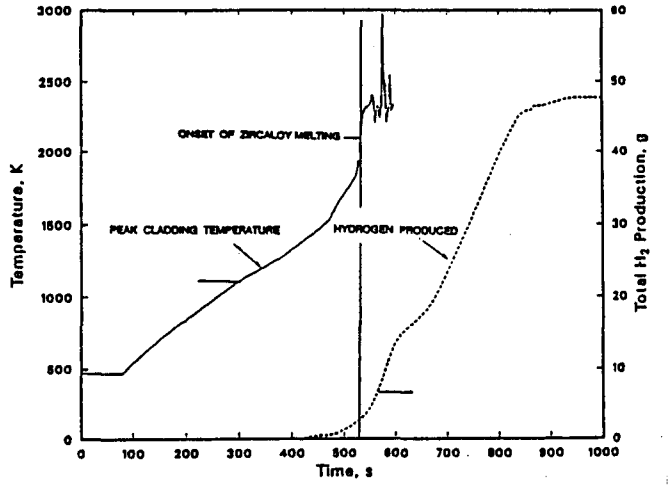

Figure 4.14 Partitioning of hydrogen production for the FLHT-5 test

FLHT-5. This reduction in the FLHT-2 hydrogen generation rate and the associated recorded relocation events are noted in the 600 to 800 s time frame of Figure 4.11. The effect of material relocation is to remove hot material from the high-temperature oxidation zone, causing a decrease in the rate of hydrogen generation. As the lower, and hence cooler regions, were heated up as the oxidation excursion zone progressed downward, hydrogen generation returned to fully-consumed conditions. Because little material relocated from the high-temperature zone to the steam cooled region, hydrogen generation continued from the onset of autocatalytic oxidation to the termination of the test. Although the rate of hydrogen generation was temporarily reduced by approximately 50% during FLHT-2 because of material relocation, the overall impact on the total amount of hydrogen generation expected during a long-term accident is quite minimal. (See Section 4.3.2 below.)

4.3.2 Effect of Zircaloy Melting on the Release of Hydrogen

As indicated in Table 4.1 and Figure 4.14, >90% of the hydrogen was generated following the onset of cladding melt temperatures. This occurred because 1) oxidation of the Zircaloy components continued uninterrupted with the steady supply of steam generated by the coolant boilaway and 2) because no physical behavior such as extensive material relocation occurred that moved material to low-temperature regions or formed a cohesive flow blockages that would limit the availability of steam. The continuing hydrogen generation is contrary to a common assumption that blockages would develop and terminate hydrogen generation. In the FLHT-5 test, only complete oxidation of the exposed Zircaloy terminated hydrogen generation; however, this occurred after 80% of the available hydrogen was generated. Only the Zircaloy below the dryout front did not contribute to the production of hydrogen.

The fact that oxidation/hydrogen generation continued at essentially fully-consumed rates following onset of Zircaloy melt temperatures suggests the following: changing surface-to-volume ratios of the reacting Zircaloy, which tend to decrease the overall oxidation process, and the destruction of the protective zirconium dioxide layer by Zircaloy melting and fuel dissolution, which would tend to enhance the oxidation process, are either negated or are in actuality second-order effects. As indicated in Section 4.2, a third of the steam generated at the coolant-to-vapor interface is consumed below the oxidation front by Zircaloy with intact geometry and where fuel dissolution effects did not occur. This represents a "base" hydrogen generation fraction; only

the remaining hydrogen generation is, therefore, susceptible to the effects of molten Zircaloy.

The limited influence of melt effects on the hydrogen generation is presented in Table 4.2. This table summarizes the percentage of steam consumed by the steam oxidation reaction during seven in-pile SFD tests. For the steam-starved tests, the percentage of steam consumed was nearly 100%; the largest difference is noted for the DF-4 test where a significant reduction in surface-to-volume ratio occurred as a result of relocated control materials.[1] Full consumption of the available steam was noted for times ranging from just over 4 min to as long as 45 min.

In conclusion, arguments for diminished hydrogen generation following Zircaloy melting and fuel rod dissolution are not supported by the test data of the FLHT tests. In fact, the results show that hydrogen will continue to be produced with the continued availability of steam and Zircaloy metal and that the entire uncovered length of the fuel rod can contribute to the total hydrogen release.

[1]An assessment of the hydrogen production from the DF-4 BWR control materials test indicated that the large amount of control material relocated to the lower elevations and that the subsequent blockage formation resulted in a temporary decrease in the hydrogen production. The short length of this test (0.5 m) makes the amount of steam consumed more likely to be affected by material relocation phenomena because the length of the high-temperature region is limited and end effects concentrate the solidification of once-molten materials in the vicinity of the inlet region.

4.4 Material Relocation Behavior

Following the oxidation excursion, local temperatures exceeded the Zircaloy melt temperature leading to the relocation of U, Zr, O. That some of these materials relocated has been inferred from abrupt, coincident changes in the response of thermocouples at different axial levels and among different bundle components. From these coincidental changes in the response of thermocouples, conclusions have been made regarding the following: 1) the origin of relocated materials, 2) the relocation distance, 3) the effect of relocation on local temperatures, and 4) the velocity at which the molten material relocated.

In spite of the extensive thermocouple instrumentation within the bundle region of the FLHT tests, only a partial picture of material relocation behavior can be derived from the temperature data because of the discrete nature of the measurements. Therefore, real-time data on relocation must be correlated with the end-state picture provided by post-test visual and metallographic

Table 4.2 Summary of steam consumption for in-pile SFD tests

Test (Environment)	H_2 (g)	Makeup Flow (g/s-rod)	Time at T>1700 K (s)	Steam Consumed (%)
INEL PBF-ST (Steam rich)	172	0.5	600	16
INEL PBF1-1 (Steam starved)	64	0.02	600	100
INEL PBF 1-4 (Steam starved)	86	0.02	750	100
PNL FLHT-2 (Steam starved)	44	0.12	250	100
PNL FLHT-4 (Steam starved)	240	0.12	1800	94
PNL FLHT-5 (Steam starved)	340	0.11	3000	83
SNL DF-4 (Steam starved)	38	0.06	570	60

examinations. To date, visual examinations through axial sections cut into the shroud have been performed on the fuel bundles from all the FLHT tests; detailed metallographic evaluations and gamma-tomography have been completed for the FLHT-2 and test bundle. The results of these post-test evaluations will be documented in a future report.

Presented below is an assessment of the material relocation behavior for the FLHT tests, based on the test results and the post-test examinations conducted to date. Material relocation behavior in these full-length tests is then compared with material relocation behavior that occurred during the short-length SFD tests to develop a comprehensive picture of material relocation behavior in early phases of a severe accident.

4.4.1 Observed Relocation Behavior

Of all the FLHT tests, FLHT-2 provided the most complete picture of material relocation behavior. This is because a greater number of thermocouples per plane were used in this test and provided more detailed data pertaining to material relocation kinetics than in the other tests. During the 4 min that the FLHT-2 test was extended following attainment of 2100 K cladding temperatures, a total of eight separate material relocation events have been inferred from the response of the thermocouples. An overview of these events for the FLHT-2 test is presented in Table 4.3[1]; the thermocouple responses that identified five of these relocation events (A-E on Table 4.3) are displayed in Figure 4.15. The eight discrete relocation events indicated in the table are 1) the location of the thermocouple that indicated relocated materials, 2) the estimated origin of relocated material, 3) the lowest axial level indicating a response, and 4) the local temperature increase.

The eight relocation events occurred over a 170-s period as the oxidation front progressed downward. The initial relocation occurred near the initial peak temperature location. Subsequently, fuel rod cladding and shroud liner temperatures at many locations responded with abrupt temperature increases, indicating extensive axial and radial relocation. The relocated source of molten

[1]FLHT-2 Data Report. N. J. Lombardo and D. D. Lanning. Pacific Northwest Laboratory, Richland, Washington.

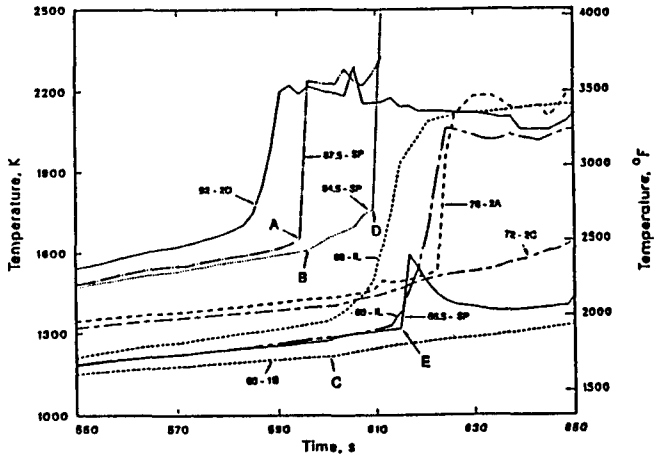

Figure 4.15 Thermocouple responses identifying FLHT-2 material relocation events A-E (see Table 4.3)

material for these eight events was estimated to have been from Level 92 to Level 62, essentially the full extent of downward oxidation progression, i.e., the severe damage region.

Whereas molten material was estimated to have relocated as much as 0.7 m from the source, this distance was not sufficient to remove the material completely out of the high-temperature zone. Hydrogen generation, therefore, continued in all tests, although a temporary reduction in the generation rate in FLHT-2 was noted (see Section 4.3).

Because cladding melt temperatures were achieved as a result of the local oxidation power, the source of the relocated material was found to correlate well with the position of the oxidation excursion (see Section 4.2). Thus, the velocity of the oxidation front (a function of the rate of coolant level decrease), as well as the length of the oxidation excursion zone (a function of the local steaming rate), affected the timing and amount of material that relocated and the distance it relocated. For the FLHT-2 test, a larger number of relocation events were recorded during the early phase of the burndown when the oxidation burn front velocity was greatest.

In instances where relocation occurred over a significant axial distance, e.g., the relocation distances at 600 s, 610 s, and 614 s, the change in the response of the

Table 4.3 Overview of FLHT-2 recorded material relocation events

Event	Time, s	Key Event Sensed by TCs	Estimated Origin of Relocation, Level	Lowermost Level Showing TC Change	Distance Detected from Origin, m	Remarks
A, B	594	Steam probe above grid Level 87.5	90	84.5	0.14	+580 K increase steam probe temperature, Level 87.5; initial material relocation; start of hydrogen generation
C	600	Liner adjacent to grid Level 88	88	60	0.71	Hot material at Level 60
D	609	Steam probe below grid Level 84.5	86[1]	76	0.25	+400 K increase liner temperature, Level 88
E	614	Steam probe above grid Level 66	84	66	0.46	+270 K increase in steam probe temperature, Level 66
--	623	Rod 2A cladding Level 76	82	72	0.25	+640 K increase in cladding temperature; secondary heatup noted; minimum of hydrogen generation
--	654	Liner at Level 72	74	66.5	0.19	+700 K increase in liner temperature; liner participation in bundle relocation behavior; hydrogen generation increasing
--	715	Steam probe below grid Level 63.5	66[1]	48	0.46	Hot material into steam-cooled region (Level 48); fully consumed conditions restored[2]
--	765	Rods 1B, 2C, and 4C, Level 60	62	60	0.1	Coplanar indications of molten material

[1]Grid spacer location.
[2]Full conversion of bundle coolant flow to hydrogen.

thermocouples was instantaneous, indicating that the material flowed rapidly down the length of the bundle, a result of the low viscosity of molten Zircaloy. Additionally, the Inconel grid spacers appeared to have a dual role in the damage progression. They acted as molten material traps (as judged by the multiple excursions sensed at the spacer locations) and as sources of molten material (because of eutectic formation). The behavior of the Inconel grid spacers noted in the FLHT tests is consistent with the behavior noted in the CORA out-of-pile experiments (Hoffman 1989).

An axial schematic of the relocation behavior in the bundle during FLHT-2 is presented in Figure 4.16. Illustrated in this figure are the relocation events presented in Table 4.3, except for the relocation event at 765 s. Also noted are the local interactions that took place between cladding and the grid spacer observed in the post-test visual examination but not recorded by the thermocouples. Note that the length of the brackets used to define the relocation event indicates the estimated axial position of the origin and the lowest level thermocouple that sensed hot material.

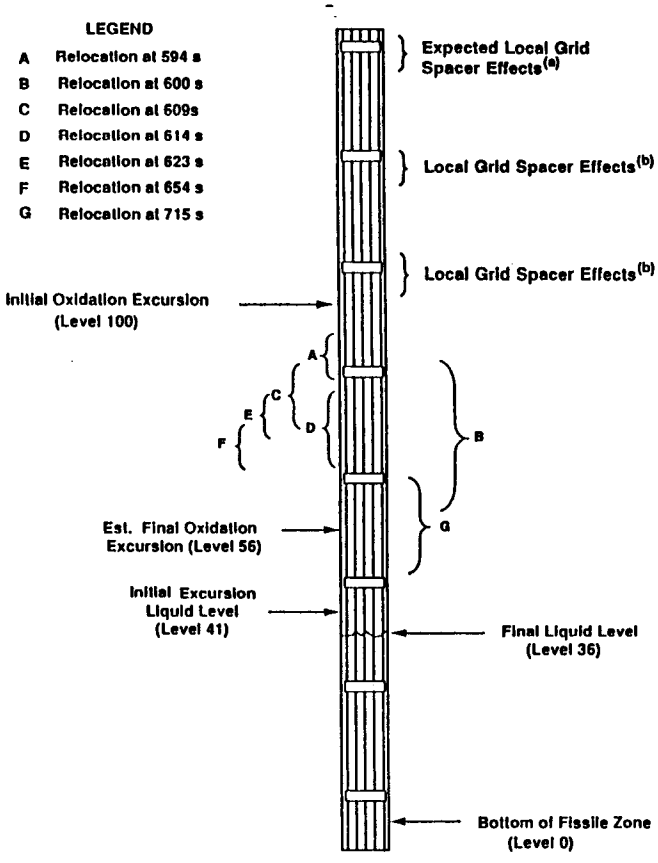

(a) Not confirmed from visual exam.
(b) From post-test visual exam.

Figure 4.16 Axial schematic of FLHT-2 material relocation events

Evident in this figure is the heterogeneous nature of the relocation behavior and the potential for once-molten materials that have relocated to reheat and possibly relocate multiple times. The axial extent of the relocation events are also indicated and are generally no longer than the axial distance between grid spacers (0.5 m).

Based on the on-line data collected during the FLHT tests and the currently available visual and metallographic results from the tests, the FLHT material relocation behavior is summarized as follows:

- The axial extent of material relocation is typically within the distance between grid spacers, i.e., <0.5 m.
- The relocation phenomenon is heterogeneous with the sources of molten material originating from different components within the oxidation burn front and freezing at different locations lower in the bundle elevations.
- The extent of the axial relocation is such that once-molten materials can remelt and relocate as the oxidation excursion region proceeds downward.
- Grid spacers act as both sources and sinks of molten metal.
- The tendency for relocation is greater early in the boiloff transient when the oxidation front velocity is highest and the amount of fresh metal the greatest.
- Once-molten materials have not been observed in the steam-cooled region above the coolant pool nor in the pool.

4.4.2 Assessment of SFD Test Relocation Behavior

While neither the short-length or full-length SFD tests are fully prototypic, each provides information on phenomena important to understanding material relocation behavior. In this section, the differences and similarities among the full- and short-length SFD tests are examined with the goal of developing a comprehensive picture of early-phase melt progression. To ensure a meaningful comparison, the assessment of the short-length tests included only tests without control materials, e.g., DF-1 (Gasser et al. 1990) and PBF 1-3 (Martinson et al. 1989). The comparison is presented below based on the similarities and differences shown in Table 4.4.

Table 4.4 Evaluation of material relocation behavior in both short- and full-length SFD tests[1]

Similarities
• heterogeneous nature
• influence of oxidation burn front
• relocation distance
• impact of grid spacers
Differences
• amount of cohesive melt found at the lower elevations

[1]Data on the degree of fuel dissolution for the FLHT tests is forthcoming; conclusions relative to the short-length test cannot be drawn at this time.

The single notable difference in the material relocation behavior between these two different kinds of tests, i.e., the amount of cohesive melt found in the lower elevation, can be related to differences in the test features and operation. The short-length tests have intrinsic design and operational features that promote the formation of large cohesive blockages, particularly at the lower elevations. These features include large axial temperature gradients resulting from the short length, the proximity of inlet region structures to the damage region, and high fission power levels. Conversely, the design and operational features of the full-length tests make the formation of large cohesive melts less likely: larger radial heat losses at SFD temperatures, a smaller fission power component, and a large distance between the melt zone and inlet fixtures. Thus the key parameters that could lead to the observed differences in test behavior are as follows:

- radial heat losses - limits superheat of melt
- increasing fission power levels - increases superheat
- axial temperature gradients - promotes freezing
- proximity of low temperature inlet fixtures - promotes blockage formation.

While the above parameters are inextricably tied to the phenomena of molten material relocation, it is important to understand the role of each and how it might impact the end-state. Presented below are discussions on how differences in these parameters can lead to the different end-states observed.

4.4.2.1 Effect of Radial Heat Losses

Differences in the bundle and shroud designs and radial boundary conditions between the full- and short-length test lead to differences in the radial heat loss component. Whereas the FLHT shroud had a thicker insulation than the Power Burst Facility (PBF) shroud (10.2 vs. 7.6 mm), the PBF bundle region had a larger number of fuel rods (28 vs. 12) that would reduce the radial temperature gradients across the bundle (both the PBF and FLHT tests had single-phase forced convection radial boundary conditions). The DF-4 test had a relatively thick shroud insulation thickness (~140 mm) and a stagnant helium gas boundary condition, making this shroud the most thermally insulating of the three. As a result, the local radial heat losses in the FLHT tests were greater than in the other SFD tests.

If, however, the FLHT radial heat losses are excessive at and below the melt location, the axial temperature profiles in the vicinity of this region would be affected. The axial temperature profile is an important thermal-hydraulic parameter that governs the heat transfer from

the melt to contacting and surrounding structures. Further, it is one of several important parameters that determines the freezing behavior of molten materials and, therefore, the axial extent of relocation.

To evaluate the effect of FLHT-type radial heat losses on the axial temperature profiles, predictions were made using BWRSAR-NRU[1] with an as-designed shroud and a shroud with an assumed adiabatic boundary. The results of this assessment (Figure 4.17) for an interior rod show that the onset of the oxidation excursion is delayed less than 2 minutes due to the heat losses, and that the axial temperature gradients at and below the melt front location are relatively unaffected.

[1]Ott, L. J. 1989. "Description of the NRU FLHT-6 Experiment-Specific Code and Preliminary Pretest Predictions." Oak Ridge National Laboratory Letter Report, September 1989.

Therefore, up to the Zircaloy melting temperature (the temperature relocation is predicted to occur by BWRSAR-NRU), one of the major thermal-hydraulic parameters that governs material relocation behavior, the local axial temperature gradient, is not affected by FLHT-type radial heat losses. This would explain the observed similarities in the relocation distance between the short- and full-length tests.

One aspect of material relocation behavior not captured by BWRSAR-NRU is the how the radial heat losses limit the potential superheat of the melt. Because the code predicts relocation to occur at the Zircaloy melt temperature, the superheat was excluded. The effect of radial heat losses on the melt superheat cannot now be quantified. An accurate and robust material relocation model would be required for the analysis. At this time such a model does not exist and therefore one can only

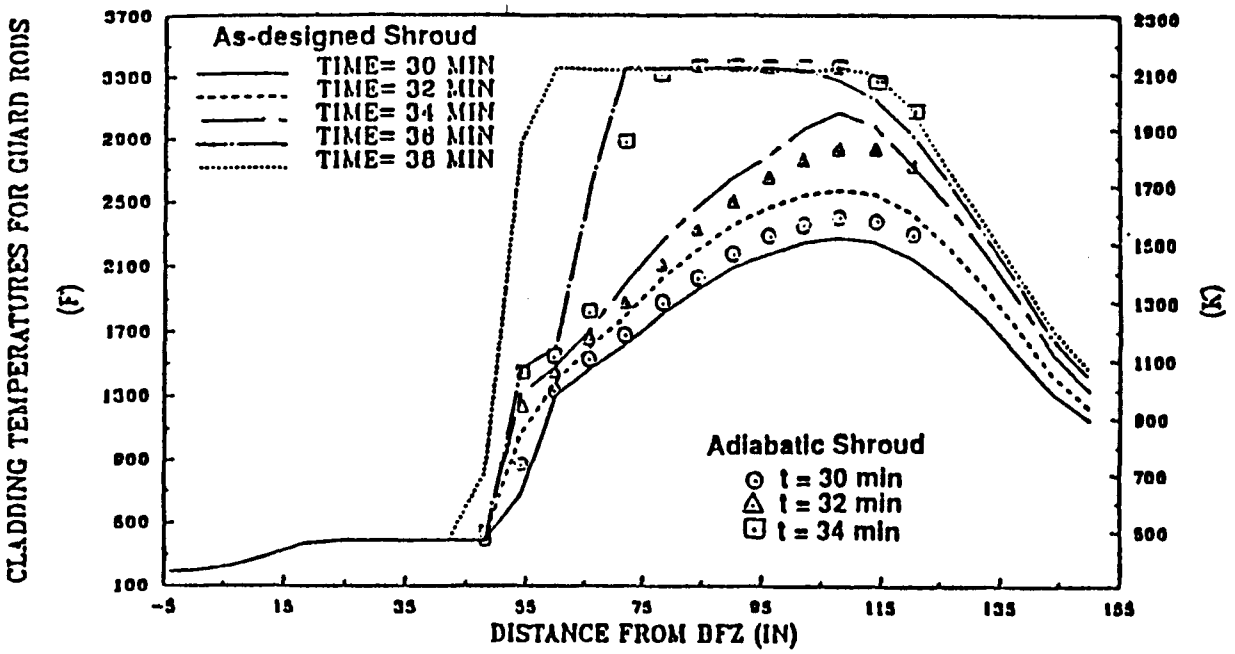

Figure 4.17 Predicted impact of shroud radial heat losses on cladding axial temperature gradients

conclude that radial heat losses do not cause atypical axial temperature gradients.

4.4.2.2 Effect of Relative Fission-to-Chemical Power Ratio

In each of the short- and full-length tests, different fission power levels and steaming rates were used. The approach used in the short-length tests was to use higher fission power levels to overcome the effect of higher radial heat losses at SFD temperatures; his approach was not chosen for the full-length FLHT tests because of the coupled relationship between coolant level and power and the ability to achieve more prototypic conditions by simulating decay heat levels. Instead, the fission power levels were maintained constant and melt temperatures were achieved as a result of the oxidation excursion. Note that in both the PBF and the FLHT test, radial heat losses were offset by rapid oxidation of the shroud liner.

A summary of the peak fission power and steaming rate levels for the three SFD tests is presented in Table 4.5.

Table 4.5 Comparison of fission and chemical powers

Parameter	FLHT-5	DF-4	PBF 1-3
Number of fuel rods	11	9	28
Steaming rate, g/s-rod	0.11	0.09[1]	0.02
Peak fission power, kW/m-rod	0.74	2.2	1.1
Relative fission/ chemical power ratio	6.5	25	51

[1]Average net steaming rate during oxidation phase.

Also presented in this table is a relative measure of the peak fission power to chemical power, computed from the ratio of peak fission to steaming rate shown in the table.[1] As evidenced by the results shown in this table, in addition to having fission power levels ranging from 50% to 300% greater than the FLHT-5 test or post accident decay heat rates seen in power reactors, the ratio of the fission-to-chemical power relative to the FLHT-5 test ranged from a factor of 4 to as high as 8 in the low-steam flow PBF test. A qualitative discussion of the impact of these higher fission-to-chemical power ratios with respect to material relocation behavior is presented below.

The impact of the higher fission power levels of the short-length tests is illustrated schematically in Figure 4.18, where the local temperature as a function of time is indicated for high- and low-fission power tests. As illustrated in this figure, the higher fission-to-chemical power ratios lead to a slower and smaller overall temperature decrease after passage of the oxidation

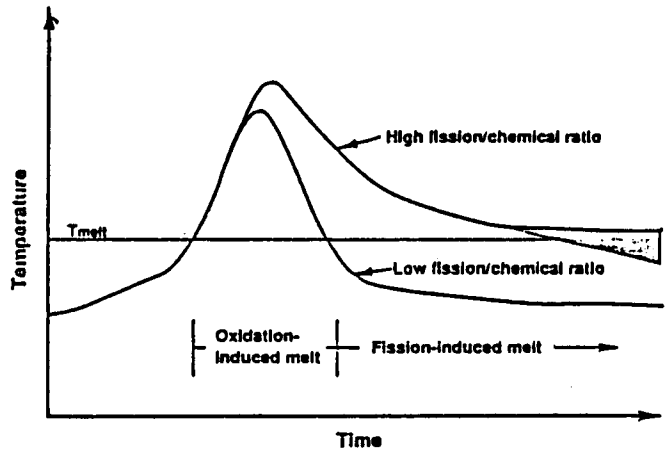

Figure 4.18 Illustration of the influence of fission-to-chemical power ratio on local temperatures

[1]The bundle steaming rate in g/s-rod is viewed as a fair representation of the chemical power production. This is because the bulk of the flowing steam was consumed within the oxidation burn front in all tests.

burn front. In addition, fission-enhanced melting can occur after the passage of the burn front. The higher fission-to-chemical power ratio, therefore, leads to the formation of larger amounts of melting and the attainment of greater superheats, both of which promote the formation of large melts that subsequently form cohesive blockages.

Again, the effect of different fission-to-chemical power ratios cannot be accurately quantified without an accurate relocation model. Independent of the fission-to-chemical power ratio, however, the greatest melt formation and relocation occurs in conjunction with the oxidation burn front and when the availability of unoxidized and previously nonrelocated metal is the greatest, i.e., during the downward burn.

4.4.2.3 Effect of Axial Temperature Profiles

The axial temperature profiles during an FLHT-type test change in magnitude over the exposed length of fuel. An example of the dynamic nature of these gradients is presented in Figure 4.19, where the cladding axial temperature gradients of the FLHT-2 test are presented as a function of time. Of particular interest are the changes in the profiles from 600 s, the time recorded for the first melt relocation event, to 800 s, just before the termination of the test.

The axial gradients along the length of uncovered fuel shown in Figure 4.19 can be segmented into three different regions: 1) an inlet region just above the coolant pool where axial gradients begin to develop, 2) the oxidation region, where the local oxidation power affects the axial temperature profile, and 3) a "transition" region between the inlet and oxidation regions. These regions are illustrated schematically in Figure 4.20.

The steepest axial temperature gradients achieved during the FLHT tests occur in the inlet region, just above the coolant pool. The gradient in this region increases with time while the region length is essentially constant. While the gradient in the inlet region approaches 35 K/cm in the full-length tests, the gradients in the short-length tests are significantly greater, exceeding 120 K/cm (for PBF 1-3 and DF-1) as a result of fission power components that are 2 to 3 times greater than for the FLHT tests.

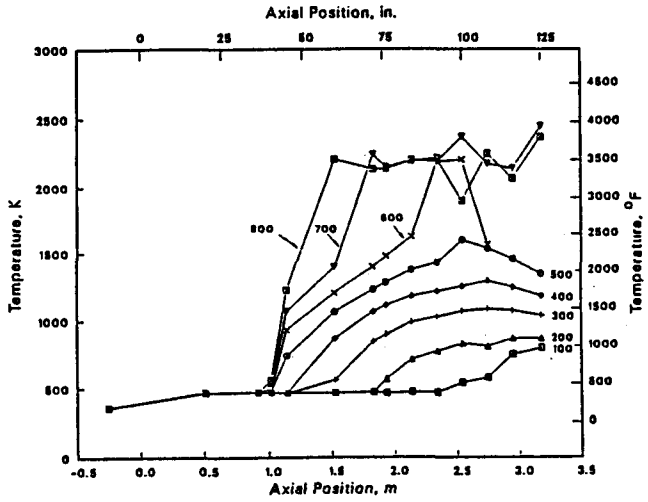

Figure 4.19 Changing nature of FLHT axial temperature gradients

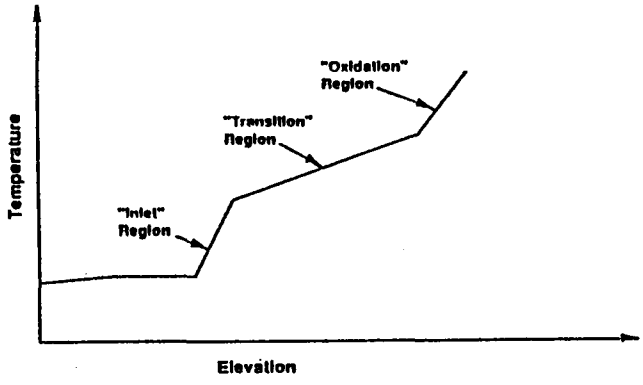

Figure 4.20 Characterization of boiloff-type axial temperature gradients

The axial gradient within the oxidation region, or the region immediately below the burn front, is on the order of 25 K/cm. Little change in the magnitude of the gradient or in the region length occurs with time. The magnitude of the gradient in this region is expected to be similar for both the short- and full-length tests as the effect of the oxidation power begins to occur at similar temperatures (1400 to 1500 K) and the rapid approach to the Zircaloy melt temperature is oxidation driven.

The axial temperature gradients in the transition region increase with time while the length of the region decreases with time. In addition, the gradients in this region are the lowest of the three regions. These two factors have several implications with respect to material relocation. The first implication is that, for the initial relocation events, conditions are such that molten material is prone to relocate farther down the length of the fuel bundle. This is because at this time the axial gradient of the transition region is the flattest and the steep axial gradients of the inlet region are not likely to occur because of the extended region length. Later, however, the axial gradients in the transition region become steeper and the length of the region becomes shorter increasing the potential for relocating material to encounter the even steeper gradients of the inlet region where cooling of the hot material is accelerated. Thus, the conditions within the transition region are such that longer material relocation distances may be promoted early in the damage sequence when cladding melting is first encountered.

While conditions in the transition region can influence material relocation as discussed above, the length of this region in the short-length tests is nonprototypically small because of the large length of the inlet region relative to the overall bundle length similarly small for the length of the oxidation region. This shortened transition region length promotes the passing of molten material from the oxidation region directly into the inlet region where the excessive temperature gradients accelerate the freezing of the material. Because the gradients are so large in this region, especially relative to the full-length tests, the likelihood of freezing the material within a small axial distance is significantly increased, as is the potential for the formation of a cohesive blockage. Also promoting the formation of cohesive blockages is the close proximity of the inlet fixtures in these tests. Together, these factors provide a rationale for why cohesive blockages are more likely to occur in the short-length tests than in the full-length tests.

4.4.2.4 Proximity of Inlet Fixtures

In comparing the relocation distances deduced for the FLHT-2 test with the data on relocation from short-length tests, the FLHT nominal relocation distance of 0.3 m for the FLHT tests is equal to 60% of the total fuel length of the DF-4 test bundle (0.5 m) and 30% of the total fuel length of the PBF test bundle (1.0 m). Recognizing that the initial relocation takes place at 2/3 to 3/4 of the heated length and proceeds downward, the relocations observed in the FLHT tests would reach the bottom of the fuel in the DF tests and the 0.4 m elevation of the PBF tests. Thus, the inlet fixtures are apparently influencing the freezing of materials in the DF tests; inlet fixtures can be expected to influence the PBF tests as the oxidation/melt zone approaches the bundle midplane.

4.4.2.5 Melt Relocation Comparison Summary

In summary, the essential features of material relocation behavior are consistent between the two types of in-reactor tests, with the exception of a larger amount of melt frozen in the lower regions of the short-length tests compared with the full-length tests. These differences appear explainable by differences in the shroud design, axial temperature gradients, fission-to-chemical power ratios, and the proximity of inlet fixtures to the oxidation burn front. The differences in the melt relocation caused by axial temperature gradients and the proximity of inlet fixtures noted above can be considered to be true length effects.

The bulk of the SFD phenomena investigated in the short-length tests are immune from length effects. These phenomena include the onset of rapid oxidation and the accompanying hydrogen generation, the interaction of core materials (eutectic reactions) including fuel dissolution), and the formation of molten materials. In these areas, the results of the short- and full-length tests tend to validate each other. However, inferences of extensive cohesive blockage formation at the bottom of the core in reactor accidents based on the observed short-length relocation phenomena should be carefully considered because of the length effects cited above.

5 SCDAP Code Analyses of FLHT Tests

In this section, the FLHT tests results are analyzed using the SCDAP severe fuel damage analysis code (Berna et al. 1984). A brief description of the code is first given, followed by an overview of the SCDAP calculations compared to key FLHT test data. This is then followed by a detailed assessment of the SCDAP predictions for the boilaway transient that occurred during the FLHT-5 test to demonstrate the applicability of the code in predicting test behavior. Included in the assessment are comparisons of predicted versus measured bundle and shroud temperatures, hydrogen generation, and fission gas release.

5.1 Description of SCDAP

The SCDAP computer code is a detailed mechanistically-based severe fuel damage code developed for the NRC by EG&G Idaho, Inc. The code is one of several computer codes developed for the analysis of severe reactor accidents and severe accident experiments and models the detailed behavior of the core during a severe damage transient sequence. It starts from an initial steady-state condition involving water-cooled, undamaged rods and continues through coolant boilaway, component heatup and oxidation, melt relocation, and fission product release. The nuclear and oxidation-driven heatup of the fuel and control rods are modeled, with account taken for convective and radiative heat losses.

The SCDAP code was developed to predict the melting and relocation of stainless steel cladding control materials (silver, indium, cadmium) and the expansion, rupture, and accelerated oxidation and melting of the Zircaloy cladding. Fission product release from the damaged fuel is also modeled as is the dissolution of uranium dioxide by metallic melt. Melt relocation is modeled as a breach of the zirconium dioxide layer on the outside of cladding, followed by downward relocation and freezing (and possible reheating and remelting) of the Zircaloy/uranium dioxide mixture. The version of the code used in the FLHT data comparisons does not model the geometry of debris, i.e., relocated melt, fractured fuel pellets, and cladding.[1]

The code can be applied to a representative LWR fuel assembly or to a test fuel assembly inside a multilayered insulated shroud with external bypass cooling, e.g., as in the FLHT tests. Thermal radiation from the assembly to the shroud and heat conduction through the shroud are modeled in the latter case.

The SCDAP code version used for the FLHT-5 analysis was MOD1, Version 20. The Zircaloy high-temperature oxidation model by Prater and Courtright (1986) was substituted for the default model of Urbanic (1978). Version 20 permitted user input of the bundle coolant level and steaming rate. It was also modified to reflect the bypass coolant boundary conditions in the NRU reactor.

5.2 Overview of SCDAP Predictions with Major FLHT-Test Parameters

Post-test SCDAP predictions presented in this report and reported previously are compared in Table 5.1 with major test results from FLHT-2, -4, and -5. The comparisons in this table show that SCDAP predicts the key peak conditions that occurred during the FLHT tests reasonably well, e.g., maximum hydrogen generation rate and maximum cladding temperature. However, the duration of accelerated oxidation and, therefore, the total hydrogen generated, are consistently underestimated by the code, as is the fraction of Zircaloy oxidized. Further analysis has shown that this underprediction is caused by 1) overprediction of the amount of Zircaloy melt relocated out of the high-temperature region and 2) underprediction of the amount of liner melt and oxidation.

Detailed code-to-data comparisons are given in the following subsections for the FLHT-5 test. For this

[1]Rod-like geometry is assumed for calculation of radiative and convective heat transfer following relocation.

Table 5.1 Post-test SCDAP predictions for FLHT tests compared with measured data

		Predicted/Measured Values		
Parameter	Units	FLHT-2	FLHT-4	FLHT-5
Maximum cladding temperature	K	2400/ >2400	2700/ >2600	3000/ >2600
Maximum hydrogen flow rate	mg/s	150/207	157/174	185/182
Total hydrogen generated[1]	g	40/48	175/265	161/340
Time interval from cladding dryout to escalation	s	800/450[2]	650/550	400/400
Fission gas release	%	--/N.A.	~10/ 25-55	20/ 22-100

[1]Divide by 398 to obtain the fraction of Zircaloy reacted.
[2]The FLHT-2 SCDAP simulation was artificially extended to permit ~5 min of hydrogen generation, as was observed in the test.

comparison, the FLHT-5 test was chosen because it permits assessment of the code's models up to and beyond the termination of the rapid oxidation phase of severe damage progression.

5.3 SCDAP Assessment of the FLHT-5 Test Data

In the following, the FLHT-5 SCDAP input model and parameters are first described. Comparisons and evaluations of the code predictions of bundle and shroud temperatures, oxidation, hydrogen generation, and fission gas release with the test data are then presented (Lanning 1986).

5.3.1 SCDAP FLHT-5 Model

The nodalization for the FLHT-5 analysis is displayed in Figure 5.1 and summarized as follows:

- The number of axial regions was 10 (the maximum allowable).

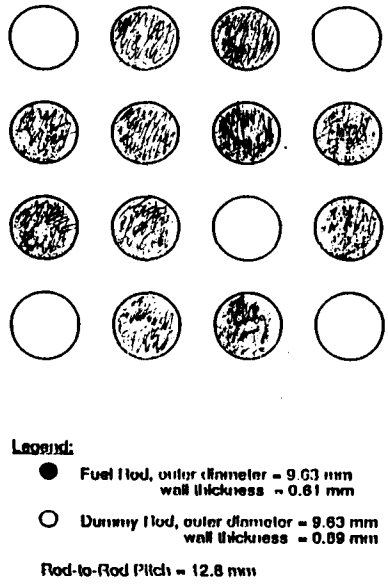

(a)

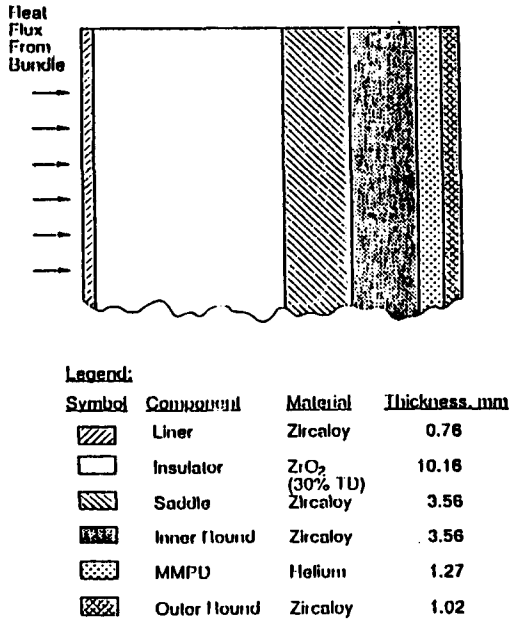

(b)

Figure 5.1 SCDAP nodalization of the FLHT-5 test: a) fuel bundle region; b) shroud region

- The number of fuel rods was 11, with as-fabricated dimensions and operating gas pressure.
- The one dummy gamma thermometer and four Zircaloy carrier pieces were modeled as non-fueled "dummy" rods with the correct mass of Zircaloy per node; see Figure 5.1.
- The shroud components were modeled and given as-fabricated thicknesses, and perfect contact was assumed between the various components. The MMPD was modeled as a helium gap (see Figure 5.1).
- Thermal properties of the shroud insulation, in particular its thermal conductivity, were input using vendor-supplied data.
- The breach temperature for the cladding oxide layer was set at a high value (3000 K) to minimize predicted Zircaloy relocation out of the reaction zone.

The bundle nuclear power history input into SCDAP for FLHT-5 was modified to include a 30% power increase because of coolant voiding during the boilaway transient. This modification was previously found to yield excellent code-to-data comparisons for bundle heatup after dryout, even though the calculated power increase from voiding predicted by PNL and CRNL neutronics codes was only 15% to 19%.[1] The boilaway coolant level and steaming rate were both input to SCDAP based on the output of the TRUMP-BD code (Lombardo et al. 1990) which in turn used measured flow rates as input. The code uses the Cunningham and Yeh (1973) void correlation for low-pressure boilaway and has proven successful at matching coolant level and dryout data for the FLHT tests.

5.3.2 Comparison of Bundle and Shroud Temperatures

An assessment of the predicted component heatup and escalation is made from comparisons of 1) predicted and measured cladding temperature, 2) liner and saddle temperatures at Level 80 just above the fuel bundle midplane, and 3) predicted and measured cladding axial temperature distributions. The agreement between measured and predicted cladding and liner temperatures is shown in Figure 5.2. As shown, the prediction for the time interval from cladding dryout to temperature escalation at Level 80 is very close to the measured values, and the heatup during that time interval is also well predicted. The predicted maximum temperature following escalation is 3000 K (corresponding with the input zirconium dioxide breach temperature of 3000 K). The estimated maximum fuel temperature attained was >2600 K.[2]

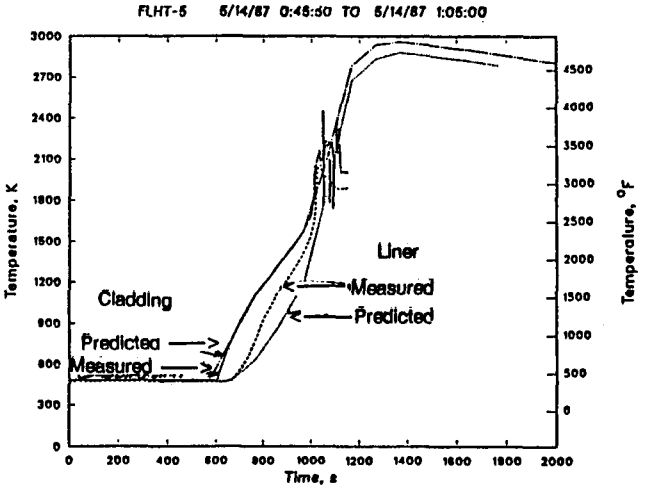

Figure 5.2 Measured and predicted cladding and liner temperatures at level 80 for FLHT-5

The approach to escalation is well matched at more than this one elevation. In Figure 5.3, the measured axial temperature profiles are plotted at 100-s intervals, from 500 s to 1000 s (i.e., from transient initiation to first escalation). The corresponding predicted axial profiles match the measurements very closely. This confirms that, given the correct boilaway history and the input power history modifications just described, SCDAP correctly predicts the subsequent bundle heatup along the entire axial length. In particular, the location and

[1]The light-water coolant in the bundle region is effectively a neutronic poison within the heavy-water moderated NRU reactor. Hence, as the coolant is boiled away, the local reactivity and power increase.

[2]Actual peak temperatures achieved will be determined by post-irradiation examinations and metallography of the fuel bundle region.

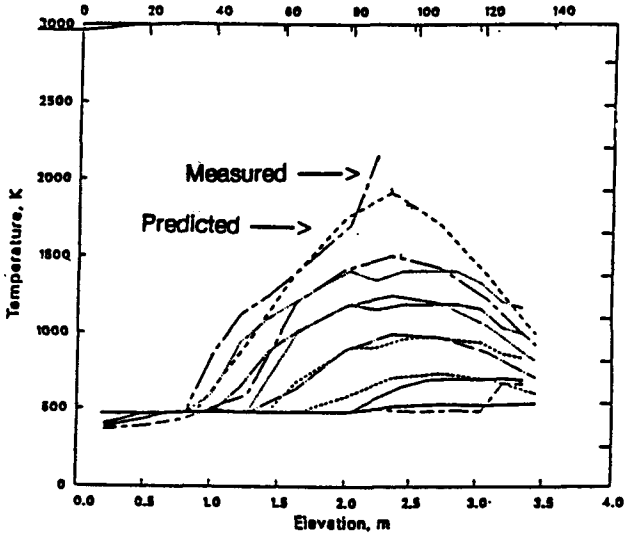

Figure 5.3 Measured and predicted cladding temperatures for FLHT-5 versus elevation, at 100 s intervals

timing of the initial temperature escalation is well predicted (i.e., at 1000 s in the 2.0- to 2.5-m range, Levels 80 to 100).

The SCDAP prediction of liner heatup is delayed relative to the measured data, as demonstrated in Figure 5.2, wherein dryout and heatup of both cladding and liner are shown for Level 80. The occurrence of dryout for the liner is well predicted, but the predicted heatup lags the measured data below 1500 K. This same pattern was noted at other axial levels.

The difference between measurement and prediction is more pronounced for saddle temperatures located on the outside of the insulation region. Figures 5.4 and 5.5 are plots of measured and predicted saddle temperatures at Levels 64 and 136, respectively. At Level 64, in Figure 5.4, the timing of the peak in saddle temperatures caused by passage of the oxidation front is predicted correctly, but the temperature rise rate is underpredicted as is the temperature decrease after passage of the front. These discrepancies can be attributed in part to the difficulty in estimating the effective thermal conductivity of the shroud. For example, the thermal conductivity of the as-fabricated insulation is well known up to 1900 K. However, the effective value during the test,

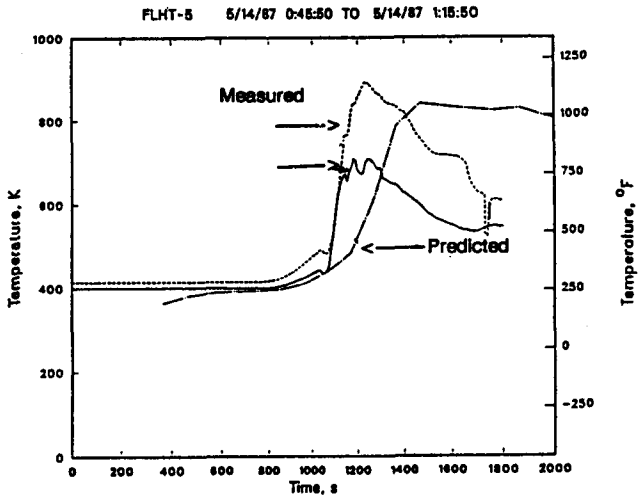

Figure 5.4 Measured and predicted saddle temperatures at level 64 for FLHT-5

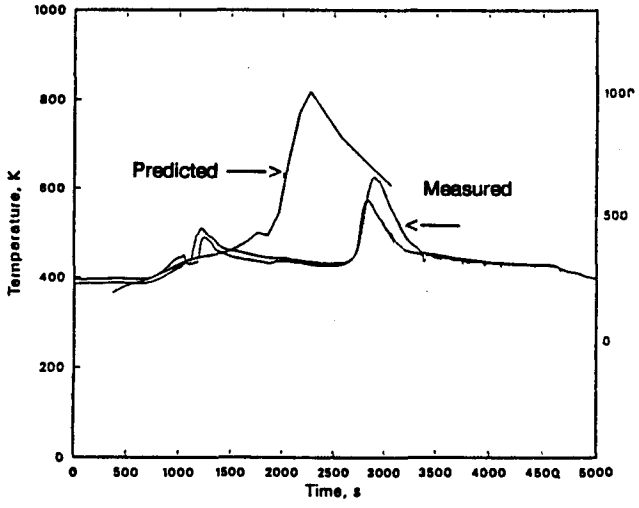

Figure 5.5 Measured and predicted saddle temperatures at level 136 for FLHT-5

especially following the escalation to higher temperatures, is uncertain because the conductance is influenced by the following factors: 1) steam ingress following liner breach, 2) cracking or displacement of the insulation, 3) reaction between the Zircaloy liner and zirconium dioxide insulation, and 4) by high-temperature radiation effects across pores in the high-porosity zirconium dioxide.

In the upper regions of the fuel bundle (Level 136), the predicted burn front and the resulting peak saddle temperature occur earlier than was observed in the test. This difference is due to premature termination of the oxidation predicted at lower levels, which resulted in the prediction of an earlier transition to an upward burn than actually occurred. The premature termination of the oxidation (before complete Zircaloy consumption) occurred because significant quantities of molten Zircaloy were predicted to relocate into the steam-cooled region above the coolant pool. The net effect was early termination of the bundle oxidation, whereby the predicted period of significant oxidation was essentially 50% of that noted for the FLHT-5 test. Copious material relocation was predicted even with a zirconium dioxide breach temperature of 3000 K.

5.3.3 Comparison of Bundle Oxidation and Hydrogen Generation

The predicted early termination of bundle oxidation was evident in the comparison of the measured and predicted hydrogen generation rate (Figure 5.6). The SCDAP code correctly predicted the onset of hydrogen generation and correctly associates the autocatalytic oxidation/hydrogen generation at 1000 s with the concurrent escalation of the bundle temperature. The peak predicted generation rates and associated oxidation power (187 mg/s, 28 kW) are also close to the peak measured values. Again the duration of the autocatalytic oxidation and hydrogen generation is underpredicted due to the predicted relocation of Zircaloy from most axial nodes and consumption of the remaining Zircaloy.

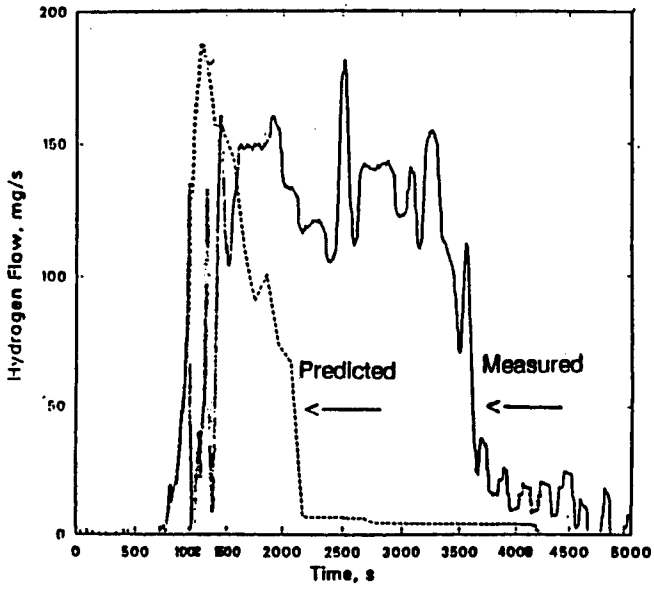

Figure 5.6 Measured and predicted hydrogen generation rates

The early termination of the accelerated Zircaloy oxidation and hydrogen generation results directly in an underprediction of total hydrogen generated and the associated fraction of bundle Zircaloy oxidized. This is summarized in Table 5.2.[1]

Table 5.2 Measured and SCDAP predicted hydrogen generation and zircaloy oxidation for FLHT-5

Parameter	Measured Value	SCDAP
Hydrogen generated, g	340[1]	168
Amount of bundle Zircaloy oxidized, %[2]	86	42
Amount of exposed Zircaloy oxidized, %[3]	100	53

[1]Best-estimate value.
[2]100% equals 398 g H_2.
[3]Steady-state coolant level following boilaway was at ~0.76 m elevation. Exposed Zircaloy represented 80% of the total Zircaloy.

Another contribution to the underpredicted hydrogen release noted in Table 5.2 was the underpredicted liner oxidation. The liner represented about one-third of the total inventory of Zircaloy in the bundle. Visual examination indicated that the liner was extensively oxidized

[1]Bundle Zircaloy included the fuel cladding, the carriers, and the liner. The steel in the dummy deposition rod was also a potential hydrogen source, as were the UO_2 pellets; however, these are not included in the calculation of potential bundle hydrogen inventory from which the fraction of Zircaloy oxidized was deduced.

within the severe damage region. However, the SCDAP code predicted minimal liner oxidation, because it predicted extensive relocation of the rapidly oxidizing cladding and, hence, lower than measured local liner temperatures within a given axial node. The predicted oxidation for the Zircaloy cladding, carriers, and liner is tabulated in Table 5.3.

Table 5.3 SCDAP predicted FLHT-5 zircaloy oxidation

	Percent Zircaloy Oxidized, by Component		
Node Number	Cladding (11 Rods, 44% of Total Zircaloy)	Carriers (+ Dummy Rod Sleeve, 22% of Total Zircaloy)	Liner (34% of Total Zircaloy)
10 (Top)	99	100	72
9	70	100	6
8	45	100	4
7	54	100	5
6	78	100	7
5	88	100	8
4	100	100	6
3	7	3	0
2	0	0	0
1 (Bottom)	1	0	0
Average	54	73	5

An improvement in code-data comparisons for the FLHT tests will require improvement in the material relocation model, in the amount of superheat that can be attained in the melt, and in the heat transfer from the melt to surrounding structures that influence the onset of freezing.

5.3.4 Comparison of Fission Gas Release

The average release rates and total release fractions for xenon and krypton for FLHT-5 were estimated from on-line gamma spectrometric data and from integration of the measured stack gas activity. These data are compared to SCDAP calculations in Table 5.4. The time history of the FLHT-5 noble gas release, as measured by the CRNL stack activity monitor and the INEL gamma spectrometer at the SCC, are shown in Figure 5.7 together with the predicted release rates.

Table 5.4 FLHT-5 fission gas release measurements and predictions

	Measured Values		Predicted Values	
Parameter/Units	CRNL Stack Monitor	Gamma Spec-trometer	SCDAP	Best-Estimate Values
Average bundle release rate, fraction/s (1500 to 2500 s)	4 to 5E-4	1 to 2E-4	1 to 2E-4	2E-4
Total Release, % of inventory (for the bundle)	88 to 100	22 (Xe) 39 (Kr)	20	20 to 80 (50 average)

The comparisons in Table 5.4 and Figure 5.7 demonstrate that the SCDAP code calculates release rates that are on the same order of magnitude as the measured values but also that these rates are not predicted to persist because the high temperatures associated with the autocatalytic oxidation reaction are terminated prematurely. If the predicted bundle oxidation were extended and the localized high temperatures associated with autocatalytic oxidation persisted longer (e.g., by a factor of 2), the predicted total fission gas release fraction would also increase by about a factor of 2, which would put it in agreement with the measurements.

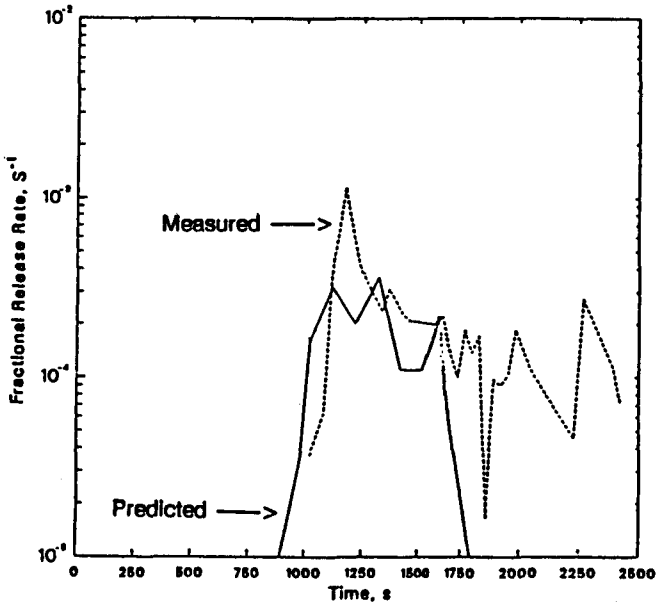

Figure 5.7 Measured and predicted xenon fractional release rates for FLHT-5

In summary, the SCDAP predictions for release rates of xenon and krypton at FLHT-5 peak temperatures are reasonable relative to measurements made during the test; the predicted total release fraction would likely approximate the measurement if the SCDAP code properly simulated the bundle oxidation and thermal history.

6 Conclusions

The results from the FLHT tests provide well-characterized data for evaluating the effects of coolant boilaway and core damage progression in an LWR. The tests provided the opportunity to investigate integral severe accident phenomena in full length LWR-type fuel bundles under coolant boilaway conditions. The test data and analysis supported the regulatory issue of hydrogen generation in BWRs during a severe accident. The tests were used to confirm the validity of most of the results obtained from separate effects and short length integral tests. Not confirmed were coherent blockage and lack of gross fuel swelling. The tests were used to help validate SCDAP for the early stage of a severe accident. We believe because of an inadequate fuel rod relocation model that the oxidation and hydrogen generation were incorrectly predicted by the code as the test data made evident. Fission product releases were also inadequately predicted but we believe that improvements in the fuel rod relocation model will also improve the fission product release predictions.

7 References

Berna, G. A., C. M. Allison, and L. J. Siefken. 1984. "SCDAP/MOD1/V>O.: Computer Code for the Analysis of LWR Vessel Behavior During Severe Accident Transients." IS-SAAM-84-002, Rev. 1, 1984.

Cathcart, J. V., and R. E. Pawel. 1977. "Zirconium Metal-Water Oxidation Kinetics IV: Reaction Rate Studies." ORNL/NUREG-17, Oak Ridge National Laboratory, Oak Ridge Tennessee.

Cronenberg, A. W., et al. 1990. "Severe Accident Zircaloy Oxidation/Hydrogen Generation Behavior Noted From In-pile Test Data." In Proceedings of the U.S. Nuclear Regulatory Commission: 17th Water Reactor Safety Information Meeting, U.S. Nuclear Regulatory Commission, NUREG/CP-0105, Vol 2., March 1990.

Cunningham, J. P., and H. C. Yeh. 1973. "Experiments and Void Correlation for PWR Small-Break LOCA Conditions." Trans. Am. Nucl. Soc. 17:269.

Gasser, R. D., C. P. Fryer, R. O. Gauntt, A. C. Marshall, K. O. Reil, and K. T Stalker. 1990. Damaged Fuel Experiment DF-1: Results and Analyses. NUREG/CR-4668, SAND86-1030, prepared by Sandia National Laboratories for the U.S. Nuclear Regulatory Commission, Washington, D.C.

Hoffman, P., S. Hogan, G. Schavy, and A. S. Kokan. 1989. "Reactor Core Materials Outer Actions at Very High Temperatures." Nuclear Technology, Vol. 87.

Lanning, D. D. 1982. Experimental Evidence for the Dependence of Fuel Relocation Upon the Maximum Local Power Attained. PNL-SA-10810, Presented at the Tenth Water Reactor Safety Research Information Meeting, Gaithersburg, Maryland, October 11-15, 1982.

NRU Full-Length High-Temperature Test SCDAP Post-Test Calculations. PNL-SA-21271. Presented at the NRC/SFD/ST Program Modeler's Workshop, October 1986, Rockville, Maryland. Pacific Northwest Laboratory, Richland, Washington.

Lombardo, N. J., T. J. Marseille, M. D. White, and P. S. Lowery. 1990. TRUMP-BD: A Computer Code for the Analysis of Nuclear Fuel Assemblies Under Severe Accident Conditions. PNL-7353, Pacific Northwest Laboratory, Richland, Washington.

Martinson, Z. R., M. Gasparini, R. R. Hobbins, D. A. Petti, C. M. Allison, J. K. Hohorst, D. L. Hagrman, and K. Vinjamuri. 1989. PBF Severe Fuel Damage Test 1-3 Test Results Report. NUREG/CR-5354, EGG-2565, prepared by Idaho National Engineering Laboratory, EG&G Idaho, Inc., for the U.S. Nuclear Regulatory Commission.

Prater, J. T., and E. L. Courtright. 1986. High Temperature Oxidation of Zircaloy-4 in Steam and Steam/Hydrogen Environments. NUREG/CR-4476, PNL-5558, prepared by Pacific Northwest Laboratory for the U. S. Nuclear Regulatory Commission, Washington D.C.

Urbanic, V. F., and T. R. Heidrick. 1978. "High Temperature Oxidation of Zircaloy-2 and Zircaloy-4 in Steam." J. Nucl. Mater. 75:251.

DISTRIBUTION

No. of Copies

OFFSITE

A. C. Thadani
U.S. Nuclear Regulatory Commission
Office of Nuclear Reactor Regulation
Washington, D.C. 20555

20 U.S. Nuclear Regulatory Commission
Office of Nuclear Regulatory Research
Washington, D.C. 20555
ATTN: E. S. Beckjord, NLS007
F. Eltawila, NLN344
R. V. Lee, NLN344
G. P. Marino, NLS007
J. A. Murphy, NLS007
Z. R. Rosztoczy, NSL169
A. M. Rubin, NLN344
B. W. Sheron, NLS007
T. P. Speis, NLS007
C. G. Tinkler, Jr., NLN344
T. J. Walker, NLN344 (9)
R. W. Wright, NLN344

M. D. Houston
U.S. Nuclear Regulatory Commission
Office of ACRS
Washington, D.C. 20555

U.S. Nuclear Regulatory Commission
Division of Technical Information and
Document Control
7920 Norfolk Avenue
Bethesda, MD 20014

D. C. Langstaff
U.S. Department of Energy
Richland Field Office
P.O. Box 550
Richland, WA 99352

B. Spencer
Argonne National Laboratory
9700 South Cass Avenue
Argonne, IL 60439

No. of Copies

C. Alexander
Battelle Columbus Laboratory
505 King Avenue
Columbus, OH 43201

T. Pratt
Brookhaven National Laboratory
130 BNL
Upton, NY 11973

A. Machiels
Electric Power Research institute
P.O. Box 10412
3412 Hillview Avenue
Palo Alto, CA 94303

2 EG&G Idaho, Inc.
P.O. Box 1625
Willow Creek Building, W-3
Idaho Falls, ID 83415
ATTN: R. Hobbins
C. M. Allison

R. J. Hammersley
Fauske and Associates, Inc.
16W070 West 83rd Street
Burr Ridge, IL 60521

3 Oak Ridge National Laboratory
P.O. Box Y
Oak Ridge, TN 37830
ATTN: S. Hodge
T. Kress
L. J. Ott

3 Sandia National Laboratories
P.O. Box 5800
Albuquerque, NM 87185
ATTN: R. O. Gauntt
J. E. Kelly
K. O. Reil

No. of Copies

I. Catton
University of California Los Angeles
Nuclear Energy Laboratory
405 Hilgaard Avenue
Los Angeles, CA 90024

M. L. Corradini
Nuclear Engineering Department
University of Wisconsin
1500 Johnson Drive
Madison, WI 53706

FOREIGN

H. Bairiot
Department of LWR Fuel
Belgonucleaire
Rue de Champde Mars. 25
B-1050 Brussels
BELGIUM

2 R. D. MacDonald
Atomic Energy of Canada, Ltd.
Chalk River, Ontario KOJ-IJO
CANADA

2 Kernforschungszentrum Karlsruhe
Postfach 3640
75 Karlsruhe
GERMANY
ATTN: S. Hagen
P. Hofmann

G. Petrangeli
Nucleare e della Protezione Sanitaria
(DISP)
Ente Nazionnle Energie Alternative
(ENEA)
Viale Regina Margherita, 125
Casella Postale M. 2358
I-00100 Roma A.D.
ITALY

K. Soda
Japan Atomic Energy Research Institute
Tokai-mura, Naka-gun, Ibaraki-ken
319-11
JAPAN

No. of Copies

H. R. Jun
Korea Advanced Energy Research
Institute
P.O. Box 7
Daeduk-Danji
Choong-Nam
KOREA

S. I. Chang
Institute of Nuclear Energy Research
P.O. Box 3
Lungtan
Taiwan 325
REPUBLIC OF CHINA

J. Bagues
Consejo de Seguridad Nuckan
SOR Angela de la Cruz No 3
Madrid 28056
SPAIN

A. Alonso
E. T. S. Ingenieros Industriales
Jost Gutierrez Abascal, 2
28006 Madrid
SPAIN

W. Frid
Statens Karnkraftinspektion
P.O. Box 27106
S-10252 Stockholm
SWEDEN

K. J. Brinkman
Reactor Centrum Nederland
1755 ZG Petten
THE NETHERLANDS

B. D. Turland, E5.157
UKAEA
Culham Laboratory
Abingdon OX14-3DB
Oxfordshire, England
UNITED KINGDOM

No. of Copies

2 UKAEA
Winfrith, Dorchester DT2-8DH
Dorset, England
UNITED KINGDOM
ATTN: S. Kinnersly, 203/A32
T. Haste

V. Asmolov
Nuclear Safety Department
I.V. Kurchatov Institute of Atomic Energy
Moscow, 123182
RUSSIA

ONSITE

30 Pacific Northwest Laboratory

G. A. Anderson, K7-28
C. E. Beyer, P8-10
M. E. Cunningham, P8-10

No. of Copies

D. E. Fitzsimmons, P8-35
M. D. Freshley, P8-10
R. J. Guenther, P8-10
L. L. King, P8-35
J. L. Ethridge, P8-10
D. D. Lanning, P8-34
N. J. Lombardo, K7-15 (3)
F. E. Panisko, P8-35 (6)
L. J. Parchen, P8-33
W. N. Rausch, P8-35
G. L. Tingey, P8-10
M. C. Wismer, P8-35
Publishing Coordination (2)
Technical Report Files (5)
NRC Project Office

NRC FORM 335 (2-89) NRCM 1102, 3201, 3202

U.S. NUCLEAR REGULATORY COMMISSION

BIBLIOGRAPHIC DATA SHEET

(See instructions on the reverse)

1. REPORT NUMBER (Assigned by NRC. Add Vol., Supp., Rev., and Addendum Numbers, if any.)

NUREG/CR-5876
PNL-8023

2. TITLE AND SUBTITLE

Full-Length Fuel Rod Behavior Under Severe Accident Conditions

3. DATE REPORT PUBLISHED

MONTH	YEAR
December	1992

4. FIN OR GRANT NUMBER

B2277

5. AUTHOR(S)

N. J. Lombardo, D. D. Lanning, F. E. Panisko

6. TYPE OF REPORT

Technical

7. PERIOD COVERED *(Inclusive Dates)*

1984 to 1991

8. PERFORMING ORGANIZATION – NAME AND ADDRESS *(If NRC, provide Division, Office or Region, U.S. Nuclear Regulatory Commission, and mailing address; if contractor, provide name and mailing address.)*

Pacific Northwest Laboratory
Richland, WA 99352

9. SPONSORING ORGANIZATION – NAME AND ADDRESS *(If NRC, type "Same as above"; if contractor, provide NRC Division, Office or Region, U.S. Nuclear Regulatory Commission, and mailing address.)*

Division of Systems Research
Office of Nuclear Regulatory Research
U.S. Nuclear Regulatory Commission
Washington, DC 20555

10. SUPPLEMENTARY NOTES

11. ABSTRACT *(200 words or less)*

This document presents an assessment of the severe accident phenomena observed from four Full-Length High-Temperature (FLHT) tests that were performed by the Pacific Northwest Laboratory (PNL) in the National Research Universal (NRU) reactor at Chalk River, Ontario, Canada. These tests were conducted for the U.S. Nuclear Regulatory Commission (NRC) as part of the Severe Accident Research Program. The objectives of the test were to simulate conditions and provide information on the behavior of full-length fuel rods during hypothetical, small-break, loss-of-coolant severe accidents, in commercial light water reactors.

12. KEY WORDS/DESCRIPTORS *(List words or phrases that will assist researchers in locating the report.)*

Fuel Performance
Melt Progression
Hydrogen Generation
Severe Accidents

13. AVAILABILITY STATEMENT

Unlimited

14. SECURITY CLASSIFICATION

(This Page) Unclassified

(This Report) Unclassified

15. NUMBER OF PAGES

16. PRICE